Aus dem Institut für Molekularbiologie und Tumorforschung

Geschäftsführender Direktor: Prof. Dr. Alexander Brehm

des Fachbereichs Medizin der Philipps-Universität Marburg

Distinct CoREST complexes act in a cell-type-specific manner

Inaugural-Dissertation

zur Erlangung des Doktorgrades der Naturwissenschaften

(Dr. rer. nat.)

dem Fachbereich Medizin der Philipps-Universität Marburg

vorgelegt von

Igor Mačinković

aus Belgrad, Serbien

Marburg, 2020

Angenommen vom Fachbereich Medizin der Philipps-Universität Marburg am:

17.11.2020

Gedruckt mit Genehmigung des Fachbereichs

Dekan i.V. der Prodekan: Prof. Dr. R. Müller

Referent: Herr Prof. Dr. A. Brehm

1. Korreferentin: Frau Dr. W. Baarends

„Бити човек, рођен без свога знања и без своје воље, бачен у океан постојања. Морати пливати. Постојати. Носити идентитет. Издржати атмосферски притисак свега око себе, све сударе, непредвидљиве и непредвиђене поступке, своје и туђе, који понајчешће нису по мери наших снага. А поврх свега, треба још издржати и своју мисао о свему томе. Укратко: бити човек"

- Иво Андрић (Стокхолм 10. децембар 1961)

"To be a man, to have been born without knowing it or wanting it, to be thrown into the ocean of existence, to be obliged to swim, to exist; to have an identity; to resist the pressure and shocks from the outside and the unforeseen and unforeseeable acts — one's own and those of others — which so often exceed one's capacities? And what is more, to endure one's own thoughts about all this: in a word, to be human."

— Ivo Andrić (Stockholm, 10 December 1961)

"Mensch zu sein, geboren worden zu sein, ohne es zu wissen oder zu wollen, in den Ozean der Existenz geworfen zu sein, zum Schwimmen gezwungen zu sein, zu existieren; eine Identität zu haben; dem Druck und den Schlägen von aussen sowie den unvorhergesehenen und unvorhersehbaren Taten zu widerstehen — den eigenen und denen von anderen — was so oft die eigenen Fähigkeiten übersteigt? Und darüber hinaus, muss man noch die eigenen Gedanken über all dies ertragen müssen, kurz gesagt: ein Mensch sein."

— Ivo Andric (Stockholm, 10 December 1961)

Table of contents

List of abbreviations

Amino acids are abbreviated with the standard single- or three-letter code and nucleotides with the standard single-letter code.

Abbreviation	Full name
α	anti
Å	angstrom
aa	amino acid
ac	acetyl
acetyl-CoA	acetyl coenzyme A
Act5C	actin 5C
ACV	anterior cross-vein
APS	ammonium peroxydisulfate
ATP	adenosine triphosphate
bam	bag of marbles
BLAST	basic local alignment search tool
BSA	bovine serum albumin
C-	carboxy-
Cas9	CRISPR associated protein 9
cDNA	complementary DNA
ChIP	chromatin immunoprecipitation
ChIP-seq	ChIP-sequencing
CoIP	co-immunoprecipitation
CoREST	corepressor of REST
CRISPR	clustered regularly interspaced short palindromic repeats
Ct	cycle threshold
Da	daltons
DMSO	dimethyl sulfoxide
DNA	deoxyribonucleic acid
dNTP	nucleoside triphosphates containing deoxyribose as the sugar
dsDNA	double-stranded DNA
dsRNA	double-stranded RNA
DTT	(2S,3S)-1,4-Bis(sulfanyl)butane-2,3-diol (Dithiothreitol)
EDTA	2,2',2'',2'''-(Ethane-1,2-diyldinitrilo)tetraacetic acid (Ethylenediaminetetraacetic acid)
EGFP	enhanced GFP
EGTA	ethylene glycol-bis(2-aminoethylether)-N,N,N',N'-tetraacetic acid
ELM2	Egl-27 and MTA1 homology 2 domain
en	engrailed
ES	embryonic stem (cells)
FBS	fetal bovine serum
FPKM	fragments per kilobase of transcript per million mapped reads
FT	flow-through

Abbreviation	Full name
fw	forward
G9a	histone-lysine N-methyltransferase
GAL4	yeast transcription factor GAL4
gDNA	genomic DNA
GFP	green fluorescent protein
GLP	good laboratory practice
GO	gene ontology
H3K9	histone H3 lysine 9
HATs	histone acetyltransferases
HDACs	histone deacetylases
HeBS	HEPES buffered saline
HEPES	2-[4-(2-hydroxyethyl)piperazin-1-yl]ethanesulfonic acid
HKMTs	histone lysine methyltransferases
HMTs	histone methyltransferases
HPLC	high performance liquid chromatography
HR	homology recombination
HRP	horseradish peroxidase
IF	immunofluorescence
IgG	immunoglobulin G
IP	immunoprecipitation
ivT	*in vitro* transcription
kb	kilobases
kDa	kilodaltons
L(3)mbt	lethal (3) malignant brain tumor
LAD	lamina-associated domain
LB	Lysogeny Broth
LC-MS/MS	liquid chromatography–mass spectrometry
LDS	lithium dodecyl sulphate
Lig4	DNA ligase 4
LINT	dL(3)mbt interacting protein complex
Lint-1	L(3)mbt interacting protein 1
log2FC	log2 fold change
LSD1	lysine specific demethylase 1 (KDM1)
MBT	malignant brain tumour
MBTS	malignant brain tumour signature
me	methyl
Mi-2	Mitchell-2, nuclear ATP-dependent nucleosome remodeller of the CHD family
MMEJ	microhomology-mediated end joining
mRNA	messinger RNA
Mus308	DNA polymerase theta
N-	ammino-
NHEJ	non-homologous end joining
NP-40	nonidet P-40

Abbreviation	Full name
NTP	nucleoside triphosphate
PBS	phosphate buffered saline
PCR	polymerase chain reaction
PCV	posterior cross-vein
PHD	plant homeodomain
PMSF	phenyl-methane-sulfonyl-fluoride
ppm	particles per milion
PRC1	polycomb repressive complex 1
PRC2	polycomb repressive complex 2
PRMTs	protein arginine methyltransferases
PTMs	post-translational modifications
PVDF	poly(1,1-difluoroethylene)
qPCR	quantitative polymerase chain reaction
RNA	ribonucleic acid
RNA-seq	RNA sequencing
RNAi	RNA interference
rNTP	nucleoside triphosphates containing ribose as the sugar
RPD3	reduced potassium dependency 3, *Drosophila* HDAC1
rpm	revolutions per minute
RT	room temperature
rv	reverse
SANT	Swi3, Ada2, N-Cor, and TFIIIB domain
SDS	sodium dodecyl sulphate
SDS-PAGE	sodium dodecyl sulphate polyacrylamide gel electrophoresis
SET	Su(var)3-9, Enhancer-of-zeste and Trithorax
sgRNA	single guide RNA
shRNA	small hairpin RNA
SLC	SFMB1, LSD1 and CoREST containing complex
SWH	Salvador-Warts-Hippo
SWI/SNF	SWItch/Sucrose Non-Fermentable complex
TAD	topologically associating domain
TAE	Tris-acetate/EDTA buffer
TBST	Tris buffered saline with tween
TE	Tris/EDTA buffer
TEMED	N,N,N′,N′-tetramethylethane-1,2-diamine
Tris	2-amino-2-(hydroxymethyl)propane-1,3-diol
UAS	upstream activation sequence
ub	ubiquitination
v/v	volume per volume
VDRC	Vienna *Drosophila* Resource Center
w/v	weight per volume
WB	western blot

List of Figures

List of Tables

1. Introduction

"The fundamental problem of chemical physiology and of embryology is to understand why tissue cells do not all express, all the time, all the potentialities inherent in their genome."

— François Jacob and Jaques Mond,
article in Journal of Molecular Biology, 1961

1.1. DNA — size issue

Abiogenesis started roughly 4.28 million years ago, separating physical entities that support biological processes from non-living matter (Dodd et al., 2017). Since then, a vast number of organisms evolved that have a life cycle, can grow and adapt to their environment, respond to stimuli and reproduce. There is no clear evidence when exactly living organisms started utilising deoxyribonucleic acid (DNA) as the primary "storage" of genetic information. However, to the present day, every living cell uses this molecule to carry the information necessary to maintain all biological processes during their life cycle.

DNA molecules are long polymers of nucleotides containing four different bases (adenine (A), thymine (T), cytosine (C) and guanine (G)) organised in the form of a double-stranded helix. These polymers are tightly packed in small viral or cellular compartments. In some viruses, DNA is packed in the capsid. In prokaryotes, DNA is concentrated in a nucleoid, or present in the form of an extra, several kilobases long, plasmid. In eukaryotes, DNA is packed in up to three cell compartments where it is separated from the cytosol by a phospholipid bilayer — the nucleus, mitochondrion and chloroplast, except for some yeast and fungi that also have plasmids in the cytosol. Each organism has DNA molecules that are generally much longer than the cells containing them. For example, a diploid human cell has an approximately 1.8 meters long DNA material that is packed in the nucleus of an average diameter of 10 μm. An extraordinary degree of organisation tightly sequesters DNA molecules in small compartments while still allowing cellular processes, such as transcription, replication

and DNA repair, to take place. In particular, DNA material in almost every eukaryotic cell is apportioned into chromosomes.

1.2. The organisation of DNA in the nucleus

In the nucleus of a eukaryotic cell, negatively charged double-stranded DNA molecules are bound by proteins, and the DNA is concentrated in a compartment that occupies about 10% of the total cell volume. This DNA in the nucleus is present in the form of chromatin and is separated into chromosomes. Chromatin structural organisation starts with nucleosomes and is further organised with the help of other scaffold proteins into higher-order structures. During cell division, the highest order of chromatin organisation is the alignment of chromosomes on the metaphase plate.

1.2.1. Nucleosomes — organisational units of chromatin

DNA in all eukaryotes is tightly associated with proteins called histones and in this form is referred to as nucleosomal DNA. Histones package and order the DNA into fundamental structural units called nucleosomes. The first high-resolution structure of a nucleosome was solved in the lab of Timothy J. Richmond and was published in 1997 (Luger et al., 1997). This revealed that DNA (147 base pairs) is wound 1.65 times around the octamer of four distinct histone proteins. The winding is in the form of a left-handed solenoidal supercoil. Each canonical nucleosome contains eight core histone molecules: two copies each of H2A, H2B, H3, and H4 (**Figure 1.1**).

Histones are highly basic globular proteins with molecular masses from 11,000 to 21,000 Daltons (Da). Histones that are present in the nucleosome core have a common structural motif known as the histone fold. It consists of three α helices connected by two loops. During nucleosome assembly, the histone fold of one histone binds to a corresponding histone fold of another histone. For example, the formation of H2A—H2B heterodimers is achieved by binding of an H2A to an H2B histone fold. In the same manner, histone H3 binds H4 forming the H3—H4 heterodimer. The structure of the two histone folds in a heterodimer is referred to as a "handshake motif" (Arents et al. 1991; McGinty and Tan, 2015). Further on during nucleosome assembly the two H3

—H4 heterodimers associate forming H3—H4 tetramers. These tetramers then interact with two H2A—H2B heterodimers to form the histone octamer.
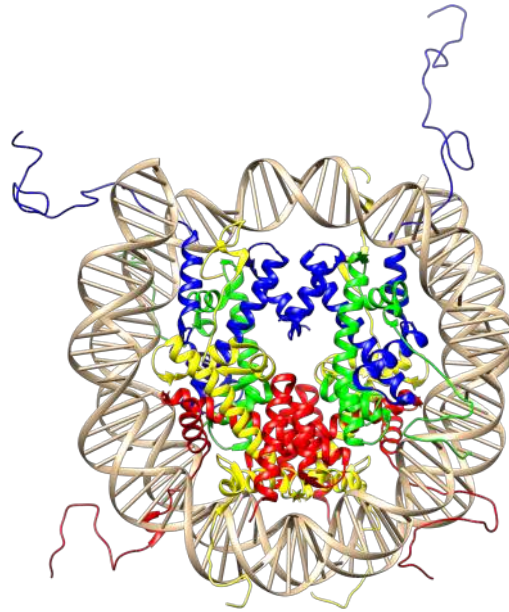
Figure 1.1. Structure of the nucleosome at 1.9 Å resolution.
147 bp DNA double helix is wound 1.65 times around the histone octamer core: H2A (yellow), H2B (red), H3 (blue) and H4 (green). The figure was generated with UCSF Chimera software using PDB accession code 1KX5 (Davey et al., 2002).

Core histone proteins are rich in arginine and lysine residues. These amino acids are positively charged at physiological pH and, hence, contribute to the overall net positive charge of the molecule. This favours negatively charged DNA to bind to and wind around the histone octamer core. This interaction is not sequence-specific. In more detail, the forces that contribute to the interaction between the histone octamer and DNA can be classified into several categories, including electrostatic interactions and intermolecular forces. For example, α-helixes in H2B, H3, and H4 form helix-dipoles causing a net positive charge to accumulate at the point of interaction with negatively charged phosphate groups on DNA; salt bridges between side chains of basic amino acids and phosphate oxygens on DNA; hydrogen bonds between the amide group on the main chain of histone proteins and the DNA backbone or non-polar interactions between the histone and deoxyribose sugars on DNA.

Histones are synthesised by ribosomes and translocated from the cytosol into the nucleus with the help of histone chaperones during S phase (Burgess and Zhang, 2013). Histone chaperone Nap1 facilitates the import of the H2A—H2B heterodimer. Several

histone chaperones, for example, HSP90, NASP, and Asf1, contribute to the import of H3—H4 tetramers. In addition, import of the H3—H4 tetramers is regulated by an array of histone modifications which predominantly involve histone acetylation. When DNA is replicated, H3—H4 tetramers are first deposited on the newly replicated DNA strand forming a tetrasome. DNA is wound once around the H3—H4 tetrasome before two H2A—H2B dimers are deposited. This deposition leads to the final DNA winding around the completed histone octamer core, and the nucleosome is formed (Dannehey and Tyler, 2014).

Neighbouring nucleosomes are separated by linker DNA of approximately 60 base pairs. The linker DNA is bound by the fifth histone protein — H1. As a consequence of this organisation, repeating nucleosome core particles occur on average every 200 bp throughout the genome (Kornberg, 1977). Histone H1 interacts with linker DNA at the entry and exit points of nucleosomal DNA, facilitating the formation of higher-order structures.

1.2.2. Histone variants

Most histones are synthesised during S phase to allow their rapid deposition behind replication forks. They fill in the gaps that are caused by the distribution and dilution of preexisting histones during the DNA replication process. During evolution histone-fold domain proteins have diversified from archaeal ancestors. They can be classified into the four histones, introduced above, that comprise the octamer of the eukaryotic nucleosome. These four canonical histone proteins have further diversified into variants, and this introduced new features to chromatin, giving rise to a variety of epigenetic consequences.

In eukaryotic species, histones have high sequence identity, and this classifies them among the most conserved proteins. The reason for high conservation during evolution lays in the functional importance of each amino acid in the histones. However, histone variants differ from core histones in sequence alteration that is causing their specific function and genomic localisation. In a process called histone exchange, the non-canonical histone variants are incorporated into chromatin in a DNA replication-independent manner. Incorporation of different histone variants in the core octamer can

have distinct effects on nucleosome structure and stability. Moreover, the binding of different proteins to the nucleosome is dependent on the histone variants in the nucleosome (Talbert and Henikoff, 2010 and 2017). Since a detailed discussion of histone variants is beyond the aim of this dissertation, in the following text, only a few examples will be described in order to depict the incredible diversity of chromatin molecular structure (**Figure 1.2**).
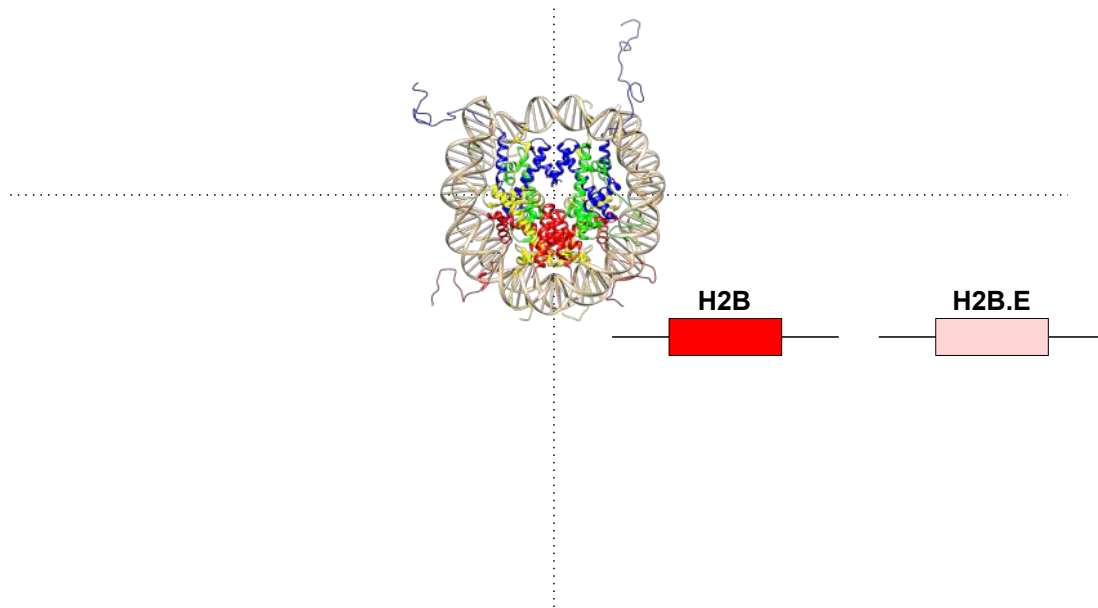
Figure 1.2. Mammalian core histone variants.
Selected variants of mammalian histone H2A (yellow), H2B (red) and H3 (blue) depicted in pale yellow, pale red and pale blue, respectively. Core regions are represented with rectangles, while lines represent flexible histone tails. Approximate percentages indicate total amino acid sequence conservation (% sequence identity) of the variants relative to their canonical counterparts. Additionally, for histone H2A, the variant-characteristic sequence in the flexible histone tails is represented by the red line (modified from Buschbeck and Hake, 2017).

At present, it is known that histone H2A has at least four different variants: H2A.Z, H2A.X, H2A.B, and macroH2A with specific functions. H2A.Z leads to the formation of less stable nucleosomes (Suto et al., 2000; Venkatesh and Workman, 2015). H2A.X has a unique C-terminal tail distinguishes this variant from H2A (Thatcher and Gorovsky, 1994). It is best known for its role in the DNA damage response (DDR). H2A.B, often described in the literature as H2A.Bbd (Bar-body deficient), is correlated with transcriptionally active regions (Bao et al., 2004; Gautier et al., 2004). MacroH2A is involved in the transcriptional repression processes that lead to X inactivation (Costanzi and Pehrson, 1998).

Currently, there are several histone H2B variants identified in mammals (Molden et al., 2015). There are highly specific for certain developmental stages. For example, histone variant H2B.E is involved in controlling olfactory gene expression in mice (Santoro and Dulac, 2012). However, their particular function remains mostly unknown.

Histone H3 has several distinct variants, and two are well characterised: histone H3.3 and CENP-A. H3.3-containing nucleosomes are incorporated into chromatin at the promoters of transcriptionally active genes (Chow et al., 2005; Mito et al., 2005). During cell mitosis, H3.3 serine 31, that is not present in the sequence of canonical histone H3, is phosphorylated in centromeres and telomeres region (Hake et al. 2005; Wong et al. 2010). CENP-A, or CenH3.3, is found in centromeric nucleosomes and it has a distinct CENP-A centromere targeting domain (CATD) that contributes to the formation of more solid and compact nucleosomes (Black et al., 2004).

In contrast to H2A, H2B and H3, histone H4 has no known variants up to date. Amino acid sequence comparison between different organisms revealed only a few amino acid changes. This makes histone H4 the most highly conserved histone (Malik and Henikoff, 2003).

1.2.3. Histone modification

The core histones have unstructured N-terminal and C-terminal "tails" that are sticking out of the nucleosome (Luger et al., 1997). Particular amino acid side chains, most of them positioned in the histone "tails" are enzymatically modified, and these histone post-translational modifications are highly dynamic. In the literature, post-translational modifications are often depicted to result in certain chromatin states, such as H3K9 trimethylation as a hallmark of constitutive heterochromatin. However, an array of histone tail modifications work synergistically to give rise to the biological outcome.

At present, different post-translational modifications (PTMs) of histones have been shown to play a role in defining the chromatin state. These modifications include acetylation, methylation, and phosphorylation as the most common histone modifications (**Figure 1.3**). Histone PTMs, such as ubiquitylation, sumoylation, ADP ribosylation, deimination and proline isomerisation are less abundant (Kouzarides, 2007). Propionylation, butyrylation and glycosylation are histone PTMs whose role in

chromatin regulation is still debated in the field (Zhang et al., 2009; Sakabe et al., 2010).
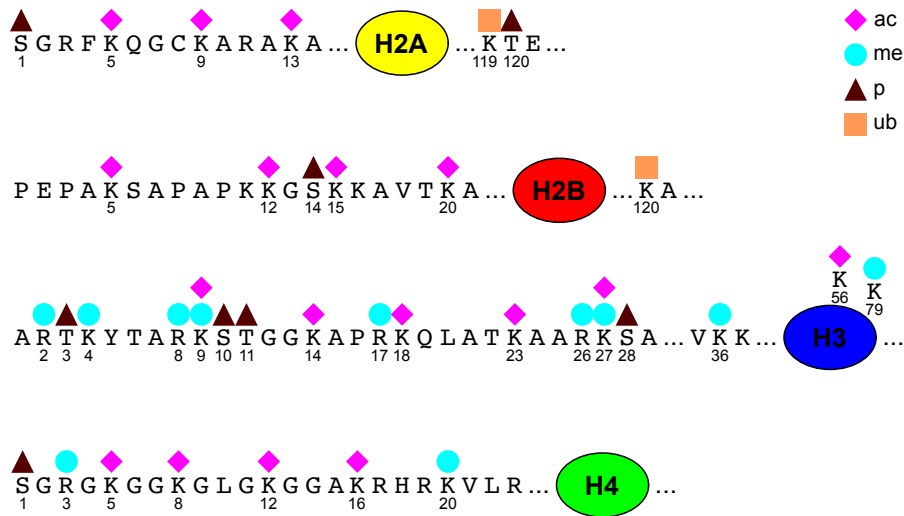
Figure 1.3. **Modifications of histone H2A, H2B, H3, and H4**
The most common PTMs of canonical histones: acetylation (ac), methylation (me), phosphorylation (p), and ubiquitylation (ub) (modified from Bhaumik et al., 2007).

Histone modifications are essential for many chromatin-associated cellular processes, such as DNA replication, DNA repair, chromosome condensation and gene regulation (Kouzarides, 2007). Moreover, histone modifications play a direct role in the regulation of alternative splicing (Luco et al., 2010). In general, it is conceivable that histone PTMs are regulating these processes via two underlying mechanisms. They contribute to the process of recruiting non-histone proteins which then regulate corresponding chromatin-associated activities. They also impact the higher-order chromatin structure by influencing inter- or intranucleosomal DNA-histone contacts (Kouzarides, 2007).

Impact of histone PTMs on higher-order chromatin structure is well documented for histone acetylation. Acetylation occurs on several lysine residues within all four core histones. The covalent attachment of an acetyl group to lysine residues of histones changes the positive charge of the ε-amino group towards the dipole. *In vitro* studies have shown that this neutralisation has a consequence by preventing the formation of higher-order chromatin compaction by affecting nucleosome—nucleosome interaction and thereby can promote transcription (Annunziato et al., 1988; Tse et al., 1998). Acetylation of histones correlates with gene activation, and deacetylated chromatin correlates with transcriptional repression (Reid et al., 2000; Shahbazian and Grunstein,

2007). Concerning the particular histone acetylation, acetylation of lysine 16 in histone H4 (H4K16) alone can cause defects in chromatin compaction (Shogren-Knaak et al., 2006; Shogren-Knaak and Peterson, 2006). In more detail, H4K16 acetylation can destabilise the interaction between the H4 tail and an "acidic patch" on the neighbouring nucleosome, affecting higher-order chromatin folding (Kalashnikova et al., 2013). During nucleosome assembly, newly synthesised histones are transiently acetylated on H4K5 and H4K12 in all eukaryotes. Acetylation of newly synthesised H3 is more species-specific. For example, H3K9 and H3K14 are acetylated in *Tetrahymena*, and H3K14 and H3K23 are acetylated in *Drosophila*. These acetylations patterns are potentially involved in the recognition of new histones by histone chaperones (Sobel et al., 1995; Shahbazian and Grunstein, 2007).

In contrast to acetylation, which is correlated with actively transcribed genes, histone methylation is associated with both, active and repressive chromatin, depending on the chromatin context and the residue it occurs on (Li et al., 2007a; Kouzarides, 2007). Two basic amino acids of histones, lysine and arginine, can be methylated. The existence of several methylation states further diversifies this modification. Lysine residues can be mono- (me1), di- (me2) or trimethylated (me3) (Murray, 1964; Black et al., 2012). Arginine methylation can also be distinguished in three states: monomethylated (me1), symmetrically dimethylated (me2s), or asymmetrically dimethylated (me2a) (Di Lorenzo and Bedford, 2010).

The complexity of histone methylation will be illustrated in this text with a few selected examples. Four histone H3 lysines are methylated in the N-terminus: H3K4, H3K9, H3K27, and H3K36; while the fifth lysine, H3K79, is located in the globular domain. H3K4me3, together with H3K36 methylation, has been associated with actively transcribed chromatin. In more detail, it has been demonstrated that trimethylation of H3K4 correlates with transcriptional start sites of active genes (Barski et al., 2007). On the other hand, trimethylation of H3K9 promotes the binding HP1 (heterochromatin protein 1) and leads to the formation of compacted chromatin that is inaccessible to the transcription machinery. H3K27me3 is catalysed by histone methyltransferase subunit of PRC2 (Polycomb repressive complex 2) and represents another example of repressive histone methylation (Lee et al., 2018). At present, only lysine 20 is known to

be methylated in histone H4. Together with the methylation of H3K9 and H3K27, H4K20 has been correlated with chromatin silencing (Pokholok et al., 2005). Methylation of arginines has also been demonstrated to have a role in transcriptional regulation (Blanc and Richard, 2017).

Histone phosphorylation, another well studied PTMs, occurs on serine, threonine, and tyrosine residues and is correlated with the processes of chromosome condensation during mitosis and meiosis (Wei et al., 1998; Nowak and Corces, 2004; Fischle et al., 2005; Banerjee and Chakravarti, 2011; Rossetto et al., 2012). Another example of the role of histone phosphorylation is in DNA damage repair where histone variant H2A.X is phosphorylated upon DNA damage (Rogakou et al. 1998).

The role of histone ubiquitination (ub) is best described for histone H2A and H2B where it is correlated with gene silencing (H2Aub) or with transcriptional activation (H2Bub) (Goldknopf et al. 1975; West and Bonner, 1980). Moreover, it has been shown that H2A, H2A.X, and H2B are ubiquitinated at DNA damage sites (Cao and Yan, 2012; Uckelmann and Sixma, 2017).

1.2.4. Higher-order chromatin structures

Higher-order chromatin structure is defined as the organisation of nucleosomes in a specific 3D conformation. The most well-known example of a higher-order structure are the mitotic or meiotic chromosomes that line up on the metaphase plate.

Nucleosomes form a nucleosomal array. The DNA spacing between nucleosomes varies depending on species, developmental stage or cell type. Even active and repressed regions in the same nuclei have different DNA spacing between nucleosomes. Different factors regulate the structure of chromatin, such as histone variants, histone modifications, DNA methylation and the binding of non-histone architectural proteins (van Holde and Zlatanova, 2007; Li and Reinberg, 2011). Nucleosomal arrays can under non-physiological conditions form a 10-nm fibre. This structure is known as "beads-on-a-string" and is considered as the first level of chromatin organisation (Thoma et al., 1979; Luger et al., 1997).

Formation of higher-order chromatin structures involves the compaction of nucleosome arrays (**Figure 1.4**). This is achieved by the inter-nucleosome interactions mediated by

the core histone tail domains and their modifications and mediated by linker histones (Fletcher and Hansen, 1995; Schwarz et al., 1996; Dorigo et al., 2003). The nucleosomal arrays are organised into a more condensed 30-nm chromatin fibre. The formation of 30-nm fibre also involves the binding of the linker histone H1 or H5 to the nucleosomes and linker DNA, and this is considered as the second structural level of DNA organisation (Robinson and Rhodes, 2006). Data from several studies of native chromatin fibres, mainly done by employing electron microscopy, have resulted in two plausible models describing the formation of the 30-nm fibre. The first model, the one-start helix/solenoid model, explains the formation of 30-nm fibre by the process in which linker DNA is bent between adjacent nucleosomes. Bending leads to positioning of the nucleosomes in the way to follow the superhelical path, with about 6 to 8 nucleosomes per turn (Widom and Klug, 1985). The second model, the two-start helix model, is based on the Zig-Zag arrangement of nucleosomes observed in the case of chromatin in low ionic strength buffers, in which straight linker DNA connects adjacent nucleosomes (Williams et al., 1986; Woodcock and Ghosh, 2010). However, both models are based on *in vitro* studies, and it is still debatable whether 30-nm fibre exists *in vivo* (Quénet et al., 2012; Ricci et al., 2015).

While the inter-nucleosome interactions within a nucleosomal array are essential for the compaction of model nucleosome arrays into a 30-nm fibre, the long-range inter-array interactions are required for the formation of tertiary chromatin structures (Zheng et al., 2005; Kan et al., 2007; Eltsov et al., 2008). Furthermore, quaternary chromatin structures are formed by interactions between tertiary structures and involve the compaction of the chromatin over domains of hundreds of kilobases (Horn and Peterson, 2002).

In murine embryonic stem (ES) cells, for example, mediator and cohesin cooperatively facilitate the formation of chromatin loops. These loops are formed between the enhancer regions and core promoter regions of active genes, and they are described in the literature as chromatin contact domains or topologically associating domains (TADs) (Kagey et al., 2010). TADs further aggregate into active and inactive compartments and chromosome territories. Chromatin looping should not be considered as a rigid conformation, but as a dynamic compartment that is regulated by various

factors, such as mediator protein MED1, histone deacetylation (HDAC4) and histone demethylation (LSD1) (Saramäki et al., 2009).
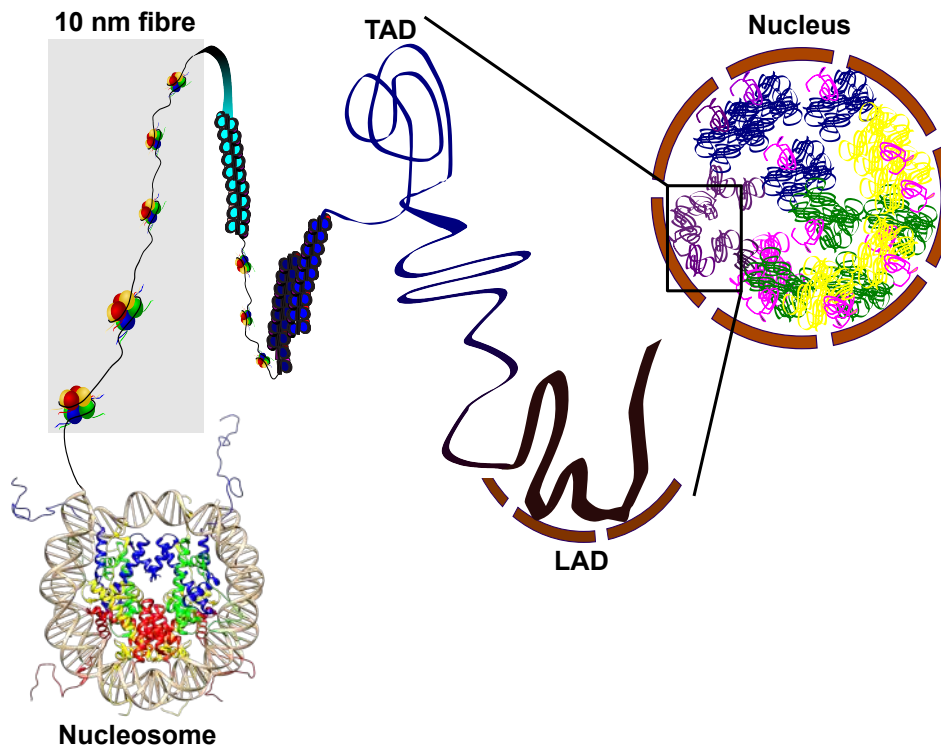
Figure 1.4. Chromatin organisation in the cell nucleus.
Chromatin organisation in the cell nucleus starts with a nucleosome and finishes with chromosomal territories. Structure detected only under non-physiological conditions is in grey rectangle.
TAD - topologically associating domain; LAD - lamina-associated domain.

Recent studies have identified large genomic domains with distinct epigenetic signatures that are associated with the nuclear lamina in fly and mammalian cells (Pickersgill et al., 2006; Guelen et al., 2009). These studies have shown that these lamina-associated domains (LADs) have low gene-density and associate with specific epigenetic signatures. Moreover, the majority of the genes identified within LADs have very low expression levels (Guelen et al., 2009).

Although the terms heterochromatin and euchromatin are not considered as categories of chromatin higher-order structure *per se*, they refer to states of compaction and transcriptional potential. These terms are used quite often in the literature to describe the chromatin state in the nucleus that can be clearly distinguished in light and electron micrographs. Years before the discovery of DNA, heterochromatin has been initially well defined as regions of nuclei that stained strongly with basic dyes (Heitz, 1928). In general, heterochromatin is located at the nuclear periphery and surrounding the

nucleolus. Almost one century after their discovery, eu- and heterochromatin still give a useful qualitative indication of chromatin compaction states.

1.3. Chromatin-regulating proteins

For cellular processes, such as transcription, DNA replication, and DNA repair controlling the chromatin structure is crucial. Packing of DNA into chromatin allows DNA molecule to fit into the nucleus of a cell, but, at the same time, it limits access of binding factors to DNA. Chromatin states need to be highly dynamic and tightly regulated in order to allow molecular machinery to access DNA. This regulation is achieved on different levels. For example, it involves DNA modifications, such as methylation, regulation mediated through RNA interference (RNAi) or long non-coding RNAs, a wide variety of histone variants, covalent modification of histones by histone-modifying enzymes and structural changes introduced by chromatin remodelling enzymes. In general, the molecular machinery that regulates chromatin, so-called chromatin-regulating proteins, can be arbitrarily divided into three classes. The first class consists of enzymes that modify histones and histone readers that are involved in recruiting the other proteins by sensing histone post-translational modification signature. The second class are the enzymes that remodel DNA-histone structure with energy derived from ATP hydrolysis (Zhang et al., 2016). The third class are the enzymes that affect the chromatin via DNA methylation (Lyko et al., 2010). Since chromatin remodellers and DNA methylation are beyond the aim of this dissertation, the main focus will be on the first class of chromatin-regulating proteins.

Histone modifications are dependent on enzymes catalysing the covalent attachment of PTMs, referred to as histone code writers, or the enzymatic removal of PTMs, so-called histone code erasers. The third subclass of proteins, histone code readers or effector proteins, specifically recognise histone modifications introduced by the first two subclasses. They associate with chromatin via specific binding modules recognising a particular modification or set of modifications (**Figure 1.5**).
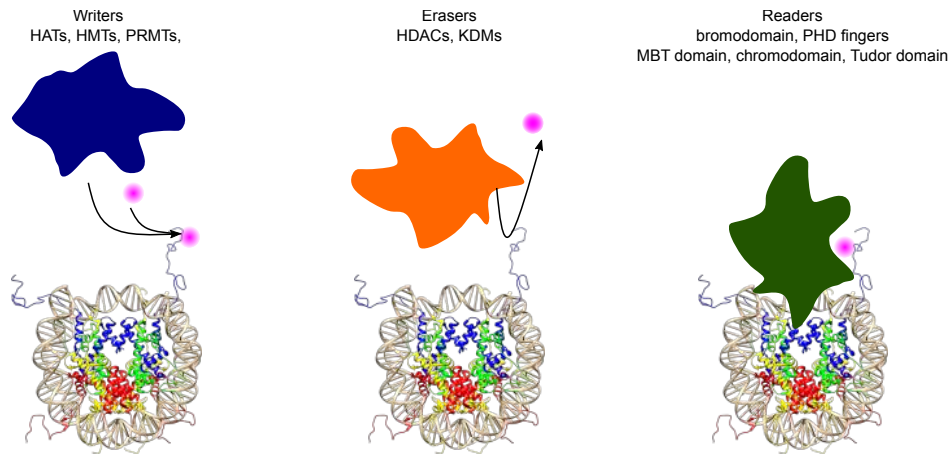
Figure 1.5. Generation, removal and binding of histone modifications by chromatin-regulating proteins. Writers covalently attach PTMs (magenta circle) to histones (left panel), while erasers remove them (middle panel), and readers (also termed effectors) bind to specific modifications (right panel). Named are the classes of enzymes writing or erasing histone marks, or, in case of histone readers, the common domains that recognise histone marks (explained in Sections 1.3.1 and 1.3.2).

In general, chromatin-regulating proteins often come in the form of multisubunit protein complexes. They are classified into families of related complexes based on a common core of dedicated subunits (Meier and Brehm, 2014). These core subunits can associate with diverse complex-specific signature subunits to yield alternative complexes with new functionality. In order to understand the complexity of chromatin regulation, it is useful to understand the role of each subunit in the complex.

1.3.1 Histone writers and erasers

Histone modifications are highly dynamic. The catalytic activity of "writers" introduces a specific mark. The marks are removed by the "erasers," which catalyse selective removal. "Writing" function is performed by enzymes from the group of histone acetyltransferases (HATs), histone methyltransferases (HMTs), protein arginine methyltransferases (PRMTs). Histone deacetylases (HDACs) and lysine demethylases (KDMs) are the representatives of the group of enzymes that "erase" these marks (Shahbazian and Grunstein, 2007; Alam et al., 2015).

Acetylation of histones is a highly transient mark crucial for precise temporal transcriptional control (Zheng et al., 2013). Histone acetyltransferases (HATs) catalyse the transfer of an acetyl group from acetyl-CoA to the ε-amino group of a histone lysine residue. For example, together with histone deacetylases (HDACs), HATs rapidly turn over acetylation on K4 trimethylated histone H3 tails (Crump et al., 2011). Interestingly,

HATs are often not specific to individual lysines. For example, the catalytic subunit of SAGA complex and elongator complex acetylates both H3K9 and H3K14. However, SAGA complex acetylates histones at promoters, while elongator complex acetylates histones in coding regions (Wittschieben et al., 1999). This is achieved via the non-catalytic domains of HAT complexes since these subunits are directing the complex to the proper genomic location (Yun et al., 2011).

Histone deacetylases (HDACs) are a class of enzymes that catalyse the removal of acetyl moiety from lysines of histones. This allows the DNA to wind the histones more tightly, and, hence, has a consequence in transcriptional repression (Grunstein, 1997). Similar to HATs, HDACs specificity is regulated via partner proteins within multi-protein complexes. So far, 11 subclasses of HDACs are described in the literature. The most studied representatives are HDAC1 and HDAC2, from subclass I, that are found together in repressive complexes such as the CoREST, PRC2, Sin3, and NuRD complexes (Yang and Seto, 2008).

A variety of histone methyltransferases and demethylases that catalyse the addition or removal of methylation marks have been discovered so far (Greer and Shi, 2012). Histone methyltransferases are classified into three distinct groups (Bannister and Kouzarides, 2011). The first group are histone lysine methyltransferases (HKMTs) that belong to a class of proteins with a SET domain. SET domain, named after the *Drosophila* proteins Su(var)3-9, E(z) and Trx, is an enzymatic domain that catalyses the transfer of a methyl group from *S*-adenosyl-L-methionine to the amino group of a lysine residue on the histone or other protein (Upadhyay and Cheng, 2011). The second group DOT1-like proteins, also methylate lysine residues. However, this group is structurally not related to SET-domain proteins (Feng et al., 2002). The third group, protein arginine methyltransferases (PRMTs), are the enzymes that are responsible for methylation of arginines. They catalyse the transfer of a methyl group from *S*-adenosylmethionine (SAM) to the guanidino nitrogen of arginines (Di Lorenzo and Bedford, 2010).

Histone demethylases catalyse the removal of the methyl groups introduced by histone methyltransferases. In general, these enzymes are divided into two major groups. The first group are amino oxidases, such as LSD1 (Lysine-specific histone demethylase 1A), that remove the mark via a flavin-dependent amine oxidation reaction (Shi et al., 2004;

Karytinos et al., 2009). LSD1 demethylates mono- and di-methylated lysines H3K4 and H3K9, an active mark, and functions as a transcriptional repressor (Shi et al. 2004, Rudolph et al., 2013). The second group of histone demethylases are dioxygenases that remove the mark via Fe^{2+} and α-ketoglutarate-dependent reaction. These are Jumonji C (JmjC) domain-containing proteins, such as JHDM1 that demethylates H3K36 (Tsukada et al. 2006).

Histone arginine demethylases remove methyl mark from arginines, introduced by PRMTs. PAD4, JMJD6, and JMJD1B are, to date, three histone arginine demethylases identified (Cuthbert et al., 2004; Chang et al., 2007; Li et al., 2018). However, the mechanism of arginine demethylation is still somewhat elusive (Mantri et al., 2010; Zhang et al., 2019)

Histone methylation has a broad role in transcription control, from organising chromatin architecture to the regulation of specific genomic loci (Greer and Shi, 2012). Mainly focusing on the *Drosophila* system, the histone lysine methylation mark — H3K9 was chosen to be illustrated in more details due to its relevance for this study.

1.3.1.1 H3K9 methylation

Post-translational modifications of histone H3 lysine 9 (H3K9) have a dual role in epigenetic control of transcription. When acetylated, H3K9ac is correlated with active promoters. This modification has a high co-occurrence with the hallmarks of active gene promoters, such as H3K4me3, H3K14ac, and H3K23ac. On the other hand, methylation of H3K9 is assigned to gene silencing (Karmodiya et al., 2012).

Methylation of H3K9 is one of the best studied histone modifications marks. It can come in the form of mono, di, and tri H3K9 methylation, and each has very distinct distribution patterns over the genome. For example, H3K9me1 is enriched at the transcriptional start site of active genes, while H3K9me2/3 mark is found often at silenced genes (Barski et al., 2007). However, these correlations are not very strong, and the promoters of many highly transcribed genes show, indeed, H3K9me2/3 enrichment. However, overall H3K9 methylation is still considered as the hallmark of heterochromatin, the transcriptionally inactive state of chromatin.

The role of H3K9 methylation in heterochromatin formation was mainly determined by the mutation studies of enzymes that methylate H3K9. Notably, this approach has certain limitations. For example, cells contain multiple H3K9 methyltransferases that are partially redundant (Elgin and Reuter, 2013). Moreover, these enzymes often have numerous non-histone substrates; hence, the analysis of the biological contribution of a given PTM can be complex (Huang and Berger, 2008; Sims and Reinberg, 2008; Biggar and Li, 2014; Zhang et al., 2015).

In *Drosophila*, there are three methyltransferases depositing H3K9 methylation marks: Su(var)3-9, dG9a, and SetDB1/Eggless. In general, they function in different regions of the genome. However, these enzymes are partially redundant and show complex genetic interactions. For example, Su(var)3-9 and dG9a single mutants are viable and fertile. On the other hand, double mutants have reduced viability (Schotta et al., 2003; Mis et al., 2006). In contrast to Su(var)3-9, which is predominantly located at the centromeric regions of polytene chromosomes, dG9a is considered to act as a euchromatic histone H3K9-methyltransferase on loosely packed DNA (Stabell et al., 2006).

Although mono- and dimethyl H3K4 are demethylated by recombinant Su(var)3-3 (also known as dLSD1) directly, the enzyme is not active on mono- or dimethylated H3K9. Nevertheless, the demethylation of H3K4 by Su(var)3-3 is necessary for the subsequent methylation of H3K9 by Su(var)3-9 (Rudolph et al., 2007).

1.3.2 Histone readers

The class of proteins that recognise the histone PTM signature, introduced by histone code "writes/erasers," is referred to as the histone code "readers." These proteins regulate chromatin state via a complex mechanism that involves recruiting other proteins (Strahl and Allis, 2000; Yun et al., 2011). Depending on the histone marks that they recognise, histone code "readers" can be further sorted into groups. For example, proteins that recognise histone acetylation marks often have a characteristic bromodomain or tandem PHD (plant homeodomain) domain (also known as PHD fingers). However, some PHD fingers also bind to histone methylation marks. In general, histone methylation marks are recognised by the proteins that contain methyl binding domains, such as WD40 repeats (40 amino acid repeat terminating with

tryptophan-aspartic acid dipeptide), CW (cysteine and tryptophan) domains, and the already mentioned PHD fingers. Moreover, the "Royal family" of histone code "readers," which includes proteins with MBT (malignant brain tumour) domains, chromodomains, chromobarrels, and Tudor domains, is also responsible for recognition of histone methylation marks (Kouzarides, 2007). Due to its relevance for this study, the "Royal family" of histone binding domains, with a focus on MBT domains, will be described in more detail.

The histone methylation mark can be recognised by various binding modules of so-called "Royal family" histone code "readers." Common for all the family members is that they share a three β-stranded core region involved in recognition of the methyl mark (Maurer-Stroh et al., 2003). In general, different domains of the "Royal family" act via a common mechanism that involves the formation of hydrophobic cavities or cages for the specific recognition of differentially methylated lysine residues (Taverna et al., 2007). This feature allows the "reading" of both higher (Kme2, Kme3) and lower (Kme1, Kme2) lysine methylation states. In more detail, chromodomains are considered to be the modules that bind higher methylation states of lysines. For example, the chromodomain of Polycomb (Pc) specifically binds to H3K27me3, and the chromodomain of HP1 binds preferentially to H3K9me2 and H3K9me3 (Fischle et al., 2003). In contrast to chromodomains, the binding of Tudor domains can be correlated to both higher and lower methylation states. For example, the tandem Tudor domain of human JMJD2A binds to H3K4me3, while the tandem Tudor domain of 53BP1 recognises H4K20me1 and H4K20me2 (Huang et al., 2006; Botuyan et al., 2006). MBT domains, on the other hand, have a binding preference towards the low methylation states (Li et al., 2007b; Min et al., 2007).

The MBT domain was initially discovered in the *D. melanogaster* tumour suppressor gene *lethal (3) malignant brain tumour* (*l(3)mbt*) (Wismar et al., 1995). This novel motif of approximately 100 aa belongs to a class of methyl-lysine binding modules (Kim et al., 2006). Many structural and mechanistic studies have been performed to understand the binding properties of MBT domains using the human ortholog L3MBTL1 (Wang et al., 2003; Li et al., 2007b; Min et al., 2007; Kalakonda et al., 2008; Bonasio et al., 2010). The results from these studies showed a preferential binding of

MBT domains to mono- and dimethylated lysines within histone tails (Li et al., 2007b). *In vitro* studies of the three MBT domains of human L3MBTL1 demonstrated their ability to compact oligo-nucleosomal arrays in an H4K20me1/2- and H1bK26me1/2-dependent manner (Trojer et al., 2007). The precise mechanism of how this is achieved and the physiological relevance of this activity *in vivo* remains to be determined.

1.4. CoREST — Co-repressor of REST

CoREST was identified by Gail Mandel's lab (Andrés et al., 1999). REST, RE1 silencing transcription factor, is responsible for silencing the brain type II voltage-dependent sodium channel in non-neuronal cells. REST also contains zinc finger motifs that often mediate protein-protein interactions. This prompted a search for other nuclear factors that could interact with REST to regulate its functions, which resulted in the discovery of CoREST, a co-repressor of REST. CoREST mediates the repression of pro-neuronal genes and is an important factor in the establishment of non-neural cell specificity.

CoREST and its role in neurogenesis is conserved in a variety of vertebrate and invertebrate species, showing its functionally conserved role in neurogenesis (Tontsch et al., 2001; de la Calle-Mustienes et al., 2002; Jarriault and Greenwald, 2002; Dallman et al., 2004). CoREST regulates the expression of many genes, including genes encoding members of key neural developmental signalling pathways. CoREST regulates these genes in both REST-dependent and REST-independent manners. In many cell types CoREST is predominantly a repressor of transcription (Abrajano et al., 2009a; Abrajano et al., 2009b; Abrajano et al., 2010; Qureshi et al., 2010).

In non-neural tissue of vertebrates, REST is a central player in blocking the neuronal phenotype. On the other hand, despite the conservation of CoREST, no obvious REST orthologues exist in invertebrates. Using a yeast two-hybrid screen for CoREST interactors to identify functional analogues of REST in *Drosophila*, the repressor Tramtrack88 (Ttk88) was discovered (Dallman et al., 2004). On the sequence level, Ttk88 has no noticeable homology to REST. However, it interacts with *Drosophila* CoREST and regulates a set of genes encoding the same neuronal hallmarks that are

regulated by REST in vertebrates. Moreover, this study suggested that *Drosophila* uses Ttk88, that is functionally similar to REST, although it has evolved independently, for regulating neuronal phenotype.

In mammals, CoREST is an integral component of multi-subunit complexes which modify nucleosomes by histone deacetylation and demethylation to repress transcription. In these complexes, CoREST acts as a scaffold for recruitment of epigenetic factors, as well as transcriptional regulators (Humphrey et al., 2001; You et al., 2001; Hakimi et al., 2002; Lee et al., 2005; Shi et al., 2005; Lakowski et al., 2006; Qureshi et al., 2010). The precise composition of CoREST complexes in mammals differs and depends on cell type and purification conditions. Beside CoREST, several subunits have been identified in independent studies, such as LSD1, histone deacetylases HDAC1 and HDAC2, CtBP1, ZNF217, BHC80 and BRAF35 (Lee et al., 2005; Shi et al., 2005). Moreover, CoREST and LSD1 are found to be part of distinct molecular assemblies. For example, they form the SFMBT1-LSD1-CoREST (SLC) complex together with SFMBT1, which represses histone genes in a cell-cycle-dependent manner (Zhang et al., 2013). Together with SIRT1, both CoREST and LSD1 also coexist in a complex that represses Notch target genes (Mulligan et al., 2011). These findings suggest that CoREST and LSD1 form a core of the LSD1/CoREST complexes that can associate with different accessory subunits. Notably, it has not been demonstrated so far that CoREST and LSD1 can also exist in separate complexes in mammals.

LSD1, like CoREST, is conserved in *Drosophila*. Two-hybrid interaction studies showed that *Drosophila* CoREST (dCoREST) interacts with Su(var)3-3, the *Drosophila* LSD1 homologue, and dRPD3, the *Drosophila* HDAC1 homologue (Dallman et al., 2004). Moreover, genetic studies implied that dCoREST and Su(var)3-3 (referred to as dLSD1 in the following) cooperate in differentiation. They have a role in the regulation of signalling pathways, such as Notch and DPP/TGFβ, during the development of wing structures and the mitotic-to-endocycle switch of follicle cells during oogenesis (Mulligan et al., 2011; Domanitskaya and Schupbach, 2012; Curtis et al., 2013; Lee and Spradling, 2014). Co-immunoprecipitation studies demonstrated that dCoREST and dLSD1 interact when overexpressed in S2 cells, and both proteins are associated in

lysates prepared from fly ovaries (Dallman et al., 2004; Lee and Spradling, 2014). Taken together, these results suggest that, similar to their mammalian counterparts, *Drosophila* LSD1/CoREST complexes exist. However, subunits of mammalian LSD1/CoREST complexes, such as ZNF217, BHC80 and BRAF35, do not have apparent homologues in *Drosophila*. This absence of clear homologues raises questions about the existence and subunit composition of putative dLSD1/dCoREST complexes in flies. Moreover, the *dCoREST* gene expresses two major isoforms by alternative splicing: dCoREST-L and dCoREST-M. Both isoforms contain an ELM2 (Egl-27 and MTA1 homology 2) domain and two SANT (Swi3, Ada2, N-Cor, and TFIIIB) domains. A 234 amino acid unique insertion in the linker that is separating the two SANT domains characterises dCoREST-L, and this insertion is absent in dCoREST-M. It is unknown if these two isoforms reside in different complexes and/or are fully redundant.

So far, the L(3)mbt-interacting (LINT) complex is the only *Drosophila* CoREST-containing complex biochemically characterised. Beside dCoREST, the other subunits identified in the LINT complex are dL(3)mbt, the dL(3)mbt-interacting protein 1 (dLint-1), and histone deacetylase dRPD3 (Meier et al., 2012). Previously it was shown in two independent studies that the role of the LINT complex is to prevent the expression of lineage-inappropriate genes in Kc cells, as well as in the ovaries (Meier et al., 2012; Coux et al., 2018). However, dLSD1 is not a stoichiometric subunit of LINT and is not required to repress LINT target genes (Meier et al., 2012).

Taken together, these published results indicate the existence of multiple CoREST containing complexes in *Drosophila*. However, a systematic identification and characterisation of potential CoREST complexes has so far been lacking.

1.5 Objectives

Since its initial discovery in 1999, several hundreds of studies involving CoREST were published. The general belief is that CoREST is associated with histone methylases and deacetylases and that it plays roles in transcriptional regulation and development. However, there are still many open questions about the composition, diversity and functionality of CoREST complexes. A lot is known about mammalian CoREST

complexes, but less so about the composition, diversity and functionality for such epigenetic regulators in *Drosophila*.

The primary goal of this study was to address these questions by the systematic identification and isolation of putative dCoREST-containing complexes in the fly model system. First, by applying the gel filtration chromatography, affinity purifications, and proteomic interactome analysis, this study aimed to define different CoREST assemblies of the two major dCoREST isoforms. Although the LINT complex is the only *Drosophila* dCoREST-containing complex biochemical characterised, the existence of additional dCoREST complexes has not been systematically analysed yet (Meier et al., 2012).

This study also aimed to ascribe specific functions to potential dCoREST complexes by integrating functional genomics methods, such as chromatin immunoprecipitation (ChIP) analysis and combined RNA interference (RNAi) and transcriptome analysis, with proteomics findings. Moreover, investigating different cell-type-specific systems, this study additionally aimed to illustrate the function of potential dCoREST complexes in the regulation of lineage-specific transcription programs.

2. Material and methods

"The principles of Good Laboratory Practice (GLP) define a set of rules and criteria for a quality system concerned with the organisational process and the conditions under which non-clinical health and environmental safety studies are planned, performed, monitored, recorded, reported and archived."

Organisation for Economic Co-operation and Development

2.1. Material

2.1.1. Material sources

Common chemicals, reagents, consumables, and equipment that were used in this studies were purchased from the following companies:

Agilent Technologies Inc., Amersham Biosciences, AppliChem GmbH, B. Braun Melsungen AG, Beckman Coulter Inc., bioline meridian BIOSCIENCE, Biometra, Bio-Rad Laboratories Inc., Biozym Scientific GmbH, Boehringer Ingelheim, Calbiochem, Covance Inc., Carl Roth GmbH, Diagenode, Eppendorf AG, Fermentas, Gilson Inc., GE Healthcare, Greiner Bio-One GmbH, Heraeus, HMC Europe GmbH, invitrogen, Julabo Labortechnik GmbH, Otto E. Kobe AG, Kodak, Labnet International, Lauda Dr. R. Wobser GmbH & Co.KG, Leica Micro- systems GmbH, Life Technologies Corporation, Merck Chemicals, Millipore, MWG Biotech, PAA Laboratories GmbH, Novagen, PEQLAB Biotechnologie GmbH, Perbio Science, Pierce, Promega GmbH, Qiagen, Roche, Santa Cruz Biotechnology, Sarstedt AG & Co., Sartorius AG, Scientific Industries, Serva GmbH, Sigma-Aldrich, Sorenson BioScience, Thermo Fisher Scientific Inc., Upstate, VWR International, Whatman and Zeiss.

2.1.1.1. SDS-PAGE and Western blotting

Ammonium persulfate	AppliChem (A2941)
Immobilon™ Western Chemiluminescent HRP Substrate	Millipore (WBKLS0500)
NuPAGE® LDS Sample Buffer (4×)	invitrogen (NP0007)
PageRuler™ Prestained Protein Ladder	Thermo Scientific (26616)
Powdered milk	Carl Roth GmbH (T145.2)
Protein Assay Dye Reagent Concentrata	Bio-Rad (500-0006)
Rotiphorese Gel 30 (37.5:1)	Carl Roth GmbH (3029.1)
Roti®-PVDF, poresize 0.45 µm	Carl Roth GmbH (T830.1)
Spectra™ Multicolor High Range Protein Ladder	Thermo Scientific (26625)
^{Super}RX-N Fuji Medical X-ray film	Fujifilm (47410 19289)
TEMED (tetramethyl-ethylene-diamine)	Carl Roth GmbH (2367.3)
Tween® 20	Carl Roth GmbH (9127.1)
Whatman™ Gel Blot Paper	GE Healthcare (10426890)

2.1.1.2. Affinity purification and Chromatography

ÄKTApurifier system	GE Healthcare
AMPure XP beads	Beckman Coulter Inc. (A63881)
Anti-FLAG M2 Affinity Gel	Sigma-Aldrich (A2220)
GFP-Trap®_A	chromotek (gta-100)
nProtein A Sepharose 4 FF	GE Healthcare (17-5280)
Protein G Sepharose 4 FF	GE Healthcare (17-0618-05)
Superose 6 HR 10/30 gel filtration column	GE Healthcare (17-0537-01)

2.1.1.3. Agarose gel electrophoresis

6× Orange DNA Loading Dye	Fermentas (R0631)
Agarose NEEO ultra-quality	Carl Roth GmbH (2267.5)
GeneRuler 1 kb Plus DNA Ladder	Thermo Scientific (SM1333)
Ethidium bromide 1% solution	Carl Roth GmbH (2218.2)

2.1.1.4. Enzymes

Benzonase® Nuclease, Purity >99%	EMB Millipore (70664-10KUN)
DreamTaq DNA Polymerase	Thermo Scientific (EP0702)
Pfu DNA Polymerase (recombinant)	Thermo Scientific (EP0501)
Restriction endonucleases	Thermo Fischer
Proteinase K	Carl Roth GmbH (7528.1)
RNase A (DNase-free)	AppliChem (A3832,0050)

2.1.1.5. Enzyme inhibitors

Aprotinin	AppliChem (A2132,0100)
Leupeptin hemisulfate	AlfaAesar (J61188)
Pepstatin A	AppliChem (A2205,0100)
PMSF (phenyl-methane-sulfonyl-fluoride)	AppliChem (A0999,0025)

2.1.1.6. Kits

Table 2.1. List of kits with corresponding application and supplier.

Kits	Application	Supplier
Expand High Fidelity^{PLUS} PCR System	PCR	Roche
Fugene-HD	Transfection of S2[Cas9] cells	Promega
Immobilon™ Western Chemiluminescent HRP Substrate	Detection of Western blot signals	Millipore
MEGAscript T7 Kit	*in vitro* transcription	Ambion
MicroPlex Library Preparation Kit v2	Library preparation for ChIP-seq	Diagenode
peqGOLD DNase I Digest Kit	RNA isolation from *Drosophila* cells/testes	Peqlab
peqGOLD Total RNA Kit	RNA isolation from *Drosophila* cells/testes	Peqlab
SensiFAST™ cDNA Synthesis Kit	cDNA synthesis	Bioline
SensiFAST™ SYBR® Lo-ROX Kit	qPCR	Bioline
SilverQuest™ Staining Kit	Silver staining	invitrogen
QIAGEN Plasmid Maxi Kit	DNA isolation for cell transfection	Qiagen
QIAquick Gel Extraction Kit	gDNA isolation	Qiagen
QIAquick PCR Purification Kit	PCR product purification	Qiagen
Qubit® dsDNA High-Sensitivity Assay Kit	Determination of DNA concentration in ChIP	Thermo Scientific

Additional sources and suppliers are mentioned in the corresponding experiments of Methods section (**2.2**).

2.1.2. Standard Solutions and Buffers

Solutions and buffers are prepared and stored according to standard procedures using ultra-pure water (<0.056 μS/cm). Specific buffers are described in the corresponding experiments of Methods section (**2.2**).

Standard solutions:

0.5 M $CuSO_4$	Merck (2791.0250)
0.5 M EDTA, pH* 8.0	Carl Roth GmbH (8043.2)
50% Glycerol (v/v)	Carl Roth GmbH (3783.2)
0.1 M Glycine, pH* 3.5	Carl Roth GmbH (3790.2)
1.0 M HEPES, pH* 7.9	Carl Roth GmbH (9105.3)
3.0 M KCl	Carl Roth GmbH (6781.1)
1.0 M $MgCl_2$	Carl Roth GmbH (2189.2)
5.0 M NaCl	Carl Roth GmbH (P092.2)
10% SDS (w/v)	AppliChem (1592,0500)
1.0 M Tris, pH* 8.0	Carl Roth GmbH (9090.2)

* pH was adjusted either with 5 M KOH or 3 M HCl

Standard Buffers:

TAE buffer (Tris-acetate/EDTA buffer)	40 mM Tris-acetate, pH 8.0 1 mM EDTA, pH 8.0
TBST (Tris Buffered Saline with Tween)	20 mM Tris, pH 7.4 137 mM NaCl 1% Tween 20
PBS (Phosphate Buffered Saline) (gibco, 10010023)	2.97 mM $Na_2HPO_4 \cdot 7H_2O$, pH 7.4 1.06 mM KH_2PO_4 155.17 mM NaCl

2.1.3. Antibodies

All antibodies used in this study are listed in the following two sections (2.1.3.1 and 2.1.3.2). In the **Table 2.2** and **Table 2.3** it is indicated if they were used in immuno-precipitation (IP) Western blot (WB), or immunofluorescence (IF) experiments.

2.1.3.1. Primary antibodies

Table 2.2. **List of primary antibodies used in this study.**

Antibody	Host origin	Experiment	Amount/ Dilution	Reference
α-dCoREST	Rabbit, Polyclonal	IP	30 μg	(Dallman et al., 2004)
		WB	1:40,000	
α-FLAG	Rabbit, Polyclonal	WB	1:20,000	Sigma-Aldrich (F7425)
α-dG9a (4H1)	Rat, Monoclonal	WB	1:50	A. Imhof
α-dG9a	Rabbit, Polyclonal	WB	1:10,000	(Kato et al., 2008)
α-GFP	Rat, Monoclonal	WB	1:5,000	chromotek (3H9)
α-dL(3)mbt #3	Rabbit, Polyclonal	WB	1:10,000	(Meier et al., 2012)
α-dL(3)mbt	Guinea pig, Polyclonal	WB	1:20,000	J. Knoblich

Table 2.2. List of primary antibodies used in this study. (continuation)

Antibody	Host origin	Experi-ment	Amount/Dilution	Reference
α-dLint-1 #2	Rabbit, Polyclonal	WB	1:10,000	(Meier et al., 2012)
α-dLSD1	Rabbit, Polyclonal	WB	1:10,000	(Rudolph et al., 2007)
α-dMi-2 (N-term)	Rabbit, Polyclonal	WB	1:20,000	(Kehle et al., 1998)
α-dMst77F	Guinea pig, Polyclonal	IF	1:500	(Rathke et al., 2010)
α-dRPD3	Rabbit, Polyclonal	WB	1:10,000	(Brehm et al., 2000)
α-Tubulin beta	Mouse, Monoclonal	WB	1:10,000	Millipore (KMX-1)
α-Histone	Mouse, Monoclonal	IF	1:1,200	Millipore (MABE71)

2.1.3.2. Secondary antibodies

Table 2.3. List of secondary antibodies used in this study.

Antibody	Host origin	Experiment	Dilution	Source
HRP α-Rabbit	Donkey, Polyclonal	WB	1:20,000	GE Healthcare
HRP α-Mouse	Sheep, Polyclonal	WB	1:20,000	GE Healthcare
HRP α-Rat	Goat, Polyclonal	WB	1:20,000	Sigma-Aldrich
HRP α-Guinea pig	Goat, Polyclonal	WB	1:20,000	Sigma-Aldrich
Cy3 α-Guinea pig	Donkey, Polyclonal	IF	1:100	Dianova
Cy5 α-Mouse	Donkey, Polyclonal	IF	1:100	Dianova

2.1.4. Bacteria strains and culture media

In order to amplify plasmids for S2 cell transfection or PCR cloning, a chemocompetent *Escherichia coli* (*E. coli*) XL1-Blue strain was used.

Lysogeny Broth (LB) medium	1% (w/v) Peptone (BD, 21677) 0.5% (w/v) Yeast extract (Sigma, Y1000-1KG) 1% (w/v) NaCl
Agar plates	1.5% (w/v) Agar-agar (Roth, 5210.3) in LB medium

LB medium was supplemented with 100 µg/ml Ampicillin (Roth, K029.2).

2.1.5. Plasmids

Table 2.4. List of plasmids used in this study.

Plasmid name	Description	Source/Reference
pBS-Puro	Expression vector for *Drosophila* cells: encodes a resistance gene against puromycin under the control of the *Drosophila* heat schock promoter.	(Benting et al., 2000)
pRmHa-3	Vector for copper-inducible expression of FLAG/HA tagged proteins in *Drosophila* cells	P. Becker LMU Munich

Table 2.4. **List of plasmids used in this study.** (continuation)

Plasmid name	Description	Source/Reference
pRmHa-3-FLAG-HA-dCoREST-L	Encodes full length dCoREST-L, tagged N-terminally with a FLAG/HA-tag for inducible expression in *Drosophila* cells, driven by metallothionein promoter.	Corina Webert AG Brehm
pRmHa-3-FLAG-HA-dCoREST-M	Encodes full length dCoREST-M, tagged N-terminally with a FLAG/HA-tag for inducible expression in *Drosophila* cells, driven by metallothionein promoter.	Corina Webert AG Brehm
pRmHa-3-FLAG-HA-dLSD1	Encodes full length dLSD1, tagged N-terminally with a FLAG/HA-tag for inducible expression in *Drosophila* cells, driven by metallothionein promoter.	Corina Webert AG Brehm
pNLS-eGFP-C1	A pEGFP-C1 (Clontech) derived vector that encodes eGFP.	H. Leonhardt
pOT2-dCoREST-L	cDNA encoding for full length dCoREST-L in the pOT2 vector.	IP20671
pRmHa-3-FLAG-HA-dL(3)mbt	Encodes full length dL(3)mbt, tagged N-terminally with a FLAG/HA-tag for inducible expression in *Drosophila* cells, driven by metallothionein promoter.	Corina Webert AG Brehm
pRmHa-3-FLAG-HA-dLint-1	Encodes full length dLint-1, tagged N-terminally with a FLAG/HA-tag for inducible expression in *Drosophila* cells, driven by metallothionein promoter.	Corina Webert AG Brehm
pRB17	Vector carrying the sequence of U6-promoter fused to T7 promoter for CRISPR/Cas9 U6-sgRNA template generation.	Addgene #52527
pSK23	Vector carrying the sequence of GFP-tagged generation of homologous recombination template for tagging in CRISPR/Cas9 S2 cells.	Addgene #72851
pSK25	Vector carrying the sequence of 2×FLAG-tagged generation of homologous recombination template for tagging in CRISPR/Cas9 S2 cells.	Addgene #72853

2.1.6. Oligonucleotides

Unmodified DNA oligonucleotides used in this study were purchased from eurofins Genomics. Lyophilised DNA oligonucleotides were diluted in water at a stock concentration of 100 pmol/μl and stored at −20 °C.

2.1.6.1. Primers used for CRISPR/Cas9 tagging

Oligonucleotides used in CRISPR/Cas9 tagging experiments were designed according to the protocol described previously (Böttcher et al., 2014).

Table 2.5. List of primers used in CRISPR/Cas9 tagging experiments.

Primer name	Sequence	Reference
sgRNA scaffold	GTTTAAGAGCTATGCTGGAAACAGCATAGCA AGTTTAAATAAGGCTAGTCCGTTATCAACTT GAAAAAGTGGCACCGAGTCGGTGC	(Böttcher et al. 2014)
U6-promoter sense	GCTCACCTGTGATTGCTCCTAC	(Böttcher et al. 2014)
sgRNA antisense	gcttattctcAAAAAAGCACCGACTCGGTGC CACT	(Böttcher et al. 2014)
CRISPR act5c	cctattttcaatttaacgtcgACCGCAAGTG CTTCTAAGAgtttaagagctatgctg	(Böttcher et al. 2014)
act5c-sense	TGGATCTCCAAGCAGGAGTACGACGAGTCCG GCCCCTCCATTGTGCACCGCAAGTGCTTCgg atcttccggatggctcgag	(Böttcher et al. 2014)
act5c-antisense	CCTCCAGCAGAATCAAGACCATCCCGATCCT GATCCTCTTGCCCAGACAAGCGATCCTTCga agttcctattctctagaaagtataggaactt cCATATG	(Böttcher et al. 2014)
CRISPR dCoREST	cctattttcaatttaacgtcgCAGAGTTCCT GGCCAACTGgtttaagagctatgctg	This study
dCoREST-sense	GCGAAGAAAATCGCGCTCAGCACCGGAGGCG GAAGCAGCGTCGCAGAGTTCCTGGCCAACgg atcttccggatggctcgag	This study
dCoREST-antisense	ATGTTATGTATCGGTATATATCTATGCGTGC ATATATATCGCGAGTGAACACGTCGCTCCga agttcctattctctagaaagtataggaactt cCATATG	This study
CRISPR dLSD1	cctattttcaatttaacgtcgAACAATGTAT TTAGCGTGAgtttaagagctatgctg	This study
dLSD1-sense	TCGTCAAAGAAGTCGGAGGAGAATTCAAACT CAAACACTGCCGACTCTACGGAGCTACAGgg atcttccggatggctcgag	This study
dLSD1-antisense	CAAAACTAAACGCTCTAGGAGTAACTGCTGG GGACCAAATGCATCACGCTAAATACATTGga agttcctattctctagaaagtataggaactt cCATATG	This study
CRISPR dL(3)mbt	cctattttcaatttaacgtcgCCCTTGCGCA CGTCCTCTTgtttaagagctatgctg	This study
dL(3)mbt-sense	TCCGACGGCGATGTGGCGATGGTGCCGATGG AAGTGCGCACGCCCTTGCGCACGTCCTCTgg atcttccggatggctcgag	This study

In lowercase letters the sequence that anneals to the template plasmids are shown, and in uppercase letters is the gene-specific DNA sequence.

Table 2.5. List of primers used in CRISPR/Cas9 tagging experiments. (continuation)

Primer name	Sequence	Reference
dL(3)mbt-antisense	GGTGCAACAAAATAATCTTATAAATCAATCA ACGGAAGCGGATGCCTGGTATCCGGAGTCga agttcctattctctagaaagtataggaactt cCATATG	This study
CRISPR dG9a	cctattttcaatttaacgtcgGAGAAAATTG GACACGCGTgtttaagagctatgctg	This study
CRISPR FLAG-dG9a	cctattttcaatttaacgtcgGACAATTAAG GCAAGATGAgtttaagagctatgctg	This study
dG9a-sense-FS	CACCGGAAAATGAAACGGGAACGCTGTCGTC TACAAATACGGAGAAAATTGGACACGCGTgg atcttccggatggctcgag	This study
dG9a-sense	GCACCGGAAAATGAAACGGGAACGCTGTCGT CTACAAATACGGAGAAAATTGGACACGCGgg atcttccggatggctcgag	This study
dG9a-antisense	TTTTATTTGTTGGATGAGACTGTGAAATCTG CAATCATCTCAGGTTTAGGTGGTTTTAGCga agttcctattctctagaaagtataggaactt cCATATG	This study
dG9a-antisense-NR	TTTTATTTGTTGGATGAGACTGTGAAATCTG CAATCATCTCAGGTTTAGGTGGTTTTAGCTC ATTTATCATCATCATCTTTATAATCggctcc ggaTTTA	This study
FLAG-dG9a-sense	ATCGAAAATCAAAGAAACTAATACGCAAAGT AATCAAATAGTGACAATTAAGGCAAGATGGA TTATAAAGATGATGATGATAAAtccggagcc GATTATA	This study
FLAG-dG9a-antisense	AGTAGCACAGTCGCTATTGAATGTACTGGAC ATGCTGTTCATCAGCTCAACAAAGTCTGTTT TATCATCATCATCTTTATAATCggctccgga TTTATCA	This study

In lowercase letters the sequence that anneals to the template plasmids are shown, and in uppercase letters is the gene-specific DNA sequence.

2.1.6.2. Primers for genotyping of tagged cell lines

To check the integration of tagging constructs in S2[Cas9] cells, gDNA isolated from cell lines was genotyped according to the protocol described previously (Böttcher et al., 2014).

Table 2.6. List of primers used for genotyping of S2[Cas9] cell lines.

Primer name	Sequence	Reference
dCoREST-GFP_fw	TCTCTTCTCCTCCTCCACAG	This study
dCoREST-GFP_rv	CGTCCCCCAAAACATCAATC	
dLSD1-GFP_fw	CCCAATCTATCTGACTCCTC	This study
dLSD1-GFP_rv	TTACAGCGGCCTAGCTTCGT	
dL(3)mbt-GFP_fw	ATGGGGATGGCGATTGTGAA	This study
dL(3)mbt-GFP_rv	ATAATACCCGAATGGGCCGA	

Table 2.6. List of primers used for genotyping of S2[Cas9] cell lines. (continuation)

Primer name	Sequence	Reference
dG9a-C-fw	CACCGGAAAATGAAACGGGA	This study
dG9a-C-rv	ACCGGGCTTCGATAACGATT	
N-dG9a-fw	CGATGCACAAATCTTGTCGG	This study
N-dG9a-rv	TTAGCAAAGTACCACCCTCC	

2.1.6.3. Primers for generation of dsRNA by *in vitro* transcription (*iv*T)

To knockdown specific proteins in *Drosophila* S2[Cas9] and S2 cells, dsRNA was used in RNAi experiments. Primers used for generation of gene-specific dsRNA by *in vitro* transcription had a T7 promoter sequence at the 5' end.

Table 2.7. List of primers used for amplification of the templates for dsRNA synthesis.

Primer name	Sequence	Reference
lig4-RNAi-fw	taatacgactcactatagggCCCAATGATCCAAAGTGTTTTTGCA	(Böttcher et al. 2014)
lig4-RNAi-rv	taatacgactcactatagGGAAGTAGGATGCCTTCGCGA	
mus308-RNAi-fw	taatacgactcactataggGCTGGGACTCCACCGGAAAG	(Böttcher et al. 2014)
mus308-RNAi-rw	taatacgactcactatagggTACCGTCGCCGTCCAGTAATG	
EFGP-RNAi-fw	gaattaatacgactcactatagggAGAGCTGGACGGCGACGTAA	(Stielow at al. 2008)
EFGP-RNAi-rv	gaattaatacgactcactatagggAGACTTGTACAGCTCGTCCATG	
dCoREST-RNAi-fw	taatacgactcactatagggCATTCGCTCAGTTTTCTGACG	(Meier et al. 2012)
dCoREST-RNAi-rv	taatacgactcactatagggCCACCGAAATGTACTCCTCC	
dCoREST-L-RNAi-fw	taatacgactcactatagggAAGATTTGCAACGTGGTCTG	Corina Webert AG Brehm
dCoREST-L-RNAi-rv	taatacgactcactatagggTTCCGCCAAATAGAGACTGG	
dLSD1-RNAi-fw	taatacgactcactatagggAAAGAAACGTCAATCACCCG	(Meier et al. 2012)
dLSD1-RNAi-rv	taatacgactcactatagggCCTCTTCGTTGGGTGTCATT	
dL(3)mbt-RNAi-fw	taatacgactcactatagggGTTGGTTTGGGTGCTGTCTT	(Meier et al. 2012)
dL(3)mbt-RNAi-rv	taatacgactcactatagggGCGTCTAAAGTTCAGCCAGG	

In lowercase letters the sequence of the T7 promoter is shown, and in uppercase letters the gene-specific DNA sequence in shown.

Table 2.7. List of primers used for amplification of the templates for dsRNA synthesis. (continuation)

Primer name	Sequence	Reference
dLint-1-RNAi-fw	taatacgactcactatagggATGAAAGGGTCGCTGGATT	(Meier et al. 2012)
dLint-1-RNAi-rv	taatacgactcactatagggGCTCGGCACTGGAATCAT	
dG9a-RNAi-fw	taatacgactcactatagggAAACCAAGTGTTACTTTGAGAG	(Meier et al. 2012)
dG9a-RNAi-rv	taatacgactcactatagggTGTACAAAATATGCCACATCCT	

In lowercase letters the sequence of the T7 promoter is shown, and in uppercase letters the gene-specific DNA sequence in shown.

2.1.6.4. Primers for gene expression analysis by qPCR

Oligonucleotides that were used in this study for qPCR experiments were designed at exon-intron borders for specific isoforms and their specificity was checked first using the primer BLAST tool (https://www.ncbi.nlm.nih.gov/tools/primer-blast) and then by control qPCR and agarose gel analysis.

Table 2.8. List of primers used for qPCR gene expression analysis.

Primer name	Sequence	Reference
Rp49-RT-fw	TGTCCTTCCAGCTTCAAGATGACCATC	(Gabler et al., 2005)
Rp49-RT-rv	CTTGGGCTTGCGCCATTTGTG	
dCoREST-RT-fw	TCAAGGATGGCTCCGAGAAC	This study
dCoREST-L-RT-rv	TGTGCCATGCCCTTTCTTGT	
dCoREST-RT-fw	TCAAGGATGGCTCCGAGAAC	This study
dCoREST-M-RT-rv	CCTATTCTTCTGTATCTTGT	
dLSD1-RT-fw	ACGGCGAGTAGAGGAGAAAT	This study
dLSD1-RT-rv	GATTATGATGTCATCCGTCA	
dL(3)mbt-RT-fw	TTTCTGGCACCACATTTCTG	(Meier et al., 2012)
dL(3)mbt-RT-rv	CTCTCCTTCTGCGTACTCTGC	
dLint-1-RT1-fw	GCAGGAGCAGCAAAGACG	(Meier et al., 2012)
dLint-1-RT1-rv	CTCAAAGAGGCCGAGGAAC	
dLint-1-RT2-fw	CCGTGAAGCTGAAGGAGAAC	This study
dLint-1-RT2-rv	GGAAGTGCTTGCGAATAAGC	
dG9a-RT-fw	AACGATGACTTGGAGCGTGTA	Dr Karin Meier
dG9a-RT-rv	GGGAGTCAGCACGTTGAAGT	

2.1.7. Cell lines and tissue culture media

2.1.7.1. Insect cell lines

S2: *Drosophila melanogaster* cell line, male aneuploid, derived from a primary culture of 20 to 24 hours old *Drosophila* embryos (Schneider, 1972; Zhang et al., 2010).

Sf9: *Spodoptera frugiperda* cell line, derived from pupal tissue. Sf9 cells were used for the expression of recombinant proteins using the baculovirus system (Vaughn et al., 1977) and were kindly maintained and transfected by Jonathan Lenz.

2.1.7.2. Stably transfected S2 cell lines

For this study, stably transfected S2 cell lines were used. Generation or source of S2 cell lines is described in the corresponding sections.

S2 pRmHa3-FLAG-HA-dCoREST-M (puromycin-resistant): polyclonal S2 cells generated by co-transfection of pRmHa3-FLAG-HA-dCoREST-M and pBS-Puro. pRmHa3-FLAG-HA-dCoREST-M encodes the full length N-terminally FLAG/HA-tagged dCoREST-M protein under the control of the inducible metallothionein promoter.

S2 pRmHa3-FLAG-HA-dCoREST-L (puromycin-resistant): polyclonal S2 cells generated by co-transfection of pRmHa3-FLAG-HA-dCoREST-L and pBS-Puro. pRmHa3-FLAG-HA-dCoREST-L encodes the full length N-terminally FLAG/HA-tagged dCoREST-L protein under the control of the inducible metallothionein promoter.

S2 pRmHa3-FLAG-HA-dLSD1 (puromycin-resistant): polyclonal S2 cells generated by co-transfection of pRmHa3-FLAG-HA-dLSD1 and pBS-Puro. pRmHa3-FLAG-HA-dLSD1 encodes the full length N-terminally FLAG/HA-tagged dLSD1 protein under the control of the inducible metallothionein promoter.

For stable transfection pBS-Puro vector, that carries a resistance gene against the antibiotic puromycin, was co-transfected together with plasmid of interest. This allowed selection and maintains of the cell line by addition of 10 μg/ml puromycin into the medium.

S2[Cas9] (hygromycin-resistant): monoclonal S2 cells stably expressing Cas9 nuclease (a gift from Klaus Förstemann; Böttcher et al., 2014).

S2[Cas9] dCoREST-GFP Clone #1 (puromycin-resistant): monoclonal S2[Cas9] cells where endogenous dCoREST was tagged on the C-terminus with GFP.

S2[Cas9] dLSD1-GFP Clone #4 (puromycin-resistant): monoclonal S2[Cas9] cells where endogenous dLSD1 was tagged on the C-terminus with GFP.

S2[Cas9] dL(3)mbt-GFP Clone #2 (puromycin-resistant): monoclonal S2[Cas9] cells where endogenous dL(3)mbt was tagged on the C-terminus with GFP.

S2[Cas9] dG9a-GFP control (puromycin-resistant): polyclonal S2[Cas9] cells where a GFP-tag and a puromycin resistance sequences were introduced at the 3' end of the *dG9a* gene. Due to addition of one nucleotide upstream of the construct, the GFP-tag is not expressed due to frame shifting.

S2[Cas9] dG9a-GFP Clone #6 (puromycin-resistant): monoclonal S2[Cas9] cells where endogenous dG9a was tagged on the C-terminus with GFP.

S2[Cas9] Act5C-GFP; FLAG-dG9a (puromycin-resistant): polyclonal S2[Cas9] cells in which dG9a was FLAG-tagged on its N-terminus. Additionally, Act5C was tagged with GFP which allowed puromycin selection.

S2[Cas9] Act5C-GFP; dG9a-FLAG (puromycin-resistant): polyclonal S2[Cas9] cells in which dG9a was FLAG-tagged on its C-terminus. Additionally, Act5C was tagged with GFP which allowed puromycin selection.

In S2[Cas9] cell lines a resistance gene against puromycin was introduced after the sequence for the tag.

2.1.7.3. Tissue culture media

Schneider's *Drosophila* medium (gibco, 21720-024) supplemented with 10% (v/v) Fetal Bovine Serum (FBS, Sigma-Aldrich, F7524) and 1% (v/v) Penicillin/ Streptomycin (gibco, 15140-122) was used for all *Drosophila* cell lines. Selection medium was prepared by adding 2.5 μg/ml to 10 μg/ml puromycin (Millipore, 540411-100MG) to supplemented Schneider's *Drosophila* medium.

Sf-900 II SFM medium (gibco, 10902088) supplemented with 10% (v/v) Fetal Bovine Serum (Biochrom AG, S0115) and 1% (v/v) Penicillin/Streptomycin (gibco, 15140-122) was used for Sf9 cells.

2.1.8. Fly strains

Fly stocks were maintained in a fly incubator at 18 °C or 26°C. Fly crosses for RNAi experiments were kept in a fly incubator at 26 °C or 30 °C. Culturing of fly stocks and crosses was done according to standard procedure described previously (Kunert and Brehm, 2008).

Table 2.9. **List of fly strains used in this study.**

Fly strain	Description	Source
w[1118] isogenic	w^{1118} isogenic fly strain, isogenised chromosomes 1,2 and 3	Bloomington (BL#5905)
triple bam-GAL4	GAL4 driver strain, expresses GAL4 in a *bag of marbles* pattern	R. Renkawitz-Pohl/ H. White-Cooper
en2.4-GAL4	GAL4 driver strain, expresses GAL4 in a *engrailed* pattern	Bloomington (BL#30564)
UAS-dCoREST #1 RNAi	Transgenic line carrying a UAS-RNAi construct directed against dCoREST, inserted at the 3rd chromosome	VDRC library (ID#34179)
UAS-dCoREST #2 RNAi	Transgenic line carrying a UAS-RNAi construct directed against dCoREST, inserted at the 2nd chromosome	VDRC library (ID#34180)
UAS-dCoREST #3 RNAi	Transgenic line carrying a UAS-RNAi construct directed against dCoREST, inserted at the 2nd chromosome	VDRC library (ID#104900)
UAS-dLSD1 RNAi	Transgenic line carrying a UAS-RNAi construct directed against dLSD1, inserted at the 2nd chromosome	VDRC library (ID#106147)
UAS-dL(3)mbt RNAi	Transgenic line carrying a UAS-RNAi construct directed against dL(3)mbt, inserted at the 2nd chromosome	VDRC library (ID#104563)
UAS-dLint-1 RNAi	Transgenic line carrying a UAS-RNAi construct directed against dLint-1, inserted at the 2nd chromosome	VDRC library (ID#105932)
UAS-dG9a RNAi	Transgenic line carrying a UAS-RNAi construct directed against dG9a, inserted at the 2nd chromosome	VDRC library (ID#25473)
UAS-dChd3 RNAi	Transgenic line carrying a UAS-RNAi construct directed against dChd3, inserted at the 2nd chromosome	VDRC library (ID#102689)
UAS-CG9973 RNAi	Transgenic line carrying a UAS-RNAi construct directed against CG9973, inserted at the 2nd chromosome	VDRC library (ID#102273)
UAS-CG2083 RNAi	Transgenic line carrying a UAS-RNAi construct directed against CG2083, inserted at the 2nd chromosome	VDRC library (ID#110549)

2.2. Methods

All reactions and experiments were performed at the temperatures indicated in the corresponding sections. All buffers and solutions were sterile filtered through 0.2 μm filters and stored according to recommendations.

2.2.1. Cell biological methods

2.2.1.1. Standard cell culture procedures

Drosophila melanogaster S2 cells were cultured in Schneider's insect medium supplemented with FBS and Penicillin/Streptomycin (**2.1.7.3**) at 26 °C (BINDER K3400). Sf9 cells were cultured in Sf-900 II SFM medium supplemented FBS and Penicillin/Streptomycin. Cells were detached from the tissue culture dish surface when they had reached 100% confluence by scraping them with the cell scraper and additionally resuspended by pipetting. Cells were pelleted by centrifugation for 5 minutes (1,000 rpm, RT) (Heraeus Megafuge 1.0), medium was removed and cells were split in a 1:3 to 1:10 ratio.

2.2.1.2. Freezing and thawing of cells

From one dense 175 cm^2 tissue culture dish (T175, Sarstedt), cell monolayer was scrapped and medium was removed by centrifugation at 1,000 rpm for 5 minutes. Cell pellet was resuspended in 400 μl FBS; 1,400 μl Schneider's insect medium and 200 μl DMSO (Serva 20385.01). Cell suspension aliquots (1 ml) were transferred into cryovials (Grainer, 122277) and frozen at −80 °C. For long term storage, cryovials were transferred in liquid nitrogen.

Freezing medium:	70% (v/v) Schneider's insect medium
	20% (v/v) FBS
	10% (v/v) DMSO

Aliquots of frozen cells were thawed and resuspended in 20 ml of Schneider's insect medium supplemented with FBS and Penicillin/Streptomycin (**2.1.7.3**). In order to remove remaining DMSO, cells were pelleted by centrifugation for 5 minutes (1,000

rpm, RT) and washed with 20 ml of PBS. Finally, the cell pellet was resuspended in 20 ml of fresh medium and seeded in a 75 cm² tissue culture flask (T75, Sarstedt).

2.2.1.3. Stable transfection

To generate stable S2 cells lines expressing recombinant proteins, cells were transfected using the calcium-phosphate method (Graham and van der Eb, 1973 a/b). For introduction of transgene, pRmHa-3 plasmids expressing full-length FLAG-tagged dCoREST-L, dCoREST-M or dLSD1 under control of a metallothionein promoter were co-transfected with pBS-Puro (which confers resistance to puromycin) into S2 cells. In brief, a total of 7.4×10^6 S2 cells were seeded in 10 cm plates. The next day cells were transfected with 30 μg of plasmid containing the coding sequence of full-length FLAG-tagged dCoREST-L, dCoREST-M or dLSD1 and 1.5 μg of the pBS-Puro by calcium-phosphate transfection. The plasmid DNA was diluted in 500 μl of $CaCl_2$ solution and added dropwise to 500 μl of 2× HeBS buffer while vortexing. The transfection mixture was incubated for 30 minutes at room temperature and was added dropwise, including precipitates, onto the cells. Plates were swirled and incubated for one day. The medium was exchanged 24 hours after transfection. After three days cells were split in a 1:3 ratio and selected in 10 μg/ml puromycin for three weeks. Transgene expression was induced by adding $CuSO_4$ to a final concentration of 100 μM and nuclear extracts were prepared 24 hours later.

$CaCl_2$ solution	250 mM $CaCl_2$
	1 mM HEPES, pH 7.1
2× HeBS buffer	280 mM NaCl
	10 mM KCl
	3 mM Na_2HPO_4
	3 mM D(+)-Saccharose
	20 mM HEPES, pH 7.1

2.2.1.4. CRISPR/Ca9 gene editing in S2 cells

Endogenous dCoREST, dLSD1, dL(3)mbt, and dG9a were epitope-tagged using CRISPR/Cas9 as described in details previously (Böttcher et al., 2014). Briefly, four days before transfection, 1×10^6 cells/ml S2[Cas9] cells were first transiently depleted of the essential NHEJ-factor Lig4 and the MMEJ-factor Mus308 via RNAi to favour

homologous recombination (both dsRNA were used at the concentration of 1 μg/ml). U6-sgRNA templates and homologous recombination templates for tagging were generated by PCR (**2.2.2.2**) using sequence specific primers (**2.1.6.1**). 375 ng of both, U6-sgRNA template and homologous recombination template, were transfected into 400 μl of the cells (1.5×10^6 cells/ml) using 5 μl Fugene-HD. After four days, puromycin-resistant cells were selected in 2.5 μg/ml puromycin for two weeks. Monoclonal cell lines were prepared by serial dilution and clones were analysed by PCR (**2.2.2.2**) and Western blot (**2.2.3.7**).

2.2.1.5. Protein expression in Sf9 cells

Baculoviruses expressing dCoREST-L, dCoREST-M and dLSD1 were generated with the Bac-to-Bac Baculovirus Expression System (invitrogen) according to the manufacturer's instructions. Sf9 cells were harvested 72 hours after infection and lysed by three freeze/thaw cycles in Lysis buffer. Lysates were cleared by centrifugation for 30 minutes ($17,000 \times g$, 4 °C) and kindly provided by Jonathan Lenz.

Lysis buffer	20 mM HEPES, pH 7.6
	200 mM KCl
	10% (v/v) Glycerol
	0.1% (v/v) NP-40

2.2.2. Molecular biological methods

All experiments with DNA and RNA were carried out according to standard procedures in molecular biology (Sambrook and Russell, 2001).

2.2.2.1. Amplification of plasmids

Bacteria were transformed according to standard procedure. Bacteria were mixed gently with 100 ng of corresponding plasmid and incubated 30 minutes on ice. Heat-shock was done for 2 minutes at 42 °C and the mixture was further incubated 5 minutes on ice prior to plating on LB agar plates with resistance antibiotics. Single colonies were used to inoculate 200 ml of LB medium and the bacteria were incubated overnight at 37 °C (shaker). Isolation of the plasmids was done using QIAGEN Plasmid Maxi Kit according to the manufacturer's instruction. Plasmids were eluted from the columns

using sterile water and the concentration was estimated on a NanoDrop (Thermo Scientific). Additionally, plasmids were subjected to restriction digestion and the fragments were analysed by agarose electrophoresis.

2.2.2.2. Polymerase chain reaction (PCR)

Exponential amplification of a specific DNA sequence from a template DNA was done using sequence-specific primer pairs by PCR (Saiki et al., 1988).

Generation of the U6-sgRNA templates for transfection in CRISPR/Cas9 tagging experiment was done using the following PCR reaction mixture:

```
 2 µl  1 µM oligo sgRNA scaffold
 2 µl  1 µM primer CRISPR
 2 µl  10 ng/µl plasmid pRB17
 2 µl  10 µM primer U6-promoter sense
 2 µl  10 µM primer sgRNA antisense
10 µl  10× PCR buffer (100 mM Tris-HCl, pH 8.3; 500 mM KCl)
16 µl  25 mM MgSO4
 2 µl  10 µM (each) dNTP
60 µl  H2O
 1 µl  DreamTaq DNA Polymerase
 1 µl  Pfu DNA Polymerase (recombinant)
```

Generation of the homology recombination (HR) templates for transfection in CRISPR/Cas9 tagging experiment was done using the following PCR reaction mixture:

```
 6 µl  100 pg/µl plasmid pSK23 or pSK25
 2 µl  10 µM primer sense
 2 µl  10 µM primer antisense
10 µl  10× PCR buffer (100 mM Tris-HCl, pH 8.3; 500 mM KCl)
 6 µl  25 mM MgSO4
 2 µl  10 µM (each) dNTP
70 µl  H2O
 2 µl  Expand HiFiPLUS enzyme
```

U6-sgRNA template DNA and HR template DNA sequence was amplified in a T Professional gradient Thermocycler (Biometra) using the following program:

```
1:       94 °C   2 min
2:       94 °C   30 s
3:    50-55 °C   30 s       | 30 cycles
4:       72 °C   2 min      |
5:        4 °C   Pause
```

The annealing temperature was dependent on the primers used. The concentration of PCR products was estimated by comparing the intensities of the bands in agarose gel electrophoresis to the known standards.

To generate the templates for double-stranded RNA synthesis, DNA amplification was done using the following PCR reaction mixture:

```
 1.0 µl  100 ng/µl of plasmid or cDNA from S2 cells
 5.0 µl  5 µM primer sense
 5.0 µl  5 µM primer antisense
10.0 µl  5× Expand HiFiPLUS buffer
 1.0 µl  10 mM (each) dNTP
27.5 µl  H2O
 0.5 µl  Expand HiFiPLUS enzyme
```

DNA templates were amplified in a T3000 Thermocycler (Biometra) using the following program:

```
1:      94 °C   2 min
2:      94 °C   15 s
3:      60 °C   30 s      35 cycles
4:      72 °C   45 s
5:      72 °C   7 min
6:       4 °C   Pause
```

PCR products were purified from the agarose gel using the QIAquick Gel Extraction Kit and the DNA concentration was determined using a NanoDrop (Thermo Scientific). The first PCR products were reused as a template for the second PCR amplification under the same conditions. The second PCR products were purified using the QIAquick PCR Purification Kit and, upon determination of the concentrations (NanoDrop; Thermo Scientific), were used as a template for synthesis of double-stranded RNA.

2.2.2.3. Chromatin immunoprecipitation (ChIP)

Exponentially growing S2[Cas9] cells (1×10^8) expressing GFP-tagged proteins were cross-linked with 1% Formaldehyde (Roth, 4235.1) for 10 minutes at room temperature. Cross-linking was stopped by adding Glycine to a final concentration of 240 mM and incubating samples for 10 minutes at room temperature. Cells were then washed twice in PBS and lysed in 1 ml of ChIP Lysis buffer for 10 minutes on ice. Chromatin was sheared by sonication in a Bioruptor UCD-200TM-EX (Diagenode) supplied with ice

water. Three sonication cycles were applied, each cycle lasting for 10 minutes with 30 seconds intervals of sonication at high power interrupted by 30 seconds of resting. Cell debris were pelleted by centrifugation for 20 minutes (21,100 × g, 4 °C) and the supernatant containing fragmented chromatin was stored at −80 °C. The fragment size was monitored by reverse cross-linking 50 μl of chromatin-containing lysate in the presence of RNase A (400 ng/μl) and Proteinase K (400 ng/μl) for 3 h at 55 °C followed by 65 °C overnight. DNA was purified using the QIAquick PCR purification kit (Qiagen) and the fragment size was evaluated on a 1.2% agarose gel.

For ChIP 1 ml of chromatin lysate was pre-cleared by 1:10 dilution in ChIP IP buffer and addition of 285 μl Protein A Sepharose resin (GE Healthcare) that had been blocked for 1 hour in ChIP Blocking buffer (ChIP Low salt buffer containing 2 mg/ml BSA (Sigma, 2153-100G) and 2% (w/v) Gelatin from cold water fish skin (Sigma, G7765-250ML)). After incubation at 4 °C for 1 hour with rotation, beads were precipitated by centrifugation for 10 minutes (21,100 × g, 4 °C) and the supernatant was added to 200 μl of blocked GFP-Trap® (chromotek).

Immunoprecipitation took place overnight at 4 °C with rotation followed by washing: 3× with 15 ml of ChIP Low salt buffer, 3× with 15 ml of ChIP High salt buffer, 1× with 15 ml of ChIP LiCl buffer, 2× with TE buffer. Each washing step was performed at 4 °C for 5 minutes with rotation and the resin was precipitated in between by centrifugation for 4 minutes (400 × g, 4 °C).

Cross-linked protein-DNA complexes were eluted twice from the resin in 500 μl ChIP Elution buffer for 20 minutes at room temperature with rotation followed by 10 minutes incubation at 95 °C. Pooled eluates were diluted 1:1 with 100 mM NaHCO$_3$. As "input" sample, 14 μl of pre-cleared chromatin was added to 250 μl of ChIP Elution buffer and diluted 1:1 with 100 mM NaHCO$_3$. 5 M NaCl was added to the samples to a final concentration of 200 mM. Protein-DNA complexes were reverse cross-linked overnight at 65 °C with agitation. 40 mM Tris, pH 6.8; 1 mM EDTA and 40 ng/μl Proteinase K was added to each sample and proteins were digested at 45 °C for 1 hour with agitation. The DNA was purified using the QIAquick PCR Purification Kit (Qiagen) and the concentration was determined using the Qubit® dsDNA High-Sensitivity Assay Kit according to the manufacturer's instruction.

ChIP Lysis buffer	50 mM Tris, pH 8.0
	10 mM EDTA
	1% (w/v) SDS
	1 mM DTT
	protease inhibitors (2.2.3)
ChIP IP buffer	16.7 mM Tris, pH 8.0
	1.2 mM EDTA
	167 mM NaCl
	1 mM DTT
	protease inhibitors (2.2.3)
ChIP Low salt buffer	20 mM Tris, pH 8.0
	2 mM EDTA
	150 mM NaCl
	1% (w/v) Triton X-100,
	0.1% (w/v) SDS
	1 mM DTT
	protease inhibitors (2.2.3)
ChIP High salt buffer	20 mM Tris, pH 8.0
	2 mM EDTA
	500 mM NaCl
	1% (w/v) Triton X-100,
	0.1% (w/v) SDS
	1 mM DTT
	protease inhibitors (2.2.3)
ChIP LiCl buffer	10 mM Tris pH 8.0
	1 mM EDTA
	250 mM LiCl
	0.1% (w/v) NP-40
	1 mM DTT
	protease inhibitors (2.2.3)
TE buffer	10 mM Tris, pH 8.0
	1 mM EDTA
	1 mM DTT
ChIP Elution buffer	100 mM NaHCO$_3$
	2% (w/v) SDS)

2.2.2.4. Synthesis of double-stranded RNA (dsRNA)

The synthesis of dsRNA by *in vitro* transcription (*iv*T) was done using the MEGAscript T7 Kit (Ambion) according to manufacturer's instruction.

First, templates for *iv*T were generated from plasmids (dsRNA for EGFP, dCoREST, dCoREST-L, dLSD1, dL(3)mbt, dLint-1; **2.1.5**) or cDNA (dsRNA for dG9a, Mus308 and Lig4) by PCR (**2.2.2.2**) using gene specific primers (**2.1.6.3**). Both, forward and reverse primers contained a minimal T7 polymerase promoter at the 5' end.

For one reaction 500 ng of DNA template was incubated with 2 µl of each rNTP, 2 µl of enzyme, and 2 µl 10× reaction buffer in total volume of 20 µl. The reaction was performed at 37 °C for 16 hours. DNA template was depleted by adding 1 µl of TURBO DNase for 15 minutes at 37 °C into the reaction mixture. The reaction was stopped by

adding an equal volume of stop solution (5 M NH$_4$OAc, 100 mM EDTA). To precipitate the RNA, 2.5 volumes of absolute ethanol was added to the mixture followed by incubation at −20 °C for 1 hour. The RNA was pelleted by centrifugation for 30 minutes (21,800 × g, 4 °C), and the pellet was washed with 200 µl 70% ethanol. Upon 5 minutes centrifugation (21,800 × g, 4 °C), the supernatant was removed and the pelleted RNA was dried at 37 °C for 10 minutes. The RNA was resuspended in 20 µl of nuclease-free water and incubated at 37 °C in a thermoshaker (G. Kisker TS-100, 400 rpm) for 1 hour for proper solubilisation. For proper alignment of dsRNA, the samples were denatured at 65 °C without shaking and then renatured by turning off the thermoshaker to cool down to room temperature. The concentration of dsRNA was determined by measuring the absorbance at 260 nm (NanoDrop; Thermo Scientific), and integrity was judged by agarose gel electrophoresis.

2.2.2.5. Knockdown by RNA interference (RNAi)

In eukaryotic cells the knockdown of protein expression can be achieved by RNA interference (Fire et al., 1998). Double-stranded RNAs (dsRNA), with a size of around 500 bp, can be directly transfected into the *Drosophila* cells (Clemens et al., 2000). dsRNAs are processed inside of the cells and bind specifically to the messenger RNA (mRNA). This binding will trigger the degradation of mRNA and suppression of protein expression.

RNAi treatment in S2 cell

To knockdown proteins of interest, dsRNAs were transfected into S2 cells using Effectene® Transfection Reagent (Qiagen, 301425) and the cells were harvested three to four days after transfection. In brief, 1.2 × 10^6 S2 cells were resuspended in 1 ml of Schneider's insect medium and the cells were seeded in a well of a 6-well plate. 15 µg of dsRNA was mixed with Effectene transfection reagent according to the manufacturer's instruction and dropwise added to the cells. After 40 minutes incubation at 26 °C, 1 ml of Schneider's insect medium containing 20% (v/v) FBS and 2% (v/v) Penicillin/Streptomycin was added. The cells were incubated for three to four days at 26 °C. The efficiency of knockdown was confirmed by qPCR (**2.2.2.8**) and Western blot analysis (**2.2.3.7**).

RNAi in flies

RNA interference experiments in flies (Dietzl et al., 2007) was performed using stocks from the VDCR RNAi Library (http://stockcenter.vdrc.at/control/main) carrying RNAi transgene under UAS control (VDRC RNAi #: dCoREST – 34179; – 34180 and – 104900 ; dLSD1 – 106147; dL(3)mbt – 104563; dLint-1 – 105932; dG9a – 25473; dChd3 – 102689; CG9973 – 102273; CG2083 - 110549). For knockdown experiments the GAL4-driver strains engrailed-GAL4 (wing) and bam-GAL4 (germ line) were used, respectively. All flies were collected as virgins before setting up the crosses. Flies were kept at 26 °C or 30 °C in a fly incubator. The efficiency of knockdown was confirmed by qPCR (**2.2.2.8**)

2.2.2.6. Total RNA isolation

Total RNA isolation was performed using the peqGOLD Total RNA Kit (S-Line, Peqlab) according to the manufacturer's instructions from three independent RNAi experiments in S2 cells or from a pool of 50 testes from 3 independent crosses. In brief, after three to four days of knockdown, cells from one well of a 6-well plate or dissected *Drosophila* testes were lysed in 350 μl RNA Lysis Buffer T. DNA was removed by applying the lysate onto the DNA Removing Column, and RNA was isolated following the manufacturer's instruction. RNA was additionally treated with DNase I (peqGOLD DNase I Digest Kit, Peqlab) according to the manufacturer's instruction. Isolated RNA was quantified (NanoDrop; Thermo Scientific) and the integrity was checked by agarose gel electrophoresis.

For RNA-seq analysis, total RNA from dissected *Drosophila* testes was isolated using the TRIzol (invitrogen) reagent according to the manufacturer's protocol. Following chloroform extraction, ethanol precipitation, and DNase digestion, RNAs were purified using a RNeasy Mini Kit (Qiagen) according to manufacturer's instruction.

2.2.2.7. Complementary DNA (cDNA) synthesis

In order to assess the levels of mRNA expression of targeted genes upon RNAi, the RNA was reversely transcribed into first-strand cDNA. cDNA synthesis was carried out in triplicate from 0.2 μg (testis) or 1.0 μg (S2 cells) of isolated RNA using the

SensiFAST™ cDNA Synthesis Kit (Bioline) according to the manufacturer's protocol. In brief, the RNA was diluted with nuclease free water in total volume of 15 μl and mixed with 4 μl 5× TransAmp buffer (containing random hexamer and anchored oligo dT primers) and 1 μl Reverse Transcriptase. The reaction mixture was first incubated at 25 °C for 10 minutes to allow annealing of the primers. Reverse transcription was done by incubating the mixture at 42 °C for 15 minutes, and the reaction was stoped by incubating the mixture at 85 °C for 5 minutes. cDNA was diluted ten times for further use in qPCR reactions.

2.2.2.8. Quantitative PCR (qPCR)

qPCR was performed using the SensiFAST™ SYBR® Lo-ROX Kit (Bioline) on a Mx3000P cycler (Agilent Technologies) according to the instruction manual. In brief, 5 μl 1:10 diluted cDNA was mixed with 15 μl PCR mix in a 0.2 ml Non-skirted 96-well PCR Plate (Thermo-Scientific, AB-0600) and sealed with an Adhesive Sealing Sheets (Thermo-Scientific, AB-0558). The samples were additional mixed by inverting the plate several times and collected by centrifugation.

PCR mix	10.0 μl 2× SensiFAST SYBR® Lo-ROX Mix
	0.8 μl 10 μM forward primer (2.1.6.4)
	0.8 μl 10 μM reverse primer (2.1.6.4)
	3.4 μl H$_2$O

Real-time PCR conditions were used as follow:

Initial denaturation	95 °C	2 min	
Denaturation	95 °C	5 s	
Annealing	60 °C	10 s	40 cycles
Elongation	72 °C	20 s	
Denaturation	95 °C	1 min	
	60 °C	30 s	
Dissociation curve	60 °C → 95 °C	gradually	
	95 °C	30 s	

Cycle threshold (Ct) values for each sample were calculated automatically by the MxPro software. Calculations for relative gene expression were done according to previously described methods (Livak and Schmittgen, 2001). Data presented in the graphs represent mean values of three biological (S2 cells) or three technical (testes)

replicates with standard deviations. For determination of RNA expression in testes, testes from several independent crosses were pooled prior to RNA preparation.

2.2.3. Biochemical methods

If not mentioned otherwise, all buffers used in the experiments in this section were kept at 4 °C and were supplemented before use with protease inhibitors.

	Final concentration
Aprotinin	0.1 mg/ml
Leupeptin	0.1 mg/ml
Pepstatin A	1.4 µg/ml
PMSF	0.2 mM

2.2.3.1. Nuclear extract preparation

Nuclear extracts from S2 cells were made when cells reached 100% confluence. Preparation of nuclear extracts was done according to a modified protocol described previously (Andrews and Faller, 1991). In brief, cells were harvested by scraping from the cell culture dish, washed with ice-cold PBS and resuspended in three volumes of low salt buffer. After incubation on ice for 10 minutes and vortexing for 10 seconds, samples were centrifuged for 1 minute ($21,100 \times g$, 4 °C). The supernatant fraction was discarded and the remaining pellet containing nuclei was resuspended in 1.5 volumes of high salt buffer. The suspension was incubated for 20 minutes on ice for high-salt extraction and subsequently centrifuged for 30 minutes ($21,100 \times g$, 4 °C). The supernatant (nuclear extract) was subjected to gel filtration (**2.2.3.3**), co-immunoprecipitation (**2.2.3.4**) or aliquoted, frozen in liquid nitrogen and stored before use at −80 °C.

Low salt buffer	10.0 mM HEPES, pH 7.6
	1.5 mM MgCl$_2$
	10.0 mM KCl
	1.0 mM DTT
High salt buffer	20.0 mM HEPES, pH 7.6
	1.5 mM MgCl$_2$
	420.0 mM NaCl
	0.2 mM EDTA
	20% (v/v) Glycerol
	1.0 mM DTT

Preparation of nuclear extract from *Drosophila* embryos (0-12 hours after egg deposition) was done as described previously (Kunert and Brehm, 2008).

2.2.3.2. Determination of protein concentration

The protein concentration of nuclear extracts was determined using Bio-Rad's Protein Assay Dye Reagent according to the manufacturer's instructions using BSA (Sigma, A2153-100G) as a standard.

2.2.3.3. Gel filtration analysis of *Drosophila* nuclear extracts

Gel filtration or size exclusion chromatography is a technique that allows separation of proteins according to their molecular weight and shape. To resolve protein complexes, a total of 1 mg of *Drosophila* S2 nuclear extract or embryo (0-12 hours after egg deposition) nuclear extract was fractionated on a Superose™ 6 10/300 GL gel filtration column. This column allows separation of molecules ranging from 44 kDa to 2,000 kDa. Before injection, sample concentration was determined, adjusted to 5 mg/ml, and centrifuged for 15 minutes (21,100 × *g*, 4 °C). Samples were applied to the column using a 200 μL sample loading loop on an Äkta purifier system. Samples were resolved in EX300 buffer to minimise the detection of protein complexes mediated by weak protein-protein interactions. Fractions (0.5 ml) were collected with a F9-R fraction collector following the manufacturer's instructions. Proteins from collected fractions were precipitated using 5 μl StrataClean resin (Agilent, 400714-61) or co-immunoprecipitated using GFP-Trap® (**2.2.3.4**) and subjected to Western blot analysis (**2.2.3.7**).

Elution volumes of proteins with known molecular weights were determined using the Gel Filtration Calibration Kit according to the manufacturer's instructions.

EX300 gel filtration buffer	10.0 mM HEPES, pH 7.6
	1.5 mM $MgCl_2$
	300.0 mM KCl
	0.5 mM EGTA
	10% (v/v) Glycerol

2.2.3.4. Co-immunoprecipitation

For co-immunoprecipitation of endogenous dCoREST, anti-CoREST rabbit polyclonal antibody was cross-linked to Protein G Sepharose and co-immunoprecipitation was performed as previously described (van den Berg et al., 2010). In brief, four independent cross-linking reactions were prepared using 30 µg of anti-CoREST rabbit polyclonal antibody or 30 µg of IgG and 70 µl of Protein G Sepharose. Additionally, the beads were blocked for one hour with 1% Gelatin from cold water fish skin (Sigma, G7765-250ML) and 0.2 mg/ml Albumin from chicken egg white (Sigma, A5253-500G). Cross-linked beads were incubated overnight with 6 mg of S2 nuclear extract. Unbound proteins were removed by washing three times with high salt buffer supplemented with 0.05% NP-40 (Fluka, 74385) for 5 minutes, followed by washing with high salt buffer, and finally two washes with 50 mM $(NH_4)HCO_3$. 10% of the affinity-purified material was electrophoresed and analysed by silver staining (**2.2.3.6**) and the rest was subjected to LC-MS/MS analysis (**2.2.4.1**).

Anti-FLAG co-immunoprecipitation was performed according to the manufacturer's instructions in high salt buffer. 200 µl of anti-FLAG® M2 Affinity Gel was equilibrated and blocked for one hour with 1% Gelatin from cold water fish skin and 0.2 mg/ml Albumin from chicken egg white in high salt buffer. 10 mg of S2 nuclear extract was incubated overnight with 200 µl of beads. Unbound proteins were removed by washing three times with high salt buffer supplemented with 0.05% NP-40 for 5 minutes, followed by washing with high salt buffer, and finally two washes with 50 mM $(NH_4)HCO_3$. 10% of the affinity-purified material was electrophoresed and analysed by silver staining, 10% of the affinity-purified material was electrophoresed and analysed by Western blot (**2.2.3.7**). The rest (80%) was subjected to LC-MS/MS analysis (**2.2.4.1**).

Anti-GFP co-immunoprecipitation of fractions (0.5 ml) collected after gel filtration was performed according to the manufacturer's instructions (GFP-Trap®, chromotek). The fractions were diluted 1:1 with 10 mM HEPES pH 7.6, to lower the salt concentration of KCl to 150 mM, and incubated with 25 µl of equilibrated GFP-Trap® overnight at 4 °C. Unbound proteins were removed by washing four times with IP-150 buffer for 5 minutes and the bound proteins were eluted by incubating the beads with 30 µl of 1×

NuPAGE® LDS Sample Buffer (invitrogen). 20 µl of the eluate was analysed by Western blot (**2.2.3.7**).

Anti-CoREST co-immunoprecipitation of proteins expressed in Sf9 cells was done as follows: 200 µl of Sf9 extracts with comparable amounts of the target proteins were mixed with 1 ml of IP-150 buffer. 3 µl of anti-dCoREST antibody was added to each sample and the reaction was rotated for two hours at 4 °C. Protein G Sepharose 4 Fast Flow beads (GE Healthcare) were blocked for one hour with 0.5 mg/ml BSA and 1% (w/v) Gelatin from cold water fish skin. 20 µl of blocked beads were added to each IP reaction and rotated for one hour at 4 °C. Immune complexes were precipitated by centrifugation for 4 minutes (1,500 × g, 4 °C) and washed four times with 1 ml of IP-150 buffer. Precipitates were eluted with SDS-loading buffer and analysed by SDS-PAGE and Western Blot (**2.2.3.7**).

IP-150 buffer	25.0 mM HEPES, pH 7.9
	150.0 mM NaCl
	12.5 mM MgCl$_2$
	0.1 mM EDTA
	10.0% (v/v) Glycerol
	0.1% (v/v) NP-40

2.2.3.5. SDS-polyacrylamide gel electrophoresis (SDS-PAGE)

Sodium dodecyl sulphate polyacrylamide gel electrophoresis (SDS-PAGE) was done using the XCell SureLock™ Electrophoresis Cell system (invitrogen, novex® Mini-Cell, EI0001) according to standard protocols. In brief, gels were prepared in disposable gel cassettes (invitrogen, novex®, NC2010) using a Rotiphorse® Ready-to-Use Gel Solution 30 (37.5:1). Resolving and stacking gels were made according to manufacturer's instruction (sufficient for 3 gels):

Resolving gel 8% (20 ml)		Stacking gel 5% (5 ml)	
H$_2$O (ml)	9.30	H$_2$O (ml)	3.40
30% acrylamide mix (ml)	5.30	30% acrylamide mix (ml)	0.83
Tris (1.5 M, pH 8.8) (ml)	5.00	Tris (1.0 M, pH 6.8) (ml)	0.63
10% SDS solution (µl)	200	10% SDS solution (µl)	50
10% APS solution (µl)	200	10% APS solution (µl)	50
TEMED (µl)	20	TEMED (µl)	5

For gradient gels, NuPAGE™ 4-12% Bis-Tris Gels (invitrogen, novex®, NP0321BOX) were used following manufacturer's instruction.

Protein samples were premixed with 4× NuPAGE® LDS Sample Buffer and reducing agent, according to the manufacture's instruction, and incubated at 70 °C for 10 minutes prior to loading. PageRuler™ Prestained Protein Ladder (5 μl) and Spectra™ Multicolor HighRange Protein Ladder (7 μl) were used as molecular weight standards. Proteins were electrophoresed at a constant voltage of 80 V in the stacking gel and at 150-180 V in the resolving gel. Gels were afterwords subjected to silver staining (**2.2.3.6**) or Western blotting (**2.2.3.7**).

SDA-PAGE running buffer	25 mM Tris
	192 mM Glycine
	0.1% SDS (w/v)

2.2.3.6. Silver staining of SDS-PAGE gels

Silver staining of protein gels was done with the SilverQuest™ Staining Kit (invitrogen, LC6070) according to manufacturer's instruction. After separating proteins by SDS-PAGE, gels were rinsed with water and fixed in 40% ethanol / 10% acetic acid for 20 minutes to overnight. Fixing solution was washed out by agitating the gels in 30% ethanol for 10 minutes and the gels were incubated in sensitising solution for 10 minutes. Sensitiser was washed out by agitating gels first in 30% ethanol and then in water for 10 minutes. Staining of the gels was done by incubating the gels for 15 minutes in staining solution, and after 1 minute washing with water, the proteins were visualised by incubating the gel in the developing solution. After the appropriate staining intensity was achieved, stopping solution was added directly and incubated for 10 minutes. Finally, the gels were rinsed and stored in water. Gels were imaged on Bio-Rad ChemiDoc System and processed in Image Lab™ software (Bio-Rad) and Inkscape.

2.2.3.7. Western blotting

For detection of proteins with specific antibodies in Western blot experiments, proteins samples were first subjected to SDS-PAGE and transferred onto polyvinylidene fluoride

(PVDF) membrane following the manufacturer's protocol (Mini Trans-Blot®
Electrophoretic Transfer Cell, Bio-Rad). In brief, the PVDF membrane was activated in
methanol for 1 minute, before assembling the gel sandwich for transfer. The gel
sandwich was assembled in the cassette of Mini Trans-Blot® Electrophoretic Transfer
Cell according to the instruction manual. The transfer was done for 2 hours at 400 mA
constant current using pre-cooled Pierce™ Western Blot Transfer Buffer (Thermo
Scientific, 35040). During the transfer a block of ice was added inside the chamber and
the transfer was carried out on ice.

After the transfer, the membrane was washed once in TBST. All incubation and washing
steps were carried out on a rocking platform. Next, the membrane was blocked for 1
hour in blocking solution (5% Powdered milk in TBST; Roth T145.2) at room
temperature to reduce non-specific binding of the antibody. After blocking, the
membrane was incubated overnight at 4 °C with a primary antibody raised against the
protein of interest. The dilution of primary antibodies was done in blocking solution
according to **Table 2.2**. On the next day the membrane was washed 4 times for 10
minutes in TBST and subsequently incubated for 2 hours at room temperature with the
appropriate HRP-conjugated secondary antibody. The dilution of secondary antibodies
was done in blocking solution according to **Table 2.3**. An excess of the secondary
antibody was removed by four washing steps in TBST and the antigen-antibody
complex was detected by chemiluminescence. The membrane was incubated for 2
minutes with the Immobilon™ Western Chemiluminescent HRP Substrate solution and
exposed to ^{Super}RX Fuji Medical X-ray films following the manufacturer's instruction.
In order to re-probe the membrane with a different antibody, it was stripped using the
Restore™ PLUS Western Blot Stripping Buffer (Thermo Scientific, 46430) following
the manufacturer's instruction. After stripping, the membrane was re-probed as
described above.

2.2.4. Sequencing methods and data analysis

2.2.4.1. LC-MS/MS data acquisition and data analysis

LC-MS/MS sample preparation and analysis was carried out according to methods
described previously (Schmidt et al., 2014) in collaboration with Dr Ignasi Forné.

Briefly, after immunoaffinity purification, beads were washed with 50 mM (NH$_4$)HCO$_3$ and incubated with 10 ng/μl Trypsin in 1 M urea, 50 mM (NH$_4$)HCO$_3$ for 30 minutes, washed with 50 mM (NH$_4$)HCO$_3$ and the supernatant was digested overnight in the presence of 1 mM DTT. Digested peptides were alkylated and desalted prior to LC-MS/MS analysis.

For LC-MS/MS purposes, desalted peptides were injected in an Ultimate 3000 RSLCnano system (Thermo), separated in a 15-cm analytical column (75 μm ID home-packed with ReproSil-Pur C18-AQ 2.4 μm from Dr. Maisch) with a 50-min gradient from 5 to 60% acetonitrile in 0.1% formic acid. The effluent from the HPLC was directly electrosprayed into a Qexactive HF (Thermo) operated in data dependent mode to automatically switch between full scan MS and MS/MS acquisition. Survey full scan MS spectra (from m/z 375–1,600) were acquired with resolution R=60,000 at m/z 400 (AGC target of 3×10^6). The 10 most intense peptide ions with charge states between 2 and 5 were sequentially isolated to a target value of 1×10^5, and fragmented at 27% normalised collision energy. Typical mass spectrometric conditions were: spray voltage, 1.5 kV; no sheath and auxiliary gas flow; heated capillary temperature, 250 °C; ion selection threshold, 33,000 counts. MaxQuant 1.5.2.8 was used to identify proteins and quantify by iBAQ with the following parameters:

Database	Uniprot_0803_Dmelanogaster_20180723
MS tol	10 ppm
MS/MS tol	20 ppm
Peptide FDR	0.1
Protein FDR	0.01
Min. peptide length	5
Variable modifications	Oxidation (M)
Fixed modifications	Carbamidomethyl (C)
Peptides for protein quantitation	razor and unique
Min. peptides	1
Min. ratio count	2

Identified proteins were analysed in Perseus with a *t*-test adjusted for multiple comparisons.

2.2.4.2. Sequencing of ChIP samples and data analysis

The libraries for ChIP-seq analysis were prepared from 500 pg of DNA using MicroPlex Library Preparation Kit v2 following manufacturer's instructions including library size selection using AMPure XP beads. In collaboration with Dr Andrea Nist, the quality of sequencing libraries was controlled on a Bioanalyzer 2100 using the Agilent High Sensitivity DNA Kit (Agilent). Pooled sequencing libraries were quantified with digital PCR (QuantStudio 3D, Thermo Fisher) and sequenced on the NextSeq 550 platform (Illumina) using a high output v2.5 flow cell and 50 base single reads.

Raw Illumina sequence reads were aligned to *D. melanogaster* genome (BDGP6_dm6, ucsc) with the Bowtie2 tool and peak calling was performed with the MACS2 callpeak tool using the Galaxy Server of University of Giessen (default settings). Peaks were filtered using fold change values ≥4 and pileup values ≥35. Genomic distribution of the peaks was analysed using CEAS: Enrichment on chromosome tool and diagrams were generated using the Venn Diagram tool of Cistrome Galaxy server.

2.2.4.3. Sequencing of RNA and data analysis

RNA quality check, library preparation and data analysis were done in collaboration with Dr Andrea Nist and Dr Boris Lamp. RNA integrity was assessed on an Experion StdSens RNA Chip (Bio-Rad). RNA-seq libraries were prepared using a TruSeq Stranded mRNA Library Prep kit (Illumina). Libraries were quantified on a Bioanalyzer (Agilent Technologies) and were sequenced on an Illumina HiSeq 1500 platform, rapid-run mode, single-read 50 bp (HiSeq SR Rapid Cluster Kit v2, HiSeq Rapid SBS Kit v2, 50 cycles) according to the manufacturer's instructions.

For transcriptome analysis, sequenced reads were aligned to the *Drosophila melanogaster* genome (Ensembl revision 89) using STAR (version 2.4.1a) (Dobin et al., 2013). Fragments per kilobase per million (FPKM) were calculated based on the total raw read count per gene and length of merged exons. For the study with cultured S2 cells, differential expression was assessed using DESeq2 (version 1.12.3) (Love et al. 2014). To investigate differential gene expression of pooled *Drosophila* testes, log2FC values were calculated between the log2 medians of each group after a constant of 1/60 to avoid undefined algorithms. For both analyses, genes that did not yield a minimum

raw count of 50 and a minimum FPKM of 0.3 in at least two samples were discarded due to insufficient coverage. Of the remaining genes, genes were considered differentially expressed if the absolute of the log2FC was at least 1 (twofold induction/ repression), and in case of DESeq2 analysis if the corrected p-value was less or equal 0.05.

2.2.5. Phase contrast and immunofluorescence microscopy

Triple-bam-GAL4 female virgins (bam-GAL4/bam-GAL4;CyO/Sp;Sb/Bam-GAL4) were crossed with males of appropriate UAS-RNAi-lines (CoREST: VDRC-34179/GD and LSD1(Su(var)3-3): VDRC-10647/KK). Offsprings were raised in standard conditions (26 °C).

For dissection and imaging up to 1-day old males were used. Only males that were non-Sb (carried 2×bam-GAL4) were selected. As controls, UAS-RNAi lines were used. Dissected testes were placed in a drop of PBS on lysin-coated slides and covered with coverslips. The slides were imaged at 10× and 20× objective lenses in phase contrast using a Leica DMR microscope equipped with a Quantifire-X1 camera (Intas Science Imaging Instruments). For imaging spermatocytes, testes were additionally squashed by removing PBS from under the coverslip.

Immunofluorescence staining of squashed testis was carried out essentially as described before (Rathke et al., 2010; Rathke et al., 2007; Hundertmark et al., 2017) and was done in cooperation with Dr Ina Theofel.

Images were processed and assembled in GIMP and Inkscape.

"If you torture the data enough, nature will always confess."

— Ronald H. Coase,
"How should economists choose?" Warren Nutter Lecture, 1981

3.1. *Drosophila* CoREST isoforms

The *Drosophila melanogaster* gene encoding *CoREST* is located on the X chromosome (FlyBase ID: FBgn0261573; X:19,521,929..19,530,896; r6.31). In macrophage-like S2 cells alternative splicing produces two main protein isoforms of dCoREST: dCoREST-L and dCoREST-M (Dallman et al., 2004). A unique 234 amino acid insertion is present in dCoREST-L that separates the two SANT domains of dCoREST (**Figure 3.1**).
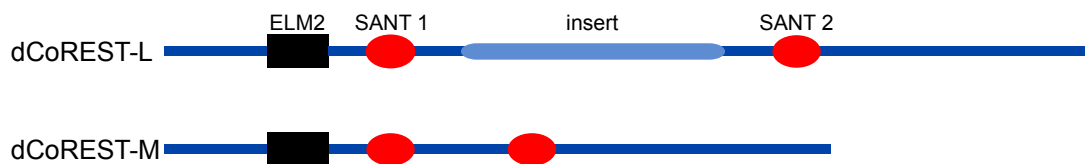
Figure 3.1. **Schematic representation of two major protein isoforms of *Drosophila* CoREST.** Black rectangles depict ELM2 domains and red ovals indicate SANT domains. The thick blue line represents a 234 amino acid insert unique to dCoREST-L.

Both dCoREST isoforms can be found in the dL(3)mbt-interacting protein (LINT) complex in *Drosophila* Kc cells (Meier et al., 2012). In the LINT complex, dCoREST associates with the malignant brain tumour (MBT) domain-containing protein dL(3)mbt, dLint-1 and the histone deacetylase dRPD3. According to the results from Meier et al. 2012, a significant portion of dCoREST is not associated with the LINT complex. I, therefore, hypothesised that additional dCoREST-containing complexes could exist. To test this hypothesis, I performed fractionation of nuclear extracts from S2 cells using size exclusion chromatography and analysed fractions by Western blot.

Western blot analysis revealed that only a minor fraction of dCoREST co-eluted with the LINT signature subunit dL(3)mbt (**Figure 3.2**). Most of dCoREST-L and dCoREST-M eluted in fractions with an apparent molecular mass of more than 440 kDa. Some dCoREST-L and dCoREST-M fractions contained little (fractions #21 and #23) or no

detectable (fractions #25 and #27) dL(3)mbt. These results indicated that dCoREST is a component of additional protein assemblies other than LINT. This gel filtration experiment also revealed that dCoREST-L (main peak in fraction #23) and dCoREST-M (main peak in fraction #25) do not peak in the same fractions pointing to the existence of isoform-specific complexes.
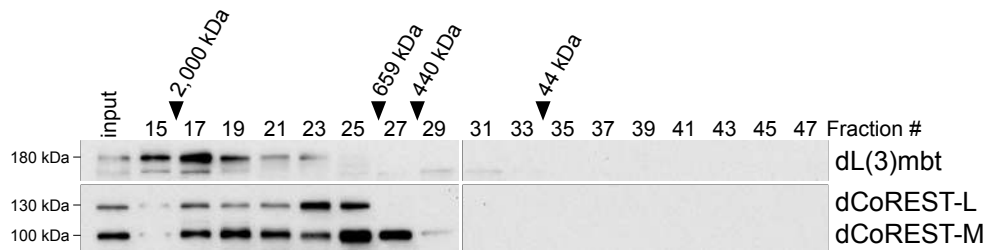
Figure 3.2. dCoREST-L and dCoREST-M have distinct elution profiles upon gel filtration.
Nuclear extract from S2 cells was fractionated over a Superose 6 column. Fractions were analysed by Western blot using the antibodies indicated on the right. Notably, anti-dCoREST antibody recognises both dCoREST isoforms. Fraction numbers and molecular mass standards are denoted on top. Input: 5% of extract loaded onto the column.

3.2. Identification of putative dCoREST interactors

Gel filtration of S2 nuclear extract revealed that dCoREST isoforms elute in high molecular fractions suggesting the existence of additional complexes. Moreover, partial overlap with the LINT complex signature subunit dL(3)mbt suggested that these additional complexes likely contain other proteins than the LINT subunits. Hence, I sought to identify novel interactors of dCoREST. Therefore I co-immunopurified dCoREST-interacting proteins from S2 nuclear extract using an antibody directed against both dCoREST isoforms (Dallman et al. 2004). In order to determine the efficiency of immunoaffinity purification, samples were subjected to Western blot analysis. Co-immunoprecipitation of dCoREST depleted most of dCoREST from the nuclear extract (**Figure 3.3.A**; compare lane 1 with lane 4). Analysis of the co-immunoprecipitated material by SDS-PAGE followed by silver staining revealed several proteins that specifically co-purified with dCoREST-L/-M, but were absent in controls (**Figure 3.3.B**; compare lane 3 with lanes 1 and 2).

Additionally, co-purified proteins were analysed by mass spectrometry (LC-MS/MS). The analysis identified 373 proteins as putative dCoREST interactors (**Figure 3.4** and **Appendix Table A1**).

B   IgG
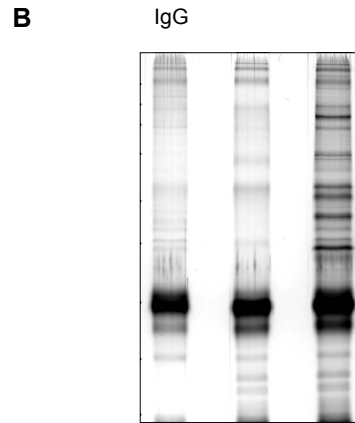
Figure 3.3. Anti-CoREST affinity purification of endogenous dCoREST.
(A) Nuclear extracts from S2 cells were subjected to IgG (lane 2) or anti-CoREST (lane 4) affinity purification and analysed by Western blot using an anti-CoREST antibody. As an additional control, the anti-dCoREST antibody not incubated with nuclear extract was used (lane 3). Input: 5% of extract used for CoIP. FT: flow-through. **(B)** Nuclear extracts from S2 cells were subjected to IgG (lane 1) or anti-CoREST (lane 3) affinity purification and the bound material was analysed by SDS-PAGE and silver staining. As an additional control the anti-dCoREST antibody not incubated with nuclear extract was loaded (lane 2).

Figure 3.4. LC-MS/MS identification of endogenous dCoREST interactors.
Volcano plot with −log10 p-values (y-axis) and log2 iBAQ fold-difference (x-axis) after comparison of anti-CoREST affinity purification versus IgG control. The point labeled "dCoREST-M" was derived from peptides common to dCoREST-M and dCoREST-L. The point labeled "dCoREST-L" was derived from peptides mapping the insert region that is exclusive to dCoREST-L. The complete list of the interacting proteins is presented in Appendix Table A1 (n=4, FDR=0.01, s0=2).

As expected, all four components of the LINT complex (dL(3)mbt, dLint-1, dRPD3 and dCoREST) were strongly enriched in the immunoprecipitate. In addition, two histone modifying enzymes were also enriched — the histone demethylase dLSD1 and the H3K9 histone methyltransferase dG9a. These results demonstrate that dCoREST interacts with proteins outside of the LINT complex and support the hypothesis that additional dCoREST complexes exist.

3.2.1. An isoform-specific dLSD1/dCoREST complex

Previous biochemical studies in mammalian cells identified CoREST as a subunit of the LSD1/CoREST complex (Humphrey et al., 2001; You et al., 2001; Hakimi et al., 2002; Lee et al., 2005; Shi et al., 2005).

Both CoREST and LSD1 are conserved in *Drosophila* (Dallman et al., 2004; Shi et al., 2004). When both dCoREST-L and dLSD1 proteins are over-expressed in S2 cells, they can interact implying that this interaction is also conserved between mammals and *Drosophila* (Dallman et al., 2004).

In addition, LC-MS/MS analysis of affinity purified endogenous dCoREST identified three potential subunits of a putative *Drosophila* LSD1/CoREST complex: dLSD1, dCoREST and the HDAC1/2 homologue dRPD3.

Figure 3.5. dLSD1 is an isoform-specific dCoREST-L interactor.
Nuclear extracts from control S2 cells (mock, lanes 1 and 2) and S2 cells stably expressing FLAG-dLSD1 (lanes 3 and 4) were precipitated with an anti-FLAG antibody (lanes 2 and 4) and analysed by Western blot using the antibodies indicated on the right. Notably, the anti-dCoREST antibody recognises both dCoREST isoforms. Lanes 1 and 3: 1% input.

In order to investigate if dLSD1 and dCoREST form a stable complex, I generated an S2 cell line allowing the copper-inducible expression of FLAG-tagged dLSD1 (**Figure 3.5**). Western blot analysis upon FLAG-affinity purification from nuclear extracts of copper-treated cells revealed that dLSD1 co-purified with dRPD3 and dCoREST-L. These data support the existence of a dLSD1/dCoREST complex. Interestingly, dCoREST-M was not detected in the dLSD1 immunoprecipitate suggesting that dLSD1 binds dCoREST in an isoform-specific manner.

Furthermore, I established two S2 cell lines for inducible expression of FLAG-tagged dCoREST-L and FLAG-tagged dCoREST-M, respectively (**Figure 3.6.A**). Western blot

analysis of anti-FLAG co-immunoprecipitates showed no interaction of dLSD1 with FLAG-tagged dCoREST-M (**Figure 3.6.B**). By contrast, dLSD1 efficiently co-purified with FLAG-tagged dCoREST-L. This isoform-specificity of the dLSD1 interaction was not observed for subunits of the LINT complex: dL(3)mbt, dLint-1 and dRPD3 all co-precipitated with both dCoREST-L and dCoREST-M.
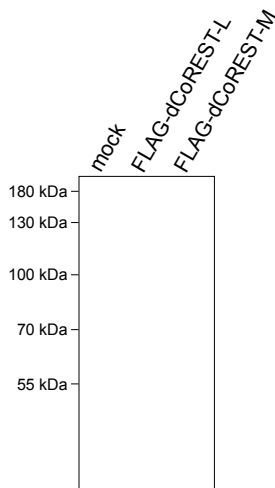
Figure 3.6. Anti-FLAG affinity purification of FLAG-tagged dCoREST-L and dCoREST-M.
(A) Stable expression of FLAG-dCoREST-L and FLAG-dCoREST-M in S2 cells. Nuclear extracts from control cells (mock, lane 1) and cells stably expressing FLAG-dCoREST-L (lane 2) and FLAG-dCoREST-M (lane 3) were analysed by anti-FLAG Western blot. **(B)** Nuclear extracts from control S2 cells (mock, lanes 1 and 4), S2 cells stably expressing FLAG-dCoREST-L (lanes 2 and 5) or FLAG-dCoREST-M (lanes 3 and 6) were immunoprecipitated with an anti-FLAG antibody (lanes 4 to 6) and analysed by Western blot using the antibodies indicated on the right. dMi-2 served as a negative control. Notably, the anti-dCoREST antibody recognises both dCoREST isoforms. Lanes 1–3: 10% input.

FLAG-dCoREST-L and FLAG-dCoREST-M co-immunoprecipitates were also analysed by LC-MS/MS. The four LINT subunits were strongly enriched in both interactomes (**Figure 3.7**; **Appendix Table A2** and **Appendix Table A3**). By contrast, dLSD1 was significantly enriched in the dCoREST-L interactome only.

Additionally, pairwise co-infection of Sf9 cells with baculoviruses expressing recombinant dLSD1 and dCoREST-L or dLSD1 and dCoREST-M followed by anti-CoREST co-immunoprecipitation confirmed that dLSD1 preferentially interacts with dCoREST-L (data generated by Jonathan Lenz; **Figure 3.8**). This data showed that the isoform-specific interaction of dLSD1 with dCoREST-L can be recapitulated with recombinant proteins.

A

dLint-1
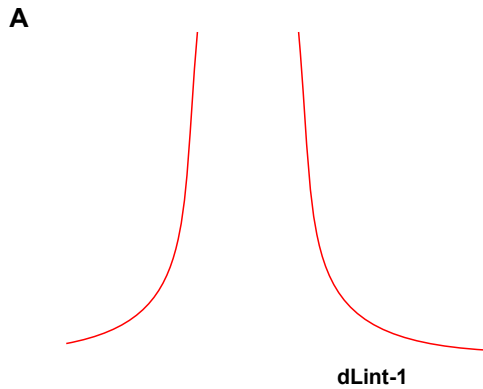
Figure 3.7. LC-MS/MS identification of dCoREST-L and dCoREST-M interactors.
Volcano plot with −log10 *p*-values (y-axis) and log2 iBAQ fold-difference (x-axis) between the mock control and either the FLAG-CoREST-L affinity purification **(A)** or the FLAG-CoREST-M affinity purification **(B)**. The complete list of the interacting proteins is presented in Appendix Tables A2 and A3. (*n*=4, FDR=0.2, s0=1).

Figure 3.8. dLSD1 preferentially interacts with dCoREST-L.
Sf9 cells were co-infected with recombinant baculoviruses directing the expression of dLSD1, dCoREST-L and/or dCoREST-M, as indicated on top. Extracts were immunoprecipitated with an anti-CoREST antibody and analysed by Western blot using the antibodies indicated on the right. Notably, the anti-dCoREST antibody recognises both dCoREST isoforms. Lanes 1-5: 5% input.

Taken together, these results support the hypothesis that dLSD1 and dCoREST-L, but not dLSD1 and dCoREST-M, form a stable complex.

3.2.2. A novel dG9a/dCoREST complex

LC-MS/MS analysis identified, in addition to LINT subunits and dLSD1, the H3K9-specific methyltransferase dG9a as one of the most abundant interaction partners of endogenous dCoREST (**Figure 3.4** and **Appendix Table A1**). dG9a was also highly enriched in immunoprecipitates according to LC-MS/MS analysis of anti-FLAG affinity purified FLAG-tagged dCoREST-L, as well as FLAG-tagged dCoREST-M (**Figure 3.7**; **Appendix Tables A2** and **Appendix Tables A3**). Western blot analysis of the

immunoprecipitates from both FLAG-tagged dCoREST isoforms also detected dG9a (**Figure 3.6**).

B
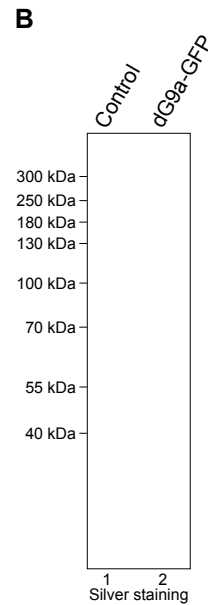
Figure 3.9. dG9a is a novel dCoREST-interacting protein.
(A) Nuclear extracts from control S2[Cas9] cells (lanes 1, 3 and 5) and a dG9a-GFP tagged S2[Cas9] cell line (lanes 2, 4 and 6) were subjected to the anti-GFP affinity purification (lanes 5 and 6) and analysed by Western blot using the antibodies indicated on the right. Notably, the anti-dCoREST antibody recognises both dCoREST isoforms. Lanes 1 and 2: 1% input. Lanes 3 and 4: 1% flow through (FT).
(B) SDS-PAGE followed by silver staining of anti-GFP affinity purified nuclear extracts from control S2[Cas9] cells (lane 1) and a dG9a-GFP tagged S2[Cas9] cell line (lane 2).

To confirm the interaction of dCoREST and dG9a, I utilised genomic tagging by CRISPR/Cas9 in *Drosophila* cells. I added a sequence encoding the GFP-tag to the 3' end of the endogenous dG9a coding sequence. Nuclear extracts from S2 cells expressing tagged dG9a were subjected to anti-GFP purification. As a control S2 cells with non-tagged dG9a were used. Western blot analysis of immunoprecipitated dG9a-GFP fusion protein confirmed both dCoREST isoforms, as well as dRPD3 as interactors of dG9a (**Figure 3.9.A**). Notably, dG9a showed a higher binding preference towards dCoREST-M compared to dCoREST-L, as judged by Western blot results. By contrast, neither dL(3)mbt nor dLSD1 were recovered to a greater extent.

These results suggest that dG9a is not part of the LINT or the dLSD1/dCoREST complexes, but forms a separate complex with dCoREST and dRPD3.

According to Western blot (**Figure 3.9.A**), less than 1% of dCoREST could be recovered after anti-GFP affinity purification. Hence, I sought to determine if dG9a forms a stoichiometric complex with dCoREST. To answer this question, I analysed

dG9a-GFP purified from nuclear extracts by SDS-PAGE and silver staining (**Figure 3.9.B**). The results showed that four polypeptides, ranging in apparent molecular masses from 250 kDa to 300 kDa, were co-purified. These masses correspond well to the mass expected for dG9a-GFP. It is currently not known if these polypeptides represent isoforms of dG9a, post-translationally modified dG9a, degradation products or, indeed, interaction partners.
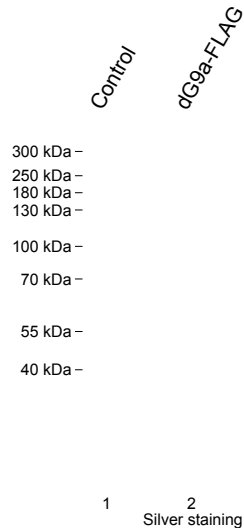
Figure 3.10. Anti-FLAG affinity purification of FLAG-tagged dG9a.
SDS-PAGE followed by silver staining of anti-FLAG affinity purified nuclear extracts from control S2[Cas9] cells (lane 1), a dG9a-FLAG tagged S2[Cas9] cell line (lane 2) and a FLAG-dG9a tagged S2[Cas9] cell line (lane 3).

This result clearly shows that under these conditions the purification did not recover polypeptides with apparent molecular masses similar to those of dCoREST-L, dCoREST-M or dRPD3. To exclude that the addition of the GFP-tag to the C-terminus of endogenous dG9a could disrupt interactions with dCoREST and dRPD3, I used CRISPR/Cas9 to create two additional cell lines where endogenous dG9 was tagged with a FLAG-tag at the N-terminus or the C-terminus, respectively. After anti-FLAG affinity purification of nuclear extracts from these cell lines, samples were electrophoresed and the SDS-PAGE gel was silver stained. Again, there were no bands with molecular masses similar to those of dCoREST or dRPD3 enriched compared the control (**Figure 3.10**).

In conclusion, these biochemical data suggest the existence of a novel CoREST complex in *Drosophila* — the dG9a/dCoREST complex. But, one must point out that the majority of dG9a molecules in *Drosophila* S2 cells nuclear extract are likely not

stably associated with dCoREST. Hence, I concluded that the bulk of dG9a is not in a complex with dCoREST and dRPD3, but rather in a still unidentified complex or exist as an entity outside of any complex.

3.3. Three distinct dCoREST complexes

The proteomic analyses suggest the existence of at least three distinct dCoREST/histone deacetylase complexes in *Drosophila*: the LINT complex, a dLSD1/dCoREST complex and a dG9a/dCoREST complex. All three complexes share a common dCoREST/ dRPD3 core and are differentiated by specific signature subunits.
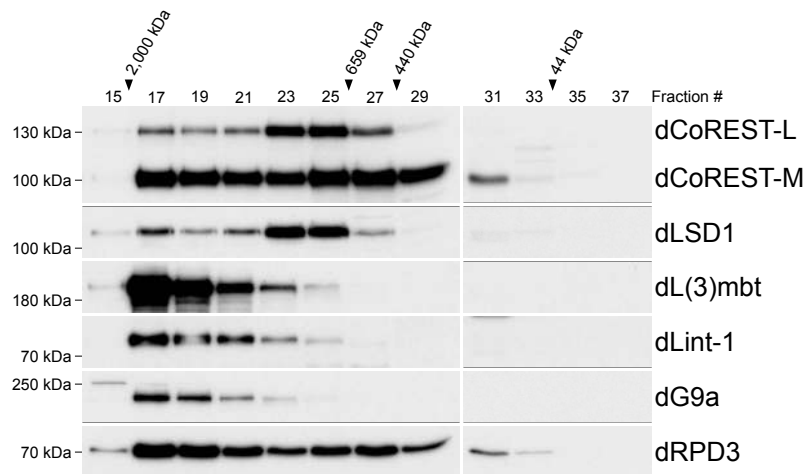
Figure 3.11. dCoREST interactors co-elute during gel filtration of S2 nuclear extract.
A total of 1 mg of nuclear extract from S2 cells was fractionated over a Superose 6 column. Fractions were analysed by Western blot using the antibodies indicated on the right. Notably, the anti-dCoREST antibody recognises both dCoREST isoforms. Fraction numbers and molecular mass standards are denoted on top.

In order to provide further support for this hypothesis, I applied S2 nuclear extract (**Figure 3.11**) and *Drosophila* embryo extract (**Figure 3.12**) to size exclusion chromatography fractionation. Wester blot analysis of obtained fractions showed the following: dCoREST-L, dCoREST-M and dRPD3 were detected in several fractions, in both extracts, representing a broad range of apparent molecular masses (440 kDa to >2,000 kDa). This is in agreement with the concept that these proteins are components of several distinct complexes. dLSD1 and dCoREST-L co-eluted in the same peak fractions #23 and #25 (S2 nuclear extract) and fractions #22 and #24 (embryo nuclear extract), further supporting the hypothesis that dLSD1 and dCoREST-L form a complex.

Contrary to dLSD1, dL(3)mbt and dLint-1 co-eluted in the same peak fraction #17 (S2 nuclear extract) and #16 (embryo nuclear extract). Interestingly, dG9a co-eluted with these LINT subunits in S2 nuclear extract (fraction #17), but not in embryo nuclear extract (peak fraction #18).
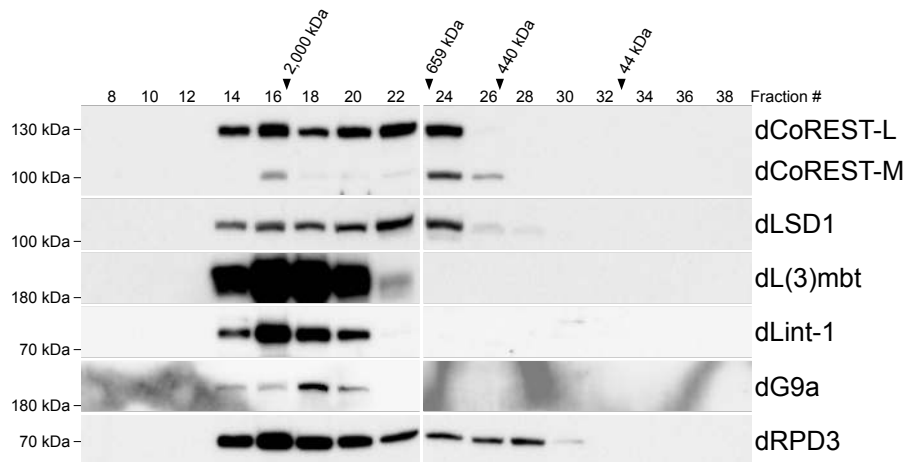
Figure 3.12. dCoREST interactors co-elute during gel filtration of *Drosophila* embryo extract. Nuclear extract from *Drosophila* embryos (1 mg) was fractionated over a Superose 6 column. Fractions were analysed by Western blot using the antibodies indicated on the right. Notably, the anti-dCoREST antibody recognises both dCoREST isoforms. Fraction numbers and molecular mass standards are denoted on top.
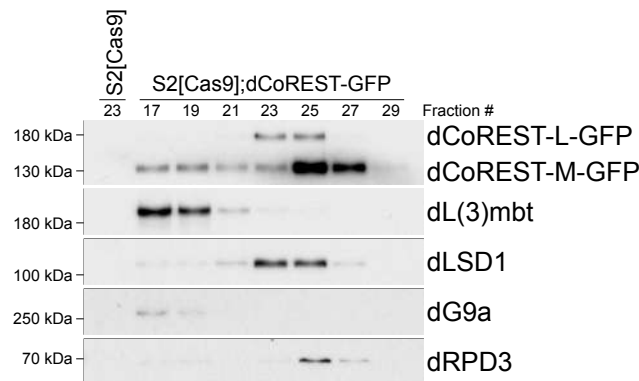
Figure 3.13. Anti-GFP affinity purification of dCoREST-GFP after gel filtration fractionation. A total of 1 mg of nuclear extract from S2[Cas9];dCoREST-GFP cells was fractionated over a Superose 6 column. Fractions were co-immunoprecipitated using the GFP-Trap resin and analysed by Western blot using the antibodies indicated on the right. Fraction numbers and molecular mass standards are denoted on top. Fraction #23 from non-tagged parental S2[Cas9] cells was used as a control.

In addition, I separated nuclear extracts of S2 cells expressing GFP-tagged dCoREST by gel filtration. I further immunoprecipitated GFP-tagged CoREST from the CoREST-containing fractions with a GFP-antibody and analysed the immunoprecipitates by Western blot (**Figure 3.13**). The results revealed that the dCoREST interaction partners; dRPD3, dLSD1, dL(3)mbt, dLint-1 and dG9a; did not only co-elute with dCoREST, but

were indeed physically associated with dCoREST in their respective gel filtration fractions.

This result further supported the hypothesis that three distinct dCoREST complexes exist as separate entities and can be isolated by both immunoprecipitation and gel filtration. Moreover, the similarity of gel filtration profiles derived from S2 nuclear extract and *Drosophila* embryo nuclear extract indicates that these complexes are present in different cell types.

3.4. Chromatin binding by dCoREST complexes

The biochemical experiments performed with soluble nuclear fractions of S2 cells suggested that three distinct dCoREST complexes exist. Furthermore, subunits of identified complexes are histone modifying enzymes and, in the LINT complex, histone modification reader. Therefore I hypothesised that these complexes are associated with chromatin. Moreover, it could be plausible that the signature subunits are involved in differential binding of identified complexes.
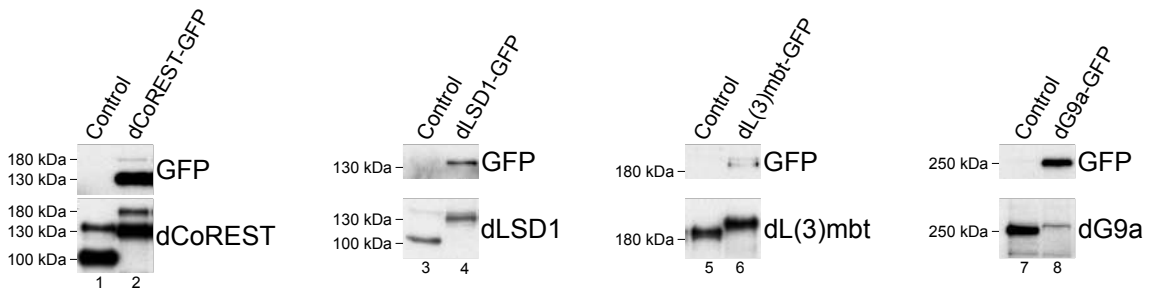
Figure 3.14. Endogenous tagging of dCoREST and its interactors.
Endogenously tagged cell lines were analysed by Western blot using anti-GFP antibody or antibody corresponding to the analysed protein. Note that in the dCoREST-GFP cell line both dCoREST isoforms are present.

To provide evidence for this hypothesis I performed ChIP-seq analyses of dCoREST and its interactors in S2 cells. Using CRISPR/Cas9-mediated genome editing I generated S2 cell lines expressing GFP-tagged dCoREST, the LINT subunit dL(3)mbt, dLSD1 or dG9a, respectively (**Figure 3.14**). This allowed me to determine the genome-wide binding profiles for these proteins by ChIP-seq using the same antibody (anti-GFP antibody) in each case.

ChIP-seq analysis identified 4,855 dCoREST binding sites in the *Drosophila* genome. Moreover, the distribution of dCoREST binding sites showed that dCoREST is greatly enriched at promoters (**Figure 3.15**). This implied a role of dCoREST in the regulation of transcription.
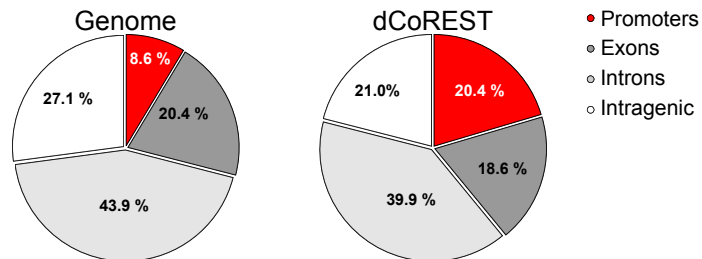
Figure 3.15. dCoREST binding is enriched at promoter regions of *Drosophila* genome. Genome-wide binding profiles of dCoREST by ChIP-seq analysis showed that dCoREST binding sites are greatly enriched in promoters.

My analysis also revealed that about 73.6% of dCoREST sites are also bound by dL(3)mbt. About 73.4% of all dL(3)mbt sites are also bound by dCoREST. In contrast to this significant overlap between dCoREST and dL(3)mbt binding sites, only 17.6% dCoREST sites are co-occupied by dLSD1. Conversely, dCoREST is associated with 79.0% of all dLSD1 binding sites. Similar to dLSD1, only 18.6% of dCoREST sites are co-occupied by dG9a, whereas dCoREST is associated with about 59.0% of all dG9a binding sites (**Figure 3.16.A** and **Figure 3.16.B**).

These data suggest that the LINT complex is more abundant on chromatin than either the dLSD1/dCoREST or the dG9a/dCoREST complexes. Moreover, the majority of dLSD1 bind chromatin as part of the dLSD1/dCoREST complex. Besides, more than half of dG9a binding sites are a part of the dG9a/dCoREST assembly, but it is clear that a significant fraction of dG9a (41.0%) associates with chromatin independently of dCoREST.

Further analysis shows that only 10.2% and 7.3% of all dL(3)mbt sites are co-occupied by dLSD1 and dG9a, respectively (**Figure 3.17**). This limited overlap further supports the hypothesis that the LINT complex is largely distinct from the dLSD1/dCoREST and the dG9a/dCoREST assemblies.

Taken together, the three dCoREST complexes that were defined by analysing soluble nuclear extract are indeed found associated with chromatin as separate entities, as judged by the results of ChIP-seq analysis.

A

B
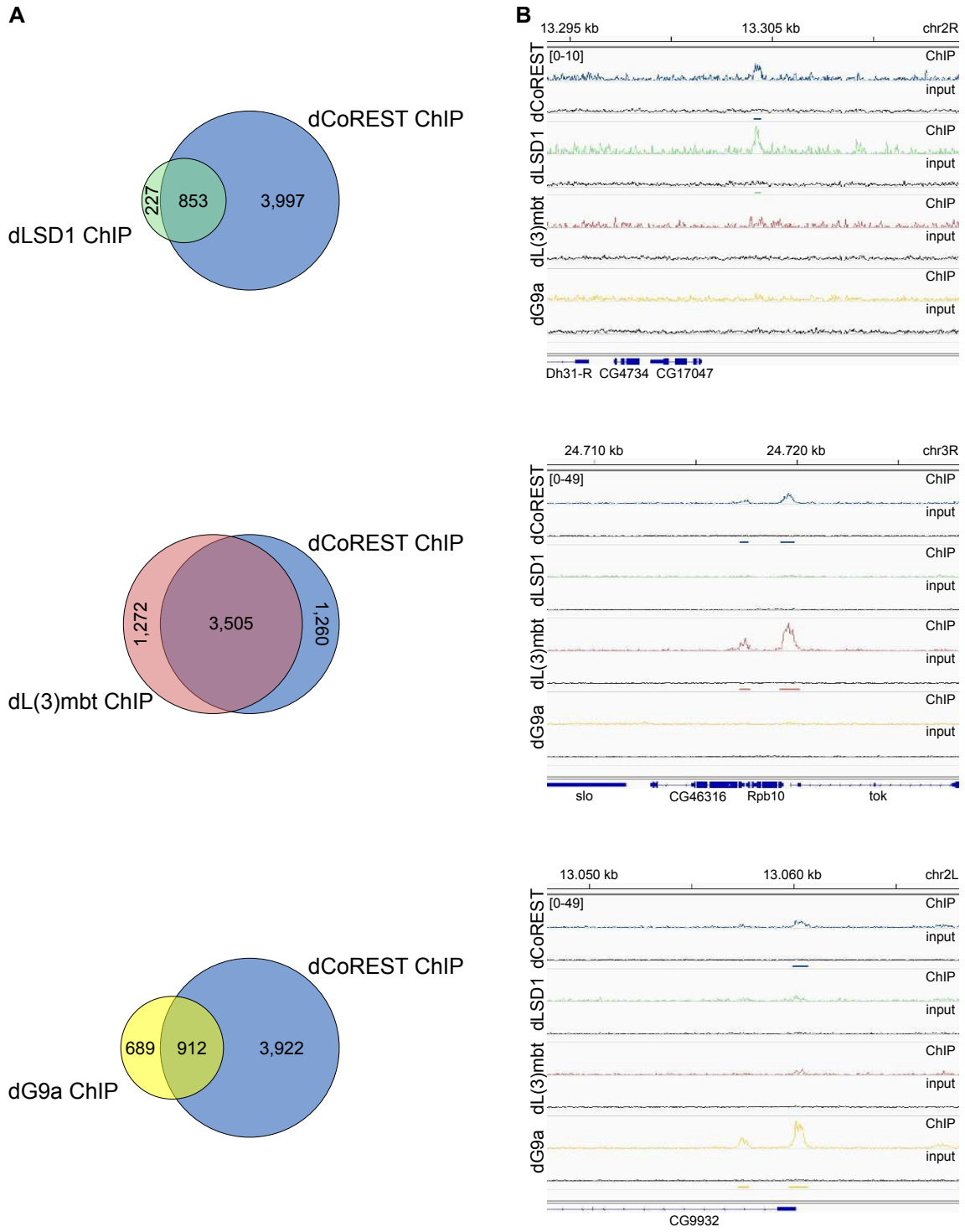
Figure 3.16. Comparison of binding sites of dCoREST complexes.
(A) Venn diagrams depicting shared and unique ChIP-seq peaks for dCoREST and dLSD1 (top panel), dCoREST and dL(3)mbt (middle panel), and dCoREST and dG9a (bottom panel). Note that one peak of one data set can simultaneously overlap with two or more peaks of the data set it is compared to. As a consequence, the total number of peaks for any given protein is slightly different between Venn diagrams. Precise numbers of peaks identified are as follows: dCoREST — 4,855; dLSD1 — 1,126; dL(3)mbt — 4,785; dG9a — 1,614. **(B)** Genome browser view of dCoREST and dLSD1 (top panel), dCoREST and dL(3)mbt (middle panel), and dCoREST and dG9a (bottom panel) chromatin associations. Data were visualised in the Integrative Genomics Viewer (Version 2.6.2) and snapshots were taken from representative regions.
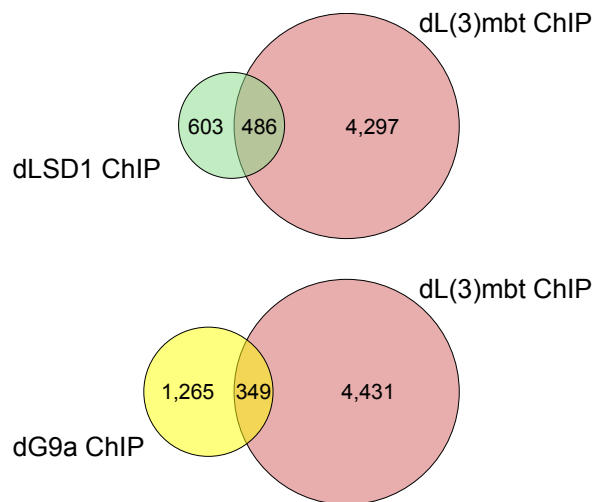
Figure 3.17. Majority of dLSD1 and dG9a do not overlap with dL(3)mbt binding sites.
Venn diagrams depicting shared and unique ChIP-seq peaks for dL(3)mbt and dLSD1 (top panel) and
dL(3)mbt and dG9a (bottom panel).

3.5. Gene regulation in S2 cells by dCoREST complexes

All three complexes identified in this study share a common dCoREST/dRPD3 core that contains the histone modifying enzyme dRPD3, the *Drosophila* homologue of histone deacetylases HDAC1 and HDAC2. Beside dRPD3, the histone methyl-lysine reader dL(3)mbt is present in the LINT complex. On the other hand, the dLSD1/dCoREST and the dG9a/dCoREST complex contain one additional histone modifying enzyme in the complex: the lysine-specific demethylase dLSD1, and the H3K9-specific methyl-transferase dG9a, respectively. It is believed that these enzymes contribute to the generation of closed chromatin structures and are involved in repression of gene transcription. Moreover, the distribution of binding sites of dCoREST complexes showed that they are greatly enriched at promoters suggesting their gene-regulatory function.

In order to evaluate the relative contribution of the three dCoREST complexes to gene regulation, I used RNAi-mediated depletion of dCoREST and its interactors followed by RNA-seq. As a control S2 cells were treated with double-stranded RNA targeting EGFP (**Figure 3.18**, lane 1). For depletion of dCoREST two double-stranded RNAs were used. One of these RNAs efficiently depleted both dCoREST-L and dCoREST-M simultaneously, because it targeted a region shared by both L- and M-isoforms (**Figure 3.18**, lane 2). The other RNA was designed to hybridise with the sequence of insert

unique to dCoREST-L, hence it depleted the dCoREST-L isoform specifically (**Figure 3.18**, lane 3). Notably, the simultaneous depletion of both dCoREST isoforms, as well as the specific depletion of dCoREST-L decreased dLSD1 protein levels (**Figure 3.18**, lanes 2 and 3). These results suggest that in S2 cells dLSD1 is stabilised by dCoREST-L binding. Previously it was reported that depletion of dL(3)mbt had a similar destabilising effect on dLint-1, a result that was reproduced in my analysis (Meier at al., 2012; **Figure 3.18**, lane 6). Interestingly, successful dLSD1 depletion only mildly decreased dCoREST-L protein levels, as judged by Western blot signal (**Figure 3.18**, lane 4). In the same manner, dLint-1 depletion only mildly decreased dL(3)mbt protein levels (**Figure 3.18**, lane 5). In contrast to the others, dG9a depletion did not have major effects on other protein levels analysed in this experiment (**Figure 3.18**, lane 7).
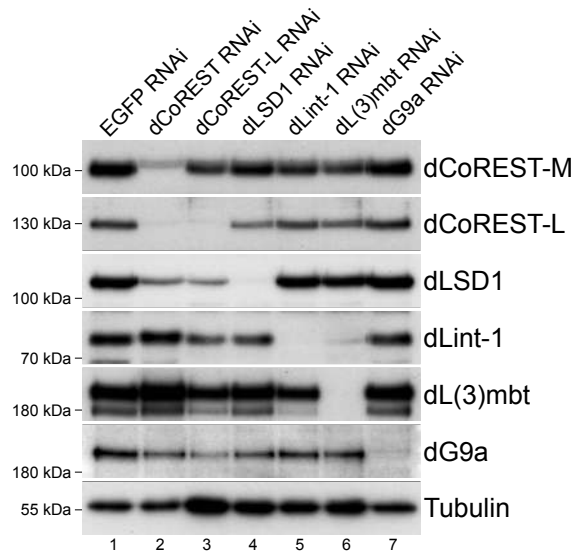
Figure 3.18. Depletion of dCoREST and its interacting partners in S2 cells.
S2 cells were treated with dsRNA directed against EGFP, dCoREST, dCoREST-L, dLSD1, dLint-1, dL(3)mbt and dG9a. Nuclear extracts of RNAi treated S2 cells were subjected to Western blot and analysed using the antibodies indicated on the right. Notably, both dCoREST isoforms are detected with the same anti-dCoREST antibody.

As determined by RNA-seq, 668 protein coding genes were up-regulated by a factor of 2.0 or more (log2FC≥1) upon simultaneous depletion of both dCoREST-L and dCoREST-M in S2 cells compared to the control (**Figure 3.19**). Only 38 protein coding genes were down-regulated. This inequality between the number of up- and down-regulated protein coding genes correlates well with the hypothesis that dCoREST complexes predominantly function to repress transcription. Moreover, 483 of the deregulated genes upon dCoREST knockdown were also bound by dCoREST, as

determined by ChIP-seq analysis. These data suggests that these genes are direct targets of dCoREST repressor complexes. Next, I analysed transcriptomes after depletion of complex-specific subunits of the three dCoREST complexes defined by biochemical analyses (**Figure 3.19**). The results of this analysis give the potential answer to the question to what extent these three dCoREST complexes contribute to gene regulation. Interestingly, RNA-seq analysis of the transcriptome in dLSD1 depleted S2 cells showed only a few genes being misexpressed: 8 genes up-regulated, 10 genes down-regulated (**Figure 3.19**). Similarly to S2 cells depleted of dLSD1, very few genes were de-regulated in dCoREST-L depleted cells: 4 genes up-regulated; 4 genes down-regulated.
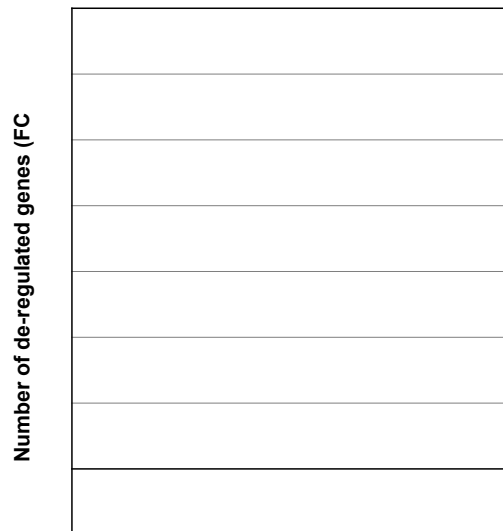
Figure 3.19. Number of de-regulated genes identified by RNA-seq.
RNA from cells depleted of dCoREST or its interactors was analysed by RNA-seq. The diagram depicts the numbers of up- and down-regulated genes (fold change ≥2) using transcript levels of EGFP RNAi treated cells as a reference (*n*=3).

A small number of de-regulated genes that does exceed a factor of 2-fold in these experiments could be due to the weak transcriptional effects of dLSD1 depletion. Notably, it has been reported previously that *Cre*-mediated deletion or RNAi-mediated depletion of LSD1 in mouse ES cells results in only weak de-repression of LSD1 target genes (Foster et al., 2010; Nair et al. 2012). Therefore, I considered genes misexpressed

by a factor of 1.5 or more (log2FC≥0.58) to gain more insight into genes that are moderately de-regulated. This, indeed, resulted in an increased number of dLSD1-repressed genes of 113 and the number of dCoREST-L-repressed genes increased to 41 (**Figure 3.20**). Comparing dLSD1 and dCoREST-L repressed genes showed that 78% of genes up-regulated by dCoREST-L depletion were likewise up-regulated by dLSD1 depletion. These results emphasise that these genes are indeed repressed by a dLSD1/dCoREST-L complex. However, the results also clearly reveal that the dLSD1/dCoREST-L complex regulates a comparatively small proportion of dCoREST-regulated genes in S2 cells.
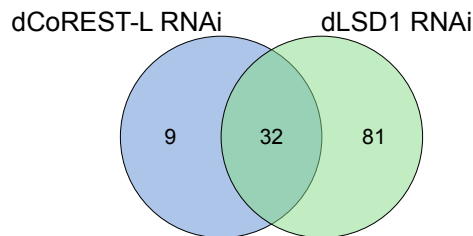
Figure 3.20. Comparison of dCoREST-L and dLSD1 up-regulated genes in S2 cells.
Venn diagram comparing dCoREST-L and dLSD1 repressed genes with fold change ≥1.5 (log2FC≥0.58, adj. p≤0.05).

Similar to dLSD1, dG9a depletion resulted in up-regulation of only a few genes by a factor of 2.0 or more: 10 genes were up-regulated, no gene was down-regulated (**Figure 3.19**). Even lowering the threshold of the analysis and considering genes misexpressed by a factor of 1.5 or more did not strikingly increase the number of affected genes. Overall, 18 genes were up-regulated, 16 genes down-regulated after adjusting log2FC to ≥0.58. According to these results, dG9a does not play a major role in regulating gene transcription in S2 cells.

Depleting the dLSD1/dCoREST complex and the dG9a/dCoREST complex-specific subunits in S2 cells had moderate to weak effects on the de-regulation of gene expression. In stark contrast, the depletion of LINT-specific subunits changed the expression levels of hundreds of genes by a factor of 2.0 or more. dL(3)mbt depletion resulted in up-regulation of 584 genes and down-regulation 56 genes, dLint-1 depletion resulted in up-regulation of 373 genes and down-regulation of 34 genes (**Figure 3.19**). This result suggests that the LINT complex in S2 cells is in control of a large fraction of dCoREST-dependent genes.
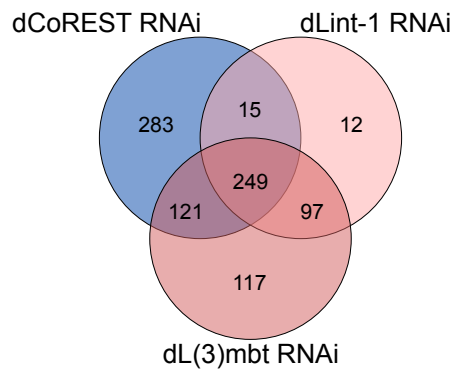
Figure 3.21. The LINT complex is a major repressor of transcription in S2 cells.
Venn diagram of genes up-regulated upon dCoREST, dL(3)mbt or dLint-1 knockdown
(log2FC≥1.0, adj. p≤0.05).

To support this hypothesis I compared genes that are de-repressed upon dCoREST, dL(3)mbt or dLint-1 depletion (**Figure 3.21**). The results show a high degree of overlap: 249 protein coding genes were up-regulated upon RNAi targeting of each of the three LINT complex subunits. I consider these to be high confidence LINT targets. Furthermore, 385 of 668 up-regulated genes in dCoREST-depleted cells were also up-regulated upon depletion of at least one other LINT complex subunit. Therefore, it appears that the LINT complex represses approximately half of the dCoREST-regulated genes. Notably, 283 genes were up-regulated in dCoREST-depleted cells but neither in dL(3)mbt nor in dLint-1-depleted cells (**Figure 3.21**). At present, it is unclear if this is a consequence of a differential requirement for LINT complex subunits at subsets of LINT target genes or if these genes represent targets of as yet unidentified dCoREST complexes.

3.5.1. LINT represses germ line genes in S2 cells

Previous studies have shown that dL(3)mbt and the LINT complex are involved in the repression of malignant brain tumour signature (MBTS) genes. MBTS genes encode mostly germ line-specific proteins that are up-regulated in brain tumours of *l(3)mbt* mutant larvae (Janic et al., 2010; Richter et al., 2011; Meier et al., 2012; Coux et al., 2018). In addition, it has been shown that dL(3)mbt is involved in the regulation of the genes targeted by the Salvador-Warts-Hippo (SWH) pathway (Richter et al., 2011). Indeed, 26 out of 101 MBTS genes were also repressed by the LINT complex in S2 cells (**Figure 3.22.A**). Interestingly, none of the SWH targets was represented in the

LINT-repressed genes (data not shown).

LINT target genes in Kc cells have been previously determined by microarray analysis (Meier et al., 2012). Both, Kc cell and S2 cell are believed to be derived from embryonal macrophages based on the comparative analysis of their transcriptomes, (Cherbas et al., 2011). I hypothesised that LINT might repress similar sets of genes in both cell lines. Therefore I compared LINT-regulated genes in Kc and S2 cells. Indeed, almost 40% of LINT target genes in S2 cells were also regulated by LINT in Kc cells (**Figure 3.22.B**).
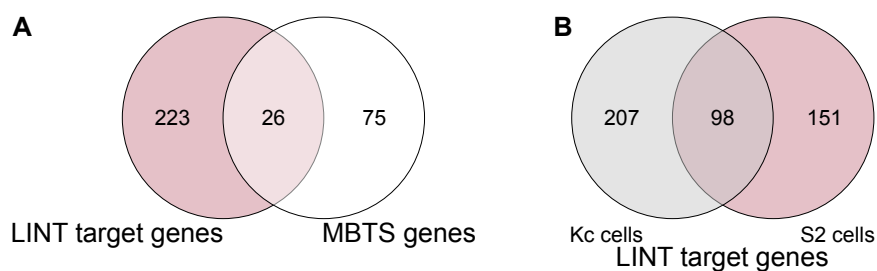
Figure 3.22. Comparison of LINT target genes.
(A) Venn diagram comparing LINT-repressed genes (this study) and malignant brain tumour signature genes (Janic et al., 2010). **(B)** Overlap of dL(3)mbt and dLint-1 repressed genes in Kc cells (microarray — Meier et al., 2012) and LINT target genes in S2 cells (this study).
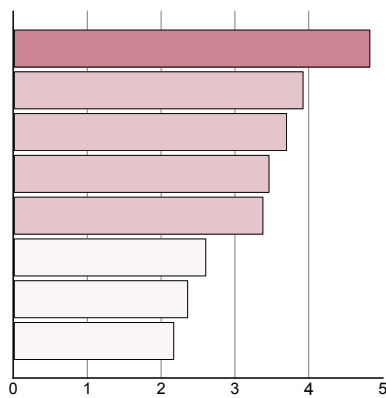
Figure 3.23. GO-term enrichment analysis of LINT-repressed genes.
GO analysis was performed using the Metascape tool to analyse 249 LINT-repressed genes identified in RNA-seq analysis.

In order to gain insight into the role of the LINT-repressed genes, I analysed these genes using gene ontology (GO)-term analysis. The GO-term analysis revealed eight terms that were significantly enriched (**Figure 3.23**). The highest enriched GO-term included genes involved in germline stem cell symmetric division. Notably, many of the germline-specific MBTS transcripts are up-regulated upon LINT subunits knockdown

(**Figure 3.22**). These findings indicate that LINT functions to repress genes involved in germ cell differentiation in S2 cells.

Taken together, these results suggest that the LINT complex maintain the cellular identity of macrophage-derived cell lines by preventing the inappropriate expression of genes characteristic for other cell types.

3.6. Role of dCoREST in differentiation of wing veins

RNAi followed by RNA-seq in S2 cells showed that the LINT complex is the major regulator of gene transcription, while the dLSD1/dCoREST and the dG9a/dCoREST complexes had only minor effect. Next I sought to investigate if these complexes have a role during fly development. In order to study this, I utilised two developmental systems, the wing and testes. Moreover, previous studies have shown that both, developing wings and spermatogenesis, are sensitive to mutation or deregulation of several chromatin regulators (Curtis et al., 2013; Kim et al., 2017; Kovač et al., 2018). For example, RNAi-mediated depletion of dCoREST and dLSD1 throughout the wing imaginal disc has been demonstrated to result in ectopic vein phenotypes (Curtis et al., 2011; Curtis et al., 2013). Therefore, I performed RNA interference using the UAS/GAL4 system in order to gain insight into the roles of different dCoREST complexes during fly development (Brand and Perrimon, 1993). The UAS/GAL4 system utilises the yeast activator GAL4 that is expressed under control of a characterised promoter of choice in *Drosophila*. This activator leads to expression of a target gene that has the Upstream Activation Sequence (UAS) array upstream of a basal promoter. Crossing the driver line that expresses the GAL4 activator with the responder line that carries UAS sequence allows the activation of the genes only within cells where GAL4 is expressed. First, I used the engrailed-GAL4 driver line to direct expression of UAS-shRNA constructs to the posterior half of the developing wing. I set up a series of crosses to knockdown dCoREST, dLSD1, dL(3)mbt, dLint-1 or dG9a. Notably, shRNA constructs for dCoREST are expected to simultaneously down-regulate both dCoREST-L and dCoREST-M.
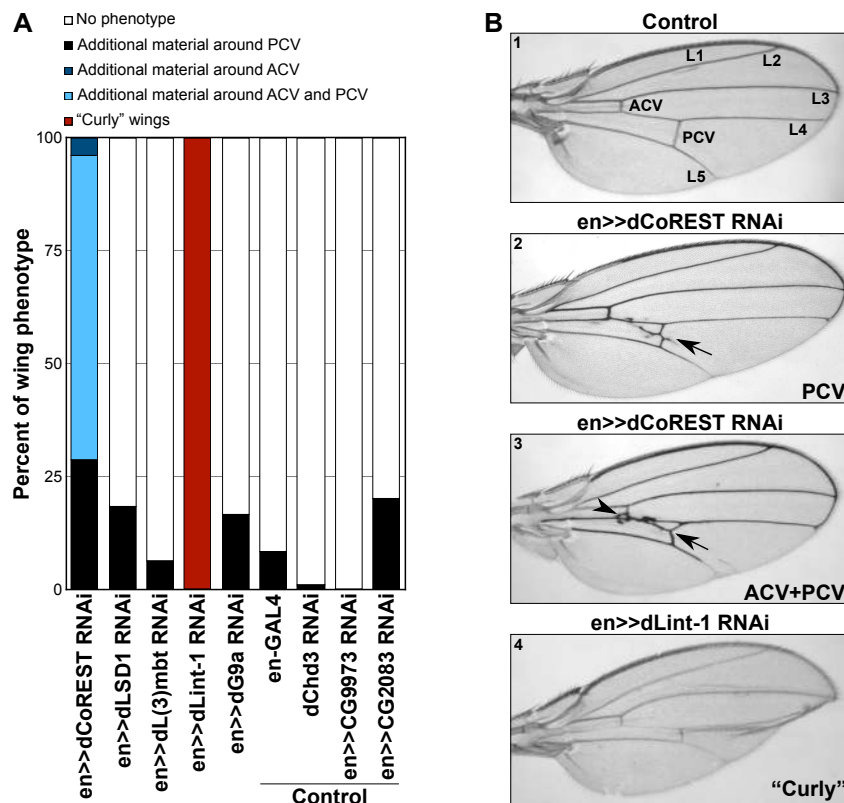
Figure 3.24. Depletion of dCoREST disrupts wing vein differentiation.
(A) Graph showing the distribution (in %) of posterior cross-vein (PCV, black), anterior cross-vein (ACV, dark blue), combined ACV and PCV (light blue), and Curly (red) phenotypes upon depletion of dCoREST, dLSD1, dL(3)mbt, dLint-1, and dG9a in fly wing discs. Depletion of dChd3, CG9973, CG2083 as well as en-GAL4 driver flies served as controls. Number of analysed wings (*n*=3): en>>dCoREST RNAi — 101; en>>dLSD1 RNAi — 92; en>>dL(3)mbt RNAi — 93; en>>dLint-1 RNAi — 90; en>>dG9a RNAi — 91; en-GAL4 — 97; en>>dChd3 RNAi — 100; en>>CG9973 RNAi — 61; en>>CG2083 RNAi — 76. **(B)** Examples of phenotypes: The positions of longitudinal veins (L1 to L5), ACV and PCV in wild type wings are shown in panel 1. PVC phenotypes are characterised by formation of additional vein material around the PCV (panel 2; arrow). ACV phenotypes are characterised by formation of additional vein material around ACV (panel 3; arrow head). Combined ACV and PCV phenotype is shown in panel 3. The characteristic dLint-1 RNAi "Curly" wing phenotype is shown in panel 4.

In flies where dCoREST was depleted by RNAi, I observed ectopic vein formations in all analysed wings (100%). I further assigned these formations to distinct phenotypes depending on the proximity to the closest wing vein (data generated together with Dr Kristina Kovač, **Figure 3.24**). In roughly 29% of analysed wings, where both dCoREST isoforms were depleted, ectopic veins were formed in the surrounding of the posterior cross-vein (PCV) only. In only 4% of analysed wing, ectopic veins were observed in the proximity of the anterior cross-vein (ACV) only. The majority (67%) of the analysed wings had additional vein material around both PCV and ACV.

Depletion of specific subunits of the three distinct dCoREST complexes: dLSD1, dL(3)mbt, or dG9a, indeed resulted in phenotypes with lower penetrance. Less then

20% of wings analysed showed characteristic PCV phenotypes. Notably, such low penetrance PCV phenotypes were also observed in the driver line (en-GAL4) and when RNAi was directed against transcripts unrelated to dCoREST complexes (dChd3, CG9973 and CG2083; **Figure 3.24.**A). Furthermore, all parental RNAi lines used in this experiments had normal wing structures without any ectopic vein material (data not shown). These results, therefore, implicate that low penetrance vein phenotypes are unlikely to be a specific consequence of depletion of these dCoREST complex subunits. Interestingly, in the fly lines where dLint-1 was depleted the wings had a strong deformation of shape manifesting as a "Curly" phenotype. This deformation largely precluded an analysis of vein phenotypes. The molecular basis for the dLint-1 phenotype is currently unclear.
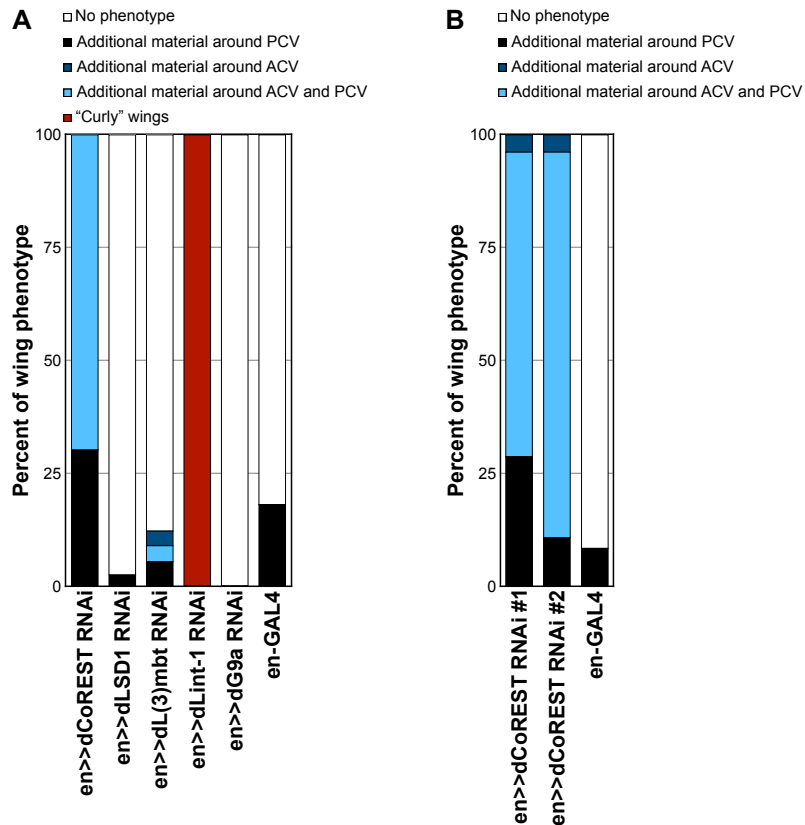
Figure 3.25. Distribution of phenotypes in fly wings.
(A) Distribution of fly wings phenotypes in flies raised at an elevated temperature of 30 °C. Graph showing the distribution (in %) of PCV (black), ACV (dark blue), combined ACV and PCV (light blue), and "Curly" (red) phenotypes upon depletion of dCoREST, dLSD1, dL(3)mbt, dLint-1, and dG9a in fly wing discs at 30 °C. Number of analysed wings ($n=3$): en>>dCoREST RNAi — 83; en>>dLSD1 RNAi — 80; en>>dL(3)mbt RNAi — 90; en>>dLint-1 RNAi —78; en>>dG9a RNAi — 52; en-GAL4 — 39. **(B)** Distribution (in %) of PCV (black), ACV (dark blue), and combined ACV and PCV (light blue) phenotypes upon depletion of dCoREST in fly wing discs by two different dCoREST RNAi fly line. The en>>dCoREST RNAi #1 and en-GAL4 quantifications are reproduced from the Figure 3.24. Number of analysed wings ($n=3$): en>>dCoREST RNAi #1 — 101; en>>dCoREST RNAi #2 — 176; en-GAL4 — 97.

I also considered the possibility that the lack of specific phenotypes caused by dL(3)mbt, dLSD1 or dG9a depletion is due to insufficient expression of RNAi constructs. It was previously reported that an elevated temperature (30 °C) enhances expression in the UAS/GAL4 system (Duffy, 2002). Therefore, I repeated all crosses at 30 °C and analysed the phenotypes. Indeed, the analysis showed enhanced severity of dCoREST and dLint-1 RNAi phenotypes (**Figure 3.25.A**). Still, enhancing the expression of shRNAs by elevating the temperature failed to produce specific wing alterations when dL(3)mbt, dLSD1 or dG9a were targeted (**Figure 3.25.A**).

Furthermore, I considered the possibility that the phenotypes caused by dCoREST depletion in the developing wing are fly line specific artefacts. To exclude this possibility, I conducted the experiment using a second dCoREST RNAi fly line to deplete dCoREST in wing imaginal discs. The results showed a similar distribution of the phenotypes (**Figure 3.25.B**). The majority of wings (85%) from the second dCoREST RNAi line crosses had additional vein material around both PCV and ACV, almost 4% had exclusive ACV phenotypes, while more than 10% had exclusive PCV phenotypes.

Using this experimental system I could demonstrate that dCoREST is critical for proper wing vein differentiation, whereas proteins specific for a particular dCoREST complex are dispensable. Moreover, these results suggest either redundancy between dCoREST complexes or the existence of as yet unidentified dCoREST complexes in this developmental setting. Notably, due to the experimental setup, I was not able to demonstrate knockdown efficiencies.

3.7. dLSD1/dCoREST is essential for spermatogenesis

Previous work on the proteins identified in this study as dCoREST complex-specific subunits implicated them in the regulation of germ cell development. Homozygous dLSD1 mutant females fail to produce oocytes and male flies are infertile (Szabad et al., 1988; Rudolph et al., 2007; Lee and Spradling, 2014). Similarly, mutations in dL(3)mbt, dLint-1 and dG9a produce ovary defects and female sterility (Lee at al., 2010; Coux et al., 2018). Taken together, these studies showed the importance of the dCoREST

interactors in germ cell development of females. However, the role in male germ cell development has not been systematically analysed yet. Therefore, I sought to compare the role of the dLSD1/dCoREST, the LINT and the dG9a/dCoREST complex subunits in spermatogenesis and male fertility.
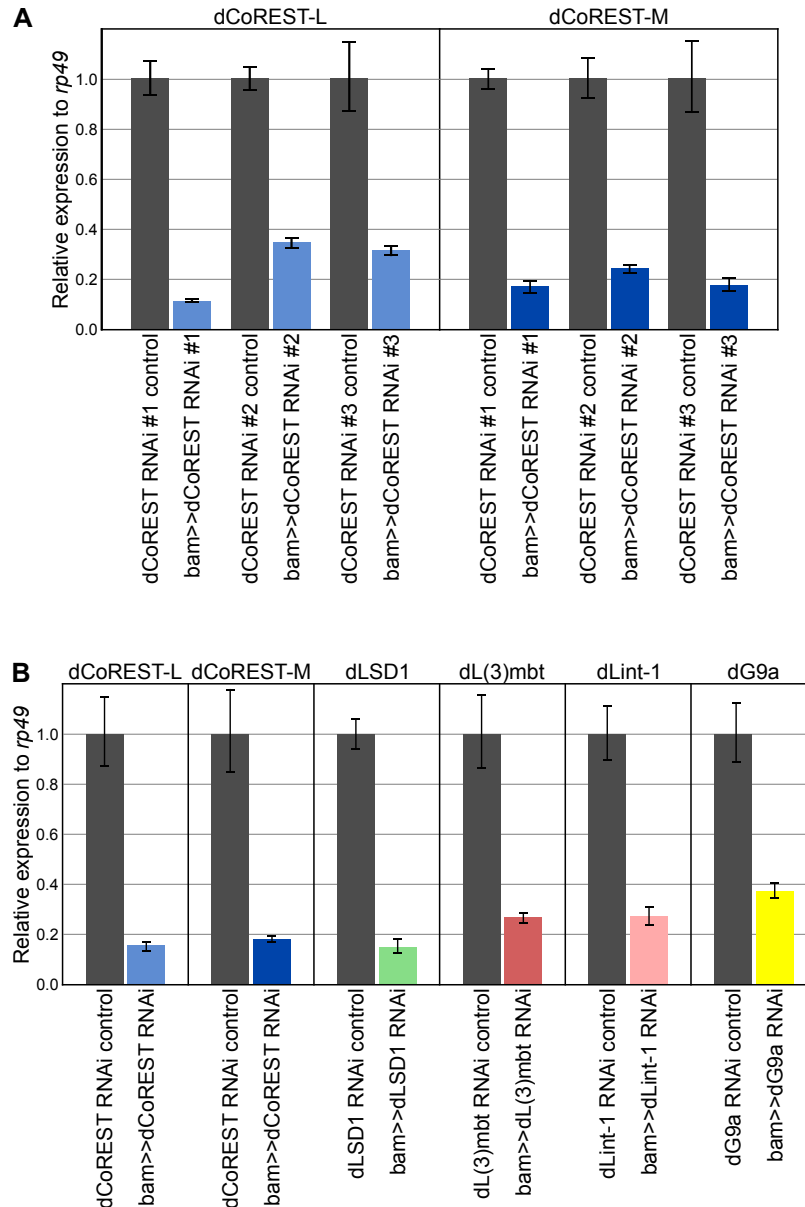
Figure 3.26. Efficiency of RNAi knockdowns of dCoREST and its interactors in fly testes.
(A) qPCR analysis of dCoREST-L and dCoREST-M expression in three bam-GAL4 driven dCoREST RNAi fly lines. (B) qPCR analysis of dCoREST-L, dCoREST-M, dLSD1, dL(3)mbt, dLint-1 and dG9a expression in bam>>RNAi fly lines. RNA levels in control testes were set to 1 and RNA levels in RNAi-depleted testes are depicted relative to the level in corresponding controls (A and B).

In order to investigate the role of the three dCoREST complexes in the male germ cells, I set up a series of crosses to knockdown dCoREST, dLSD1, dL(3)mbt, dLint-1 or dG9a in developing male germ cells. Therefore, I used the bam-GAL4 (*bag of marbles*) driver

strain to direct expression of RNAi constructs to germ cells. Moreover, I compared three different dCoREST RNAi lines expressing shRNA constructs expected to simultaneously down-regulate both dCoREST-L and dCoREST-M. I analysed RNA prepared from fly testes of corresponding crosses by qPCR to verify the efficiency of knockdowns (**Figure 3.26**).

Indeed, dCoREST-L and dCoREST-M mRNA expression in testes was reduced to levels ranging from 10% to 35% when these responder lines were crossed to bam driver lines (**Figure 3.26.A** and **Figure 3.26.B**). Furthermore, mRNA expression of all RNAi targets was efficiently reduced, levels were ranging from 10% to 40% of control values.
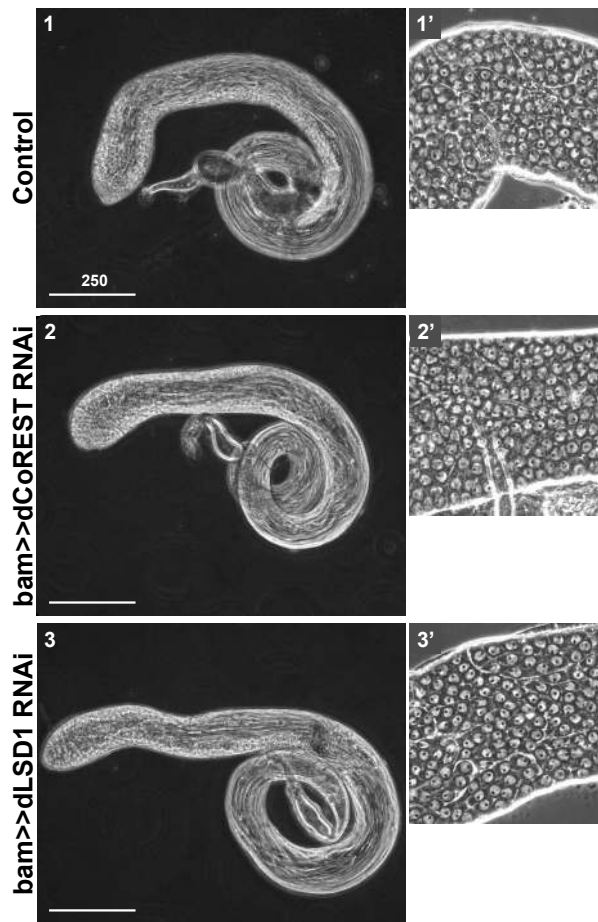
Figure 3.27. dCoREST and dLSD1 depletion impairs release of mature sperm.
Phase contrast images of 1 day old testes from control (1 and 1') and upon RNAi in bam>>dCoREST RNAi (2 and 2') and bam>>dLSD1 RNAi (3 and 3') crosses. Post-meiotic sperm with characteristic flagella (area of the testes marked by dashed lines) were visible in all testes. Full seminal vesicle (arrow in panel 1) where visible only in the control testes, whereas seminal vesicles in RNAi depleted testes (arrowheads in panel 2 and 3) were empty. Phase contrast microscopy of spermatocytes from indicated crosses (1', 2' and 3') showed no visible defects.
Scale bars: 250 μm (1, 2 and 3) and 100 μm (1', 2' and 3').

In order to assess if depletion of dCoREST or its interactors in testes leads to morphological changes, I examined the testes of corresponding fly lines with a phase contrast microscope (in cooperation with Dr Stephan Awe). Post-meiotic sperm with characteristic flagella was observed in all testes analysed in this experiment. Interestingly, only in testes where dCoREST or dLSD1 was depleted I observed that the seminal vesicles were empty with no mature sperm (**Figure 3.27**). These results suggest that depletion of dCoREST or dLSD1 in the male germ line impairs release of mature sperm into seminal vesicles.

To test the hypothesis that dCoREST-containing complexes are essential for fertility, I set up an assay to evaluate male fertility (in cooperation with Dr Ina Theofel and Dr Tim Hundertmark). I crossed virgin females with control males or RNAi-depleted males and analysed the occurrence of progeny. In total 11 lines were tested (**Table 3.1**). Only dCoREST and dLSD1-depleted males failed to generate progeny. This result was in agreement with previous observations (Kim et al., 2017). In contrast, the fertility of males depleted of dL(3)mbt, dLint-1 or dG9a was indistinguishable from that of controls.

Table 3.1. dCoREST and dLSD1 depletion leads to fly sterility.
Male fertility of wild-type flies and fly strains in which dCoREST or its interactors are depleted by RNAi (n=10). Only in dCoREST RNAi and dLSD1 RNAi flies, no offspring was detected.

#	Fly line	Fertile
1	bam-GAL4 driver	+
2	dCoREST RNAi control	+
3	bam>>dCoREST RNAi	−
4	dLSD1 RNAi control	+
5	bam>>dLSD1 RNAi	−
6	dL(3)mbt RNAi control	+
7	bam>>dL(3)mbt RNAi	+
8	dLint-1 RNAi control	+
9	bam>>dLint-1 RNAi	+
10	dG9a RNAi control	+
11	bam>>dG9a RNAi	+

This result implicates a distinctive role of dCoREST complexes in male fertility. Whereas both the LINT and the dG9a/dCoREST complexes appear to be non-essential, the dLSD1/dCoREST complex is indispensable for male fertility.

Spermiogenesis, the post-meiotic development of male germ cells, involves processes during which round spermatid nuclei elongate, individualise and eventually form mature sperm. During the elongation, the so called "*canoe*" stage, histones are removed from DNA and degraded. Concomitantly, protamines and Mst77F are expressed to replace histones in mature sperm (Rathke et al., 2007; Rathke et al., 2014). In order to analyse the defects caused by dCoREST and dLSD1 depletion in more detail, I used immunofluorescence microscopy (**Figure 3.28**).
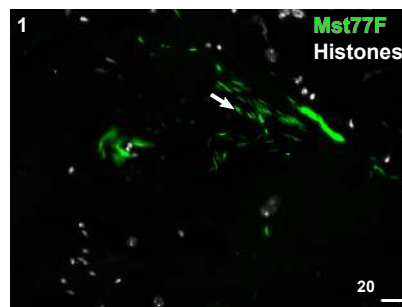
Figure 3.28. dCoREST and dLSD1 depletion affects shaping of spermatid nuclei.
Knockdown of dCoREST and dLSD1 leads to post-meiotic spermatid nuclei elongation defects. Histones (white) and the sperm protein Mst77F (green) are visualised by immunofluorescence in post-meiotic spermatid nuclei of control line (1 and 1') and upon RNAi in bam>>dCoREST RNAi (2 and 2') and bam>>dLSD1 RNAi (3 and 3') crosses. Scale bars: 20 μm.

Immunostaing of histones and Mst77F in dCoREST or dLSD1-depleted testes showed that dCoREST or dLSD1 depletion did not affect this histone-to-protamine switch, as judged by the timely expression and chromatin association of Mst77F. However, spermatid nuclei failed to elongate and no mature, elongated sperm was detected (data

generated in co-operation with Dr Ina Theofel, **Figure 3.28**). Transcription during sperm development is mainly shut down after meiotic divisions (Rathke et al., 2014), implying that these defects are probably a consequence of aberrant gene regulation during the spermatocyte phase.

Taken together, these results point out the striking similarity of the phenotypes produced after both dCoREST and dLSD1 knockdowns. This further strengthens the hypothesis that indeed the dLSD1/dCoREST complex is essential for the cellular processes that govern nuclei elongation.

The dLSD1/dCoREST complex did not appear to be a major regulator of gene transcription in macrophage-like S2 cells (**Figure 3.19**). In male germ cells, however, only depleting dCoREST and dLSD1 impaired mature sperm release into seminal vesicles, in contrast to other dCoREST interactors. Moreover, in these males spermatid nuclei failed to elongate, no mature, elongated sperm was detected and they were sterile. Hence, I hypothesised that the dLSD1/dCoREST complex might regulate gene expression during germ cell development.
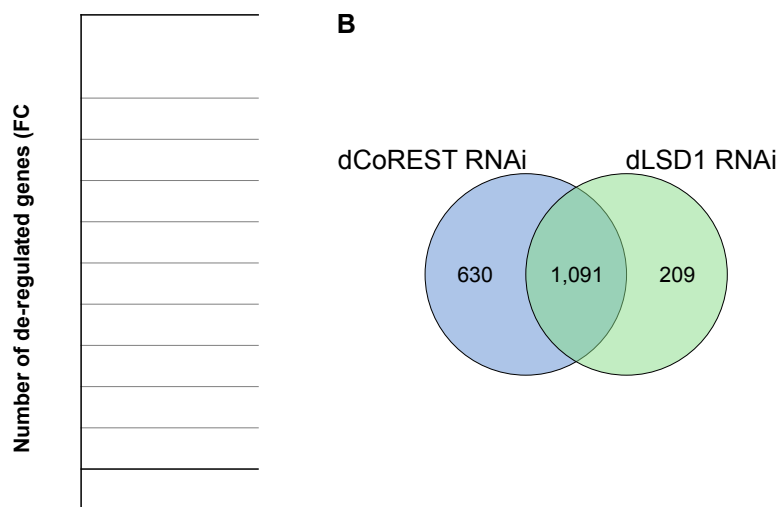
Figure 3.29. The dLSD1/dCoREST complex is a major transcriptional repressor during spermatogenesis. (**A**) Bar diagram showing the number of up- and down-regulated protein coding genes of testes depleted for dCoREST or dLSD1 as determined by RNA-seq. (**B**) Venn diagram showing comparison of dCoREST and dLSD1 repressed genes (log2FC ≥1.0, adj. p≤0.05).

To test this hypothesis I analysed RNA prepared from bam>>dCoREST RNAi, bam>>dLSD1 RNAi and control testes by RNA-seq (in cooperation with Dr Ina Theofel, Dr Tim Hundertmark, Dr Andrea Nist and Dr, Boris Lamp). A large number of genes was de-repressed by a factor of 2.0 (log2FC≥1) or more in dCoREST-depleted and dLSD1-depleted testes. In dCoREST-depleted testes 1,721 protein coding genes were up-regulated and only 61 genes were down-regulated. In dLSD1-depleted testes 1,300 protein coding genes were up-regulated and only 125 genes were down-regulated (**Figure 3.29.A**). Importantly, 1,091 genes were up-regulated in both scenarios. This number corresponds to 63% of all dCoREST-repressed genes and 84% of all dLSD1-repressed genes (**Figure 3.29.B**). I consider these genes to be high confidence targets of the dLSD1/dCoREST complex. These results further support the hypothesis that dCoREST complexes predominantly function to repress transcription. Moreover, the dLSD1/dCoREST complex is a major regulator of gene transcription during spermatogenesis.

Figure 3.30. GO-term enrichment analysis of dCoREST and dLSD1 co-repressed genes.
GO analysis was performed using the Metascape tool to analyse 1,091 common up-regulated genes identified in RNA-seq analysis.

In order to gain insight into the role of the dLSD1/dCoREST complex-repressed genes in male germ cells, I analysed 1,091 high confidence targets using GO-term analysis. The analysis identified 20 GO-terms that were significantly enriched (**Figure 3.30**). Moreover, 8 of these GO-terms were associated with genes involved in neuron development and function. This result is consistent with the hypothesis that the dLSD1/dCoREST complex is required to prevent the inappropriate expression of neuron-specific genes in the male germ line.

In conclusion, the results generated in this study demonstrate that dCoREST complexes functions to maintain cell-type-specific gene expression profiles in both macrophage-like cells and the male germ line. However, to do so, different dCoREST complexes are used in a cell-type-specific manner.

4. Discussion

"Sorting the myriad of chromatin regulating complexes neatly into different complex families satisfies the human need for order."

— Karin Meier and Alexander Brehm,
article in Epigenetics, 2014

4.1. Diversity of dCoREST complexes

The chromatin state in the living cell is tightly regulated by different multisubunit protein complexes. These complexes are often built around a common core of dedicated subunits, associated with diverse complex-specific signature subunits. Signature subunits provide specific features defining the functionality of the complex. Regulation of the enzymatic activities, the addition of new enzymatic, nucleosome or RNA binding activities and/or influencing the targeting to specific genome regions is typically achieved through these signature subunits. Moreover, the multisubunit protein complexes are grouped into (sub)families according to subunit composition (Meier and Brehm, 2014).

Several protein complex families which modulate chromatin structure and activity have been described. These include PRC1, PRC2 and SWI/SNF, and the number is increasing (Bracken et al., 2019). In contrast, identified complexes containing CoREST are comparatively small in number. Experiments performed in mammalian cells showed that the bulk of CoREST appears to reside in complexes with LSD1. In addition, it has been shown that CoREST can bind additional chromatin regulators (Lee et al., 2005; Shi et al., 2005; Zhang et al., 2013). However, systematic experiments conducted to reveal if these interactions reflect the existence of additional, stable CoREST complexes or are the products of transient binding events are currently lacking.

Both CoREST and LSD1 are conserved in *Drosophila* (Dallman et al., 2004; Rudolph et al., 2007). Endogenous proteins interact in ovary extracts and also when both proteins are over-expressed in S2 cells (Dallman et al., 2004; Lee and Spradling, 2014). The only extensive study performed in *Drosophila* to determine complex composition, up to this

point, identified dCoREST as a subunit of the L(3)mbt interacting LINT complex (Meier et al., 2012). Hence, I have used advanced proteomic approaches to systematically determine and characterise the molecular architecture of dCoREST in S2 cells.

In *Drosophila* two major protein isoforms of dCoREST are expressed: dCoREST-L and dCoREST-M. Analysing the gel filtration profile of S2 nuclear extract (**Figure 3.2**) suggested the possibility that not all of dCoREST resides in one complex. This hypothesis was also supported by analysing two-step ion exchange chromatography profiles of Kc cell nuclear extract (Meier et al., 2012). Moreover, in over-expression experiments, affinity co-purification of one dCoREST isoform did not yield detectible amounts of the other isoform (**Figure 3.6**)

In order to systematically identify and characterise dCoREST-containing complexes, I utilised immunoaffinity purification, mass spectrometry and co-immunoprecipitation approaches. In total, I have identified three distinct dCoREST-containing complexes. All three of these complexes contain a heterodimeric core composed of dCoREST itself (either the L or the M isoform) and the histone deacetylase dRPD3 (**Figure 4.1**).
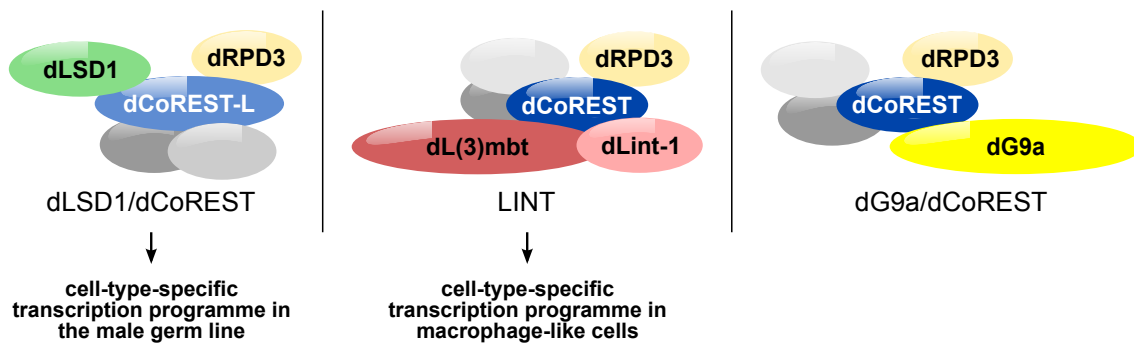
Figure 4.1. Schematic representation of different dCoREST complexes in *Drosophila*.
Three distinct dCoREST containing complexes share a common dCoREST/dRPD3 core. The dLSD1/dCoREST complex is dCoREST isoform-specific and regulates transcription in the male germ line. The LINT complex is a major repressor of transcription in macrophage-like cells. The targets of the dG9a/dCoREST complex are unknown.

The dCoREST/dRPD3 core associates further with additional protein subunits forming either the dLSD1/dCoREST complex, the LINT complex, or the dG9a/dCoREST complex. The dLSD1/dCoREST complex is defined by the histone demethylase dLSD1; dL(3)mbt and dLint-1 are the signature subunits of the LINT complex; and the H3K9 histone methyltransferase dG9a defines the dG9a/dCoREST complex. Interestingly,

these three identified dCoREST complexes have the potential to generate repressive chromatin structures by altering the histone methylation and acetylation status of nucleosomes.

The three dCoREST complexes can be separated by immunoprecipitation (**Figure 3.5**; **Figure 3.6** and **Figure 3.9**) and gel filtration under mild conditions (**Figure 3.12** and **Figure 3.13**). Moreover, genome-wide binding experiments performed in S2 cells showed only limited overlap of signature subunits belonging to different dCoREST complexes (**Figure 3.17**). Taken all together, these data demonstrate that the three identified complexes indeed exist as separate entities, not only in a soluble nuclear fraction, but as assemblies bound to the chromatin.

Notably, in proteomic screens for dCoREST interactors, additional proteins with established roles in chromatin regulation have been identified (**Appendix Table A1**; **Appendix Table A2** and **Appendix Table A3**). I have not characterised these proteins further, but this leaves open the possibility that additional dCoREST-containing complexes might exist.

4.1.1. Isoform-specific dCoREST complexes

Between the SANT domains in dCoREST-L there is a unique 234 aa insertion that is not present in dCoREST-M (**Figure 3.1**). I have found that both dCoREST isoforms can interact with the LINT and the dG9a/dCoREST complex specific subunits (**Figure 3.6** and **Figure 3.9**). By contrast, dCoREST-L forms an isoform specific complex with dLSD1. Importantly, these findings agree well with the prior observation that dLSD1 co-immunoprecipitates preferentially with dCoREST-L in ovary extracts (Lee and Spradling, 2014).

Additionally, these results also raise the question: how a unique 243 aa insertion in dCoREST-L isoform contributes to the isoform specificity of this interaction? At present, there are no structural data available of dCoREST-L. Nevertheless, the structure of a complex formed by fragments of human CoREST and human LSD1 has been solved (Yang et al., 2006): the CoREST-LSD1 interaction is established between a part of the region separating the two SANT domains and the second SANT domain of CoREST and the tower domain of LSD1. Sequence alignment of human and *Drosophila*

CoREST reveals conservation across the entire LSD1 contact region of CoREST (**Figure 4.2**). Moreover, the N-terminal part of this contact region is present only in the dCoREST-L-unique insertion, but is absent in dCoREST-M. This offers a potential explanation for why dCoREST-M cannot stably interact with dLSD1: dCoREST-M is missing a part of the dLSD1 interaction surface.

Figure 4.2. Alignment of hCoREST-LSD1 binding interface with dCoREST isoforms.
Multiple sequence alignment of human CoREST, dCoREST-L and dCoREST-M was generated with the ClustalW program. hCoREST amino acids that directly interact with LSD1 are in red (according to Yang et al., 2006). Identical residues are highlighted in light red, similar residues are highlighted in blue.

In humans, CoREST is also expressed as alternatively spliced isoforms. All three major human CoREST isoforms interact with LSD1 (Barrios et al., 2014). This implies that the strict isoform-specific dCoREST-L/dLSD1 interaction identified in *Drosophila* is not conserved in humans.

In higher metazoans, generation of cell-type-specific proteomes is achieved by alternative splicing (Graveley, 2001). Hence, the differential abundance of the three dCoREST complexes in different cell types could be generated by regulating alternative splicing of the dCoREST transcript. For example, increased expression of dCoREST-M, at the expense of dCoREST-L, would be expected to result in a higher proportion of LINT and dG9a/dCoREST complexes and a concomitant decrease in dLSD1/dCoREST complex levels. Indeed, the relative expression levels of dCoREST-L and dCoREST-M, as judged by Western blot, are significantly different in S2 cells and embryo extracts (compare **Figure 3.11** and **Figure 3.12**). Taken together, this suggests that regulation of dCoREST expression at the level of alternative splicing might occur in different cell types.

4.2. dCoREST complexes in regulation of transcription

I have identified three distinct dCoREST complexes in the soluble nuclear fraction of S2 cells. They all contain histone deacetylase as a core component, and, in the case of the dLSD1/dCoREST and the dG9a/dCoREST complex, an additional histone modifying enzyme. This complex composition has the potential to tailor the transcriptome of the cell by affecting the histone methylation and acetylation signature in nucleosomes. This raises the following question: what is the impact of the dCoREST complexes on transcriptome regulation? Moreover, can the three individual dCoREST complexes bind to the same regions in the genome and is there complex-specific regulation of transcription?

4.2.1. dCoREST complexes have distinct chromatin binding sites

dCoREST bound sites are enriched in the promoter regions of the *Drosophila* genome (**Figure 3.15**). This result implies that the dCoREST complexes regulate the expression of genes by changing the post-translational modification status of histones, mainly in promoter regions, utilising the enzymatic activities of associated subunits.

The majority of dCoREST bound sites in S2 cells are co-occupied by dL(3)mbt, but not by dLSD1 or dG9a (**Figure 3.16**). Moreover, my analysis reviled a small number of co-occupied sites by dLSD1 or dG9a and dL(3)mbt (**Figure 3.17**). According to these results it would be reasonable to expect that the majority of dCoREST dependent gene regulation in S2 cells is achieved through the LINT complex.

4.2.1. Cell-type-specific activity of dCoREST complexes

In both macrophage-like cells and male germ cells, depletion of dCoREST impacted the expression of hundreds of genes. Strikingly, in both cell types, the number of genes that was up-regulated upon dCoREST depletion was 20-fold or higher than the number of down-regulated genes (**Figure 3.19** and **Figure 3.29**). This result indicates that indeed dCoREST complexes primarily act as repressors of transcription rather than activators.

In contrast to dCoREST depletion, macrophage-like cells and the male germ line respond to the depletion of the specific subunits of the dCoREST complexes in a

different manner. RNAi depletion of dLSD1 and the dCoREST-L isoform, which are signature subunits of the dLSD1/dCoREST complex led to de-regulation of only a few genes. RNAi mediated depletion of dG9a had the same minor effect (**Figure 3.19**). Conversely, depletion of dL(3)mbt and dLint-1, the LINT complex signature subunits, in S2 cells de-regulated hundreds of genes. As in dCoREST depleted cells, the number of up-regulated genes was 20-fold higher then the number of down-regulated genes (**Figure 3.19**). Furthermore, significant overlap of up-regulated genes in dCoREST and dL(3)mbt-depleted cells showed that these genes are regulated by the LINT complex. These results reveal that the LINT complex is an important regulator of transcription, repressing inappropriate sets of genes in macrophage-like cells. For example, MBTS genes that are germline specific are repressed by the LINT complex in S2 cells.

The three dCoREST complexes I identified in this study share a common dCoREST/dRPD3 core. Nevertheless, it seems that the dLSD1/dCoREST and the dG9a/dCoREST complexes do not play important roles in shaping the S2 cell transcriptome, at least not under these experimental conditions. Interestingly, previous findings also showed that the knockdown of LSD1 in mouse ES cells does not lead to major changes in transcriptome (Nair et al., 2012). Therefore, it is conceivable that even in mammals the ubiquitous activity of the LSD1/CoREST complex is limited to the regulation transcription in a cell-type specific manner.

As it was shown in this study, knockdown of LINT subunits or dG9a has no effect on spermatogenesis, but depletion of dCoREST and dLSD1 lead to severe defects. In contrast to the results in macrophage-like cells, depletion of dLSD1 in the male germ line resulted in deregulation of more than 1,000 genes (**Figure 3.29**). Moreover, almost 84% of up-regulated genes upon dLSD1 knockdown were also up-regulated upon depletion of dCoREST. Many genes co-repressed by dLSD1 and dCoREST appear to be specific for non-germline lineages such as neurons. Previous studies showed that LSD1 indeed plays an important role in mammalian spermatogenesis and it colocalises at meiotic chromosomes together with SFMBT1 (Zhang et al., 2013). Moreover, the results demonstrated that the SLC complex, that contains SFMB1, LSD1 and CoREST, is highly expressed in mouse spermatocytes. Furthermore, in different studies it was shown that conditional ablation of LSD1 expression in mouse testis results in

misexpression of genes involved in stem cell and progenitor maintenance and differentiation (Lambrot et al., 2015; Myrick et al., 2017). Notably, published studies did not directly address the role of CoREST. But, my data strongly support the hypothesis that the role of LSD1/CoREST complexes in spermatogenesis is remarkably conserved between mouse and fruit fly.

Unlike the LINT and dLSD1/dCoREST complexes for which I have identified important functions as transcriptional regulators in S2 cells and the male germ line, respectively, dG9a depletion did not produce significant effects in any of presented experimental systems. G9a is an H3K9-specific methyltransferase responsible for histone H3 lysine 9 mono- and di-methylation. The results generated in this study agree with previous observations that dG9a mutants do not have reduced H3K9-methylation levels in germ cells, even though dG9a is abundantly expressed in the male germline (Stabell et al., 2006; Ushijima et al., 2012). dG9a is a non-essential gene, but, it was shown that dG9a *null* mutant flies have behavioural phenotypes (Seum et al., 2007; Kramer et al., 2011; Shimaji et al., 2015; Anreiter et al., 2017). Moreover, it has been published that dG9a deficient flies display severe defects under various stress conditions (Merkling et al., 2015; Shimaji et al., 2015; An et al., 2017; Riahi et al., 2019). Taken together, it is possible that the dG9a/dCoREST complex regulates transcription in cell types that have not been analysed in this study. Or, according to the recently published data, the dG9a/dCoREST complex's most prominent effects could be observed only under particular stress conditions.

4.3. dCoREST complexes in differentiation

The data in this study has revealed that at least three distinct dCoREST complexes exist in *Drosophila*. Genome-wide studies showed that these complexes have a differential impact on gene regulation, acting in a cell-type-specific manner. Utilising RNAi approaches the role of the three identified dCoREST complexes was analysed during fly development. Two developing systems were used in this study: the developing wing and spermatogenesis.

The data obtained in developing wing upon knockdown of dCoREST and its interacting partners has highlighted both redundant and specific functions of the three dCoREST complexes. In agreement with observations in this study, previously published data also reported gain of wing vein material upon depletion of dCoREST but in a different experimental setup (Curtis et al., 2011; Curtis et al., 2013). Furthermore, in the same studies it was also shown that knockout of dLSD1 leads to formation of ectopic veins as well, reflecting that different approaches were used. The results presented here show that simultaneous inactivation of all complexes, by targeting the shared dCoREST subunit for depletion, produced strong vein phenotypes with high penetrance (**Figure 3.24** and **Figure 3.25**), wheres no single dCoREST complex is critical for the developing wing. Notably, dLint-1 depletion indeed resulted in a strong phenotype that was distinct from the one caused by dCoREST depletion in this experimental setup.

Taken together, the plausible explanation of this finding is that the three dCoREST complexes contribute to wing differentiation in a redundant fashion such that inactivation of one complex is compensated for by the two remaining dCoREST complexes. Alternatively, wing cells might contain an as yet unidentified dCoREST containing complex that is crucial for vein differentiation and that we have not targeted for depletion in our experiments. However, the previous work using same en-GAL4 fly line showed indeed the effects in wing vein patterning (Kovač et al., 2018). Moreover, the same UAS-RNAi lines used in this study to deplete dCoREST complexes' specific subunit in male germ line were efficient. Taken together, it is not excluded that the spatiotemporal point or the strength of en-GAL4 depletion in the developing wing disc was not sufficient to cause any effects in these experiments.

The data obtained upon knockdown of dCoREST and its interacting partners in male germ line showed that depletion of LINT subunits or dG9a has no effect on spermatogenesis. dL(3)mbt, dLint-1, and dG9a-depleted males were fertile without any observable defects (**Table 4.1**). Supporting the observation that dG9a does not have any effect on male germ line development is that dG9a *null* flies are viable. On the other hand, dCoREST and dLSD1-depleted males failed to generate offspring (**Table 4.1**), and no mature sperm was detected in seminal vesicles (**Figure 3.27**). Moreover, depletion of dCoREST and dLSD1 in the male germ line leads to post-meiotic

spermatid nuclei elongation defects (**Figure 3.28**). Notably, depletion of LSD1 in mouse testes also resulted in the same phenotype (Lambrot et al., 2015; Myrick et al., 2017). Taken together, although the LINT complex and the dG9a/dCoREST complex seems to be dispensable for proper sperm development in *Drosophila*, the dLSD1/dCoREST complex plays a crucial role during this process. A possible mechanism that leads to this severe phenotype lies in miss-regulation of transcriptome profiling of male germ cells. Remarkably, this property of the dLSD1/dCoREST complex seems to be conserved from *Drosophila* to mice.

4.4. Cell-type specificity of dCoREST complexes

In this study three distinct dCoREST complexes were biochemically characterised. Interestingly, the two dCoREST complexes described here, the dLSD1/dCoREST complex and the LINT complex, act in a cell-type-specific manner. How is dCoREST complex activity limited to particular cell types?

Differences in expression levels of dCoREST complex signature subunits in the investigated cells types could be a simple explanation for the cell-type- and lineage-specific differences in dCoREST complexes functions. In S2 cells the expression of dLSD1 is more than three fold higher compared to testis, as judged by RNA levels reported in modENCODE expression data analysis (data retrieved from www.flybase.org). Nonetheless, transcriptome analysis revealed only few genes repressed by the dLSD1/dCoREST complex in S2 cells. By contrast, results obtained in this study showed that the dLSD1/dCoREST complex is a major repressor of transcription in testis and essential for spermatogenesis. According to modENCODE expression data analysis dLint-1 is slightly lower expressed in S2 cells compared to fly testes. Notably, its mRNA levels in S2 cells and testis are both comparable to the expression of dLSD1 in S2 cells. Interestingly, the LINT complex is a major regulator of transcription in S2 cells, while it has no detectable effects on spermatogenesis. The expression of dG9a is very low in S2 cell and in fly testes and the mRNA is roughly half the level of mRNA of dLSD1 expressed in fly testes. This could explain why there were only weak effects on the transcriptome in dG9a-depleted cells. At the protein level,

however, it has been demonstrated that dG9a is abundantly expressed in testis (Stabell et al., 2006; Ushijima et al., 2012). Taken together, the differences in dCoREST complex activity in the cell types analysed in this study cannot simply be the result of differences in their expression levels.

It is conceivable that post-translational modifications of CoREST complexes, that are cell-type-specific, alter their functions. The role of post-translational modifications was beyond the aims of this study, but it would be interesting to address experimentally the impact of PTMs on the function of dCoREST complexes. For example, affinity purification of dCoREST complexes from S2 cells and fly testis followed by MS analysis of PTMs of signature subunits could give a possible answer to this hypothesis.

Alternatively, cell-type-specific transcription factors could play an important role in recruiting dCoREST complexes to specific genes, hence restricting their repression activity only to certain sets of genes. These cell-type-specific transcription factors would specifically interact with one or more signature subunits of a particular dCoREST complex, potentially recruiting the complex to the sets of genes that need to be silenced in this cell type. An illustration of this concept was recently provided in a description of the mechanism for recruiting the chromatin regulator dMi-2 by the germline-specific transcription factor Kumgang. This enables "dMi-2—mediated" repression of hundreds of genes in the male germline (Kim et al., 2017). Furthermore, the recruitment of a particular dCoREST complex by cell-type-specific transcription factors could be further diversified by restricting the interaction to specific post-translational modification signatures of a dCoREST complex. Some types of post-translational modifications occur as a consequence of stimuli sensed by the cell, for example hormone action, oxidative stress, heat stress, genotoxic stress, and starvation. Taken together, this could open the possibility that distinct dCoREST complexes not only act in a cell-type-specific manner, but could act as sensors of changes in cell metabolism.

In conclusion, a set of distinct histone deacetylase complexes, that are built around a dCoREST/dRPD3 core, were identified in this study. These complexes have the potential to generate repressive chromatin structures by altering nucleosome acetylation and methylation. They repress lineage inappropriate genes, such as neuronal genes in

the male germ line or germline-specific genes in macrophage-like cells, and are, therefore, playing critical roles in differentiation. The results have revealed an unexpected division of labour among these complexes with individual dCoREST complexes being dedicated to preventing inappropriate gene expression in specific cell lineages and cell types.

5. Summary

5.1. Summary

Regulation of chromatin in the cell is achieved by protein complexes that are assembled in a combinatorial fashion. These complexes often contain different isoforms of the same subunit, thus, greatly increasing the number of related, but still diverse complexes. We are just beginning to unravel the rules that dictate isoform-specific complex assembly and the contributions that distinct subunit isoforms make to complex function. CoREST has been identified as a subunit of complexes that typically combine several histone modifying activities. For example, it directly binds to HDAC1 and KDM1A/ LSD1 and enhances their activity on nucleosome substrates. However, the CoREST interactome has not been systematically characterised. CoREST complexes are considered to generate transcriptionally repressive chromatin structures during development.

Drosophila expresses two isoforms of CoREST, dCoREST-L and dCoREST-M.

In this study analysis of *Drosophila* macrophage-like S2 cell nuclear extracts by size exclusion chromatography has suggested that the two dCoREST isoforms reside in different complexes. Additionally, the dCoREST interactome was determined by affinity chromatography and mass spectrometry identifying subunits of both the LINT and the dLSD1/dCoREST complexes. Notably, whereas both dCoREST-L and dCoREST-M bound the LINT complex subunits, only dCoREST-L was capable of interacting with dLSD1 *in vitro* and *in vivo*, providing support for isoform-specific complex formation. Proteomic analysis also identified the histone methyltransferase dG9a as a novel dCoREST interactor. dG9a itself did not bind dLSD1 or the LINT complex subunits suggesting it forms an independent assembly with dCoREST. These proteomic data indicate that at least three distinct dCoREST complexes exist: LINT, dLSD1/dCoREST and dG9a/dCoREST.

Genome-wide experiments established that dCoREST complexes associate with chromatin predominantly at promoters. To assess the relative contributions of the three

dCoREST complexes to gene regulation and to wing and male germ cell development, RNA interference approaches targeting individual complex subunits were used. RNA-seq revealed that the LINT complex, but not dLSD1/dCoREST or dG9a/dCoREST, is a major regulator of transcription in S2 cells. In particular, LINT repressed a set of malignant brain tumour (MBTS) genes. Conversely, the dLSD1/dCoREST complex was essential for spermatogenesis, whereas the LINT and the dG9a/dCoREST complexes appeared dispensable. Indeed, RNA-seq analysis of dissected testes demonstrated that dLSD1/dCoREST is required to repress the inappropriate expression of cell-type-specific genes during spermatogenesis.

These results define isoform-specific dCoREST complexes and suggest that distinct dCoREST complexes are differentially utilised to maintain appropriate transcriptional programmes in different cell types.

5.2. Zusammenfassung

In der Zelle wird Chromatin durch Proteinkomplexe reguliert, die aus verschiedenen Untereinheiten zusammengesetzt sind. Häufig beinhalten diese Komplexe verwandte Isoformen ihrer charakteristischen Untereinheiten, wodurch die Zahl ähnlicher aber doch diverser Komplexe zunimmt. Wir beginnen gerade erst zu verstehen, nach welchen Regeln sich diese isoform-spezifischen Proteinkomplexe zusammensetzen und welchen Beitrag sie zu komplexen Funktionen innerhalb der Zelle leisten.

In dieser Arbeit wurde CoREST als Untereinheit von Proteinkomplexen identifiziert, die typischerweise mehrere Histon-modifizierende Aktivitäten kombinieren. Zum Beispiel bindet es direkt an HDAC1 und KDM1A/LSD1, um deren Aktivität an Nukleosomsubstraten zu verstärken. Das CoREST Interaktom selbst wurde jedoch bisher noch nicht systematisch charakterisiert. Es wird angenommen, dass CoREST Komplexe während der Entwicklung zur Ausbildung Transkriptions-hemmender Chromatinstrukturen beitragen.

In *Drosophila* werden zwei unterschiedliche Isoformen des CoREST-Proteins exprimiert, dCoREST-L und dCoREST-M.

Mit Hilfe der Größenausschluss-Chromatographie wurden Zellkernextrakte von Makrophagen-ähnlichen S2 Zellen aus *Drosophila* analysiert. Die Ergebnisse deuten daraufhin, dass die zwei CoREST Isoformen Bestandteil unterschiedlicher Proteinkomplexe sind. Zusätzlich wurde das CoREST Interaktom mithilfe von Affinitätschromatographie und Massenspektrometrie untersucht. Dadurch konnten Untereinheiten des LINT und des dLSD1/dCoREST-Komplexes identifiziert werden. Während *in vitro* und *in vivo* dLSD1 ausschließlich mit dCoREST-L interagiert, beinhaltet der LINT-Komplex sowohl dCoREST-L als auch dCoREST-M. Dies deutet auf eine Isoform-spezifische Komplexbildung hin. Proteom-Analysen identifizierten außerdem die Histonmethyltransferase dG9a als neuen Interaktionspartner von CoREST. Allerdings bindet dG9a selbst nicht an Untereinheiten des dLSD1/dCoREST oder des LINT Komplexes. Dies spricht für eine von diesen Untereinheiten unabhängige Bindung von dG9a an CoREST. Die Proteom-Analyse legt nahe, dass drei

verschiedene dCoREST Komplexe existieren: LINT, dLSD1/dCoREST und dG9a/dCoREST.

Genom-weite Analysen haben etabliert, dass dCoREST-Komplexe vornehmlich in Promotorbereichen mit Chromatin assoziieren. Die Beteiligung der drei dCoREST Komplexe an der Regulierung der Geneexpression sowie an der Flügelentwicklung und Spermatogenese wurde mithilfe von RNA-Interferenz untersucht. Dadurch konnte die Expression einzelner Untereinheiten der gefundenen Proteinkomplexe gezielt gehemmt werden. Die nachfolgende RNA-Sequenzierung (RNA-seq) zeigte, dass weder der dLSD1/dCoREST noch der dG9a/dCoREST Komplex die Transkription in S2 Zellen beeinflussen. Der LINT Komplex hingegen scheint eine große Rolle bei der Regulation der Transkription zu spielen. Dieser reprimiert eine Gruppe von *malignant brain tumour signature* Genen (MBTS). Der dLSD1/dCoREST Komplex ist für die Spermatogenese essentiell, während der LINT und der dG9a/dCoREST Komplex hierfür nicht notwendig sind. Die RNA-seq Analyse von Hodengewebe zeigte, dass der dLSD1/dCoREST Komplex nötig ist, um die Expression von zelltypspezifischen Genen zu reprimieren, die andernfalls die Spermatogenese verhindern würden.

In dieser Arbeit konnten Isoform-spezifische dCoREST Komplexe identifiziert werden, die eine differentielle Funktion zur Aufrechterhaltung von zelltypspezifischen Transkriptionprogammen nahelegen.

6. References

Abrajano,J.J., Qureshi,I.A., Gokhan,S., Zheng,D., Bergman,A. and Mehler,M.F. (2009a) Differential deployment of REST and CoREST promotes glial subtype specification and oligodendrocyte lineage maturation. *PLoS One*, **4**, e7665.

Abrajano,J.J., Qureshi,I.A., Gokhan,S., Zheng,D., Bergman,A. and Mehler,M.F. (2009b) REST and CoREST modulate neuronal subtype specification, maturation and maintenance. *PLoS One*, **4**, e7936.

Abrajano,J.J., Qureshi,I.A., Gokhan,S., Molero,A.E., Zheng,D., Bergman,A. and Mehler,M.F. (2010) Corepressor for element-1-silencing transcription factor preferentially mediates gene networks underlying neural stem cell fate decisions. *Proc. Natl. Acad. Sci. U. S. A.*, **107**, 16685–16690.

Alam,H., Gu,B. and Lee,M.G. (2015) Histone methylation modifiers in cellular signaling pathways. *Cell. Mol. Life Sci.*, **72**, 4577–4592.

An,P.N.T., Shimaji,K., Tanaka,R., Yoshida,H., Kimura,H., Fukusaki,E. and Yamaguchi,M. (2017) Epigenetic regulation of starvation-induced autophagy in *Drosophila* by histone methyltransferase G9a. *Sci. Rep.*, **7**, 1–14.

Andrés,M.E., Burger,C., Peral-Rubio,M.J., Battaglioli,E., Anderson,M.E., Grimes,J., Dallman,J., Ballas,N. and Mandel,G. (1999) CoREST: a functional corepressor required for regulation of neural-specific gene expression. *Proc. Natl. Acad. Sci. U. S. A.*, **96**, 9873–9878.

Andrews,N.C. and Faller,D. V. (1991) A rapid micrqpreparation technique for extraction of DNA-binding proteins from limiting numbers of mammalian cells. *Nucleic Acids Res.*, **19**, 2499.

Annunziato,A.T., Frado,L.L., Seale,R.L. and Woodcock,C.L. (1988) Treatment with sodium butyrate inhibits the complete condensation of interphase chromatin. *Chromosoma*, **96**, 132–138.

Anreiter,I., Kramer,J.M. and Sokolowski,M.B. (2017) Epigenetic mechanisms modulate differences in *Drosophila* foraging behavior. *Proc. Natl. Acad. Sci. U. S. A.*, **114**, 12518–12523.

Arents,G., Burlingame,R.W., Wang,B.I.C., Love,W.E. and Moudrianakis,E.N. (1991) The nucleosomal core histone octamer at 3.1 Å resolution: A tripartite protein assembly and a left-handed superhelix. *Proc. Natl. Acad. Sci. U. S. A.*, **88**, 10148–10152.

Banerjee,T. and Chakravarti,D. (2011) A Peek into the Complex Realm of Histone Phosphorylation. *Mol. Cell. Biol.*, **31**, 4858–4873.

Bannister,A.J. and Kouzarides,T. (2011) Regulation of chromatin by histone modifications. *Cell Res.*, **21**, 381–395.

Bao,Y., Konesky,K., Park,Y.J., Rosu,S., Dyer,P.N., Rangasamy,D., Tremethick,D.J., Laybourn,P.J. and Luger,K. (2004) Nucleosomes containing the histone variant H2A.Bbd organize only 118 base pairs of DNA. *EMBO J.*, **23**, 3314–3324.

Barrios,A.P., Gomez,A. V., Saez,J.E., Ciossani,G., Toffolo,E., Battaglioli,E., Mattevi,A. and Andres,M.E. (2014) Differential Properties of Transcriptional Complexes Formed by the CoREST Family. *Mol. Cell. Biol.*, **34**, 2760–2770.

References

Barski,A., Cuddapah,S., Cui,K., Roh,T.Y., Schones,D.E., Wang,Z., Wei,G., Chepelev,I. and Zhao,K. (2007) High-Resolution Profiling of Histone Methylations in the Human Genome. Cell, **129**, 823–837.

Benting,J., Lecat,S., Zacchetti,D. and Simons,K. (2000) Protein expression in *Drosophila* Schneider cells. *Anal. Biochem.*, **278**, 59–68.

Bhaumik,S.R., Smith,E. and Shilatifard,A. (2007) Covalent modifications of histones during development and disease pathogenesis. *Nat. Struct. Mol. Biol.*, **14**, 1008–1016.

Biggar,K.K. and Li,S.S.-C. (2015) Non-histone protein methylation as a regulator of cellular signalling and function. *Nat. Rev. Mol. Cell Biol.*, **16**, 5–17.

Black,B.E., Foltz,D.R., Chakravarthy,S., Luger,K., Woods,V.L., and Cleveland D.W. (2004) Structural determinants for generating centromeric chromatin. *Nature*, **430**, 578–582.

Black,J.C., Van Rechem,C. and Whetstine,J.R. (2012) Histone Lysine Methylation Dynamics: Establishment, Regulation, and Biological Impact. *Mol. Cell*, **48**, 491–507.

Blanc,R.S. and Richard,S. (2017) Regenerating muscle with arginine methylation. *Transcription*, **8**, 175–178.

Bonasio,R., Lecona,E. and Reinberg,D. (2010) MBT domain proteins in development and disease. *Semin. Cell Dev. Biol.*, **21**, 221–230.

Böttcher,R., Hollmann,M., Merk,K., Nitschko,V., Obermaier,C., Philippou-Massier,J., Wieland,I., Gaul,U. and Förstemann,K. (2014) Efficient chromosomal gene modification with CRISPR/cas9 and PCR-based homologous recombination donors in cultured *Drosophila* cells. *Nucleic Acids Res.*, **42**.

Botuyan,M.V., Lee,J., Ward,I.M., Kim,J.-E., Thompson,J.R., Chen,J. and Mer,G. (2006) Structural basis for the methylation state-specific recognition of histone H4-K20 by 53BP1 and Crb2 in DNA repair. *Cell*, **127**, 1361–1373.

Bracken,A.P., Brien,G.L. and Verrijzer,C.P. (2019) Dangerous liaisons: Interplay between SWI/SNF, NURD, and polycomb in chromatin regulation and cancer. *Genes Dev.*, **33**, 936–959.

Brand,A.H. and Perrimon,N. (1993) Targeted gene expression as a means of altering cell fates and generating dominant phenotypes. *Development*, **118**, 289–295.

Brehm,A., Längst,G., Kehle,J., Clapier,C.R., Imhof,A., Eberharter,A., Müller,J. and Becker,P.B. (2000) dMi-2 and ISWI chromatin remodelling factors have distinct nucleosome binding and mobilization properties. *EMBO J.*, **19**, 4332–4341.

Burgess,R.J. and Zhang,Z. (2013) Histone chaperones in nucleosome assembly and human disease. *Nat. Struct. Mol. Biol.*, **20**, 14–22.

Buschbeck,M. and Hake,S.B. (2017) Variants of core histones and their roles in cell fate decisions, development and cancer. *Nat. Rev. Mol. Cell Biol.*, **18**, 299–314.

Cao,J. and Yan,Q. (2012) Histone ubiquitination and deubiquitination in transcription, DNA damage response, and cancer. *Front. Oncol.*, **2**, 1–9.

Chang,B., Chen,Y., Zhao,Y. and Bruick,R.K. (2007) JMJD6 is a histone arginine demethylase. *Science*, **318**, 444–447.

Cherbas,L., Willingham,A., Zhang,D., Yang,L., Zou,Y., Eads,B.D., Carlson,J.W., Landolin,J.M., Kapranov,P., Dumais,J., *et al.* (2011) The transcriptional diversity of 25 *Drosophila* cell lines. *Genome Res.*, **21**, 301–314.

Chow,C.M., Georgiou,A., Szutorisz,H., Maia e Silva,A., Pombo,A., Barahona,I., Dargelos,E., Canzonetta,C. and Dillon,N. (2005) Variant histone H3.3 marks promoters of transcriptionally active genes during mammalian cell division. *EMBO Rep.*, **6**, 354–360.

Clemens,J.C., Worby,C.A., Simonson-Leff,N., Muda,M., Maehama,T., Hemmings,B.A. and Dixon,J.E. (2000) Use of double-stranded RNA interference in *Drosophila* cell lines to dissect signal transduction pathways. *Proc. Natl. Acad. Sci. U. S. A.*, **97**, 6499–6503.

Costanzi,C. and Pehrson,J.R. (1998) Histone macroH2A1 is concentrated in the inactive X chromosome of female mammals. *Nature*, **393**, 599–601.

Coux,R.-X., Teixeira,F.K. and Lehmann,R. (2018) L(3)mbt and the LINT complex safeguard cellular identity in the *Drosophila* ovary. *Development*, 10.1242/dev.160721.

Crump,N.T., Hazzalin,C.A., Bowers,E.M., Alani,R.M., Cole,P.A. and Mahadevan,L.C. (2011) Dynamic acetylation of all lysine-4 trimethylated histone H3 is evolutionarily conserved and mediated by p300/CBP. *Proc. Natl. Acad. Sci. U. S. A.*, **108**, 7814–7819.

Curtis,B.J., Zraly,C.B., Marenda,D.R. and Dingwall,A.K. (2011) Histone lysine demethylases function as co-repressors of SWI/SNF remodeling activities during *Drosophila* wing development. *Dev. Biol.*, **350**, 534–547.

Curtis,B.J., Zraly,C.B. and Dingwall,A.K. (2013) Drosophila LSD1-CoREST demethylase complex regulates DPP/TGFβ Signaling during wing development. *Genesis*, **51**, 16–31.

Cuthbert,G.L., Daujat,S., Snowden,A.W., Erdjument-Bromage,H., Hagiwara,T., Yamada,M., Schneider,R., Gregory,P.D., Tempst,P., Bannister,A.J., *et al*. (2004) Histone deimination antagonizes arginine methylation. *Cell*, **118**, 545–553.

Dallman,J.E., Allopenna,J., Bassett,A., Travers,A. and Mandel,G. (2004) A Conserved Role But Different Partners for the Transcriptional Corepressor CoREST in Fly and Mammalian Nervous System Formation. *J. Neurosci.*, **24**, 7186–7193.

Dennehey BK, Tyler J. (2014) Histone chaperones in the assembly and disassembly of chromatin. In: Workman JL, Abmayr SM, editors. *Fundamentals of chromatin*. New York: Springer; pp. 29–67.

Davey,C.A., Sargent,D.F., Luger,K., Maeder,A.W. and Richmond,T.J. (2002) Solvent mediated interactions in the structure of the nucleosome core particle at 1.9 a resolution. *J. Mol. Biol.*, **319**, 1097–1113.

de la Calle-Mustienes,E., Modolell,J. and Gómez-Skarmeta,J.L. (2002) The Xiro-repressed gene CoREST is expressed in Xenopus neural territories. *Mech. Dev.*, **110**, 209–211.

Di Lorenzo,A. and Bedford,M.T. (2011) Histone arginine methylation. *FEBS Lett.*, **585**, 2024–2031.

Dietzl,G., Chen,D., Schnorrer,F., Su,K.C., Barinova,Y., Fellner,M., Gasser,B., Kinsey,K., Oppel,S., Scheiblauer,S., *et al.* (2007) A genome-wide transgenic RNAi library for conditional gene inactivation in *Drosophila*. *Nature*, **448**, 151–156.

Dobin,A., Davis,C.A., Schlesinger,F., Drenkow,J., Zaleski,C., Jha,S., Batut,P., Chaisson,M. and Gingeras,T.R. (2013) STAR: Ultrafast universal RNA-seq aligner. *Bioinformatics*, **29**, 15–21.

Dodd,M.S., Papineau,D., Grenne,T., Slack,J.F., Rittner,M., Pirajno,F., O'Neil,J. and Little,C.T.S. (2017) Evidence for early life in Earth's oldest hydrothermal vent precipitates. *Nature*, **543**, 60–64.

Domanitskaya,E. and Schüpbach,T. (2012) CoREST acts as a positive regulator of Notch signaling in the follicle cells of Drosophila melanogaster. *J. Cell Sci.*, **125**, 399–410.

Dorigo,B., Schalch,T., Bystricky,K. and Richmond,T.J. (2003) Chromatin fiber folding: requirement for the histone H4 N-terminal tail. *J. Mol. Biol.*, **327**, 85–96.

Duffy,J.B. (2002) GAL4 system in *Drosophila*: A fly geneticist's Swiss army knife. *Genesis*, **34**, 1–15.

Elgin,S.C.R. and Reuter,G. (2013) Position-effect variegation, heterochromatin formation, and gene silencing in Drosophila. *Cold Spring Harb. Perspect. Biol.*, **5**, a017780.

Eltsov,M., Maclellan,K.M., Maeshima,K., Frangakis,A.S. and Dubochet,J. (2008) Analysis of cryo-electron microscopy images does not support the existence of 30-nm chromatin fibers in mitotic chromosomes in situ. *Proc. Natl. Acad. Sci. U. S. A.*, **105**, 19732–19737.

Feng,Q., Wang,H., Ng,H.H., Erdjument-Bromage,H., Tempst,P., Struhl,K. and Zhang,Y. (2002) Methylation of H3-lysine 79 is mediated by a new family of HMTases without a SET domain. *Curr. Biol.*, **12**, 1052–1058.

Fire,A., Xu,S., Montgomery,M.K., Kostas,S.A., Driver,S.E. and Mello,C.C. (1998) Potent and specific genetic interference by double-stranded RNA in *Caenorhabditis elegans. Nature,* **391**, 806–811.

Fischle,W., Wang,Y., Jacobs,S.A., Kim,Y., Allis,C.D. and Khorasanizadeh,S. (2003) Molecular basis for the discrimination of repressive methyl-lysine marks in histone H3 by Polycomb and HP1 chromodomains. *Genes Dev.*, **17**, 1870–1881.

Fischle,W., Tseng,B.S., Dormann,H.L., Ueberheide,B.M., Garcia,B.A., Shabanowitz,J., Hunt,D.F., Funabiki,H. and Allis,C.D. (2005) Regulation of HP1-chromatin binding by histone H3 methylation and phosphorylation. *Nature*, **438**, 1116–1122.

Fletcher,T.M. and Hansen,J.C. (1995) Core histone tail domains mediate oligonucleosome folding and nucleosomal DNA organization through distinct molecular mechanisms. *J. Biol. Chem.*, **270**, 25359–25362.

Foster,C.T., Dovey,O.M., Lezina,L., Luo,J.L., Gant,T.W., Barlev,N., Bradley,A. and Cowley,S.M. (2010) Lysine-Specific Demethylase 1 Regulates the Embryonic Transcriptome and CoREST Stability. *Mol. Cell. Biol.*, **30**, 4851–4863.

Gabler,M., Volkmar,M., Weinlich,S., Herbst,A., Dobberthien,P., Sklarss,S., Fanti,L., Pimpinelli,S., Kress,H., Reuter,G., *et al.* (2005) Trans-splicing of the mod(mdg4) complex locus is conserved between the distantly related species *Drosophila melanogaster* and *D. virilis. Genetics*, **169**, 723–736.

Gautier,T., Abbott,D.W., Molla,A., Verdel,A., Ausio,J. and Dimitrov,S. (2004) Histone variant H2ABbd confers lower stability to the nucleosome. *EMBO Rep.*, **5**, 715–720.

Goldknopf,I.L., Taylor,C.W., Baum,R.M., Yeoman,L.C., Olson,M.O., Prestayko,A.W. and Busch,H. (1975) Isolation and characterization of protein A24, a 'histone-like' non-histone chromosomal protein. *J. Biol. Chem.*, **250**, 7182–7187.

Graham,F.L. and van der Eb,A.J. (1973a) A New Technique for the Assay of Infectivity of Human Adenovirus 5 DNA. *Virology*, **52**, 456–467.

Graham,F.L. and van der Eb,A.J. (1973b) Transformation of rat cells by DNA of human adenovirus 5. *Virology*, **54**, 536–539.

Graveley,B.R. (2001) Alternative splicing: Increasing diversity in the proteomic world. *Trends Genet.*, **17**, 100–107.

Greer,E.L. and Shi,Y. (2012) Histone methylation: a dynamic mark in health, disease and inheritance. *Nat. Rev. Genet.*, **13**, 343–357.

Grunstein,M. (1997) Histone acetylation in chromatin structure and transcription. *Nature*, **389**, 349–352.

Guelen,L., Pagie,L., Brasset,E., Meuleman,W., Faza,M.B., Talhout,W., Eussen,B.H., de Klein,A., Wessels,L., de Laat,W., *et al.* (2008) Domain organization of human chromosomes revealed by mapping of nuclear lamina interactions. *Nature*, **453**, 948–951.

Hake,S.B., Garcia,B.A., Kauer,M., Baker,S.P., Shabanowitz,J., Hunt,D.F. and Allis,C.D. (2005) Serine 31 phosphorylation of histone variant H3.3 is specific to regions bordering centromeres in metaphase chromosomes. *Proc. Natl. Acad. Sci. U. S. A.*, **102**, 6344–6349.

Hakimi,M.A., Bochar,D.A., Chenoweth,J., Lane,W.S., Mandel,G. and Shiekhattar,R. (2002) A core-BRAF35 complex containing histone deacetylase mediates repression of neuronal-specific genes. *Proc. Natl. Acad. Sci. U. S. A.*, **99**, 7420–7425.

Heitz,E. (1928) Das heterochromatin der moose. *Jahrb Wiss Bot* **69**:762–818

Horn,P.J. and Peterson,C.L. (2002) Molecular biology. Chromatin higher order folding--wrapping up transcription. *Science*, **297**, 1824–1827.

Huang,J. and Berger,S.L. (2008) The emerging field of dynamic lysine methylation of non-histone proteins. *Curr. Opin. Genet. Dev.*, **18**, 152–158.

Huang,Y., Fang,J., Bedford,M.T., Zhang,Y. and Xu,R.-M. (2006) Recognition of histone H3 lysine-4 methylation by the double tudor domain of JMJD2A. *Science*, **312**, 748–751.

Humphrey,G.W., Wang,Y., Russanova,V.R., Hirai,T., Qin,J., Nakatani,Y. and Howard,B.H. (2001) Stable Histone Deacetylase Complexes Distinguished by the Presence of SANT Domain Proteins CoREST/kiaa0071 and Mta-L1. *J. Biol. Chem.*, **276**, 6817–6824.

Hundertmark,T., Theofel,I., Eren-ghiani,Z., Miller,D. and Rathke,C. (2017) Analysis of Chromatin Dynamics During *Drosophila* Spermatogenesis. *Meiosis. Methods Mol. Biol.*, **1471**, 289–303.

Janic,A., Mendizabal,L., Llamazares,S., Rossell,D. and Gonzalez,C. (2010) Ectopic expression of germline genes drives malignant brain tumor growth in *Drosophila. Science (80-.).*, **330**, 1824–1827.

Jarriault,S. and Greenwald,I. (2002) Suppressors of the egg-laying defective phenotype of sel-12 presenilin mutants implicate the CoREST corepressor complex in LIN-12/Notch signaling in C. elegans. *Genes Dev.*, **16**, 2713–2728.

Kagey,M.H., Newman,J.J., Bilodeau,S., Zhan,Y., Orlando,D.A., van Berkum,N.L., Ebmeier,C.C., Goossens,J., Rahl,P.B., Levine,S.S., *et al.* (2010) Mediator and cohesin connect gene expression and chromatin architecture. *Nature*, **467**, 430–435.

Kalakonda,N., Fischle,W., Boccuni,P., Gurvich,N., Hoya-Arias,R., Zhao,X., Miyata,Y., Macgrogan,D., Zhang,J., Sims,J.K., *et al.* (2008) Histone H4 lysine 20 monomethylation promotes transcriptional repression by L3MBTL1. *Oncogene*, **27**, 4293–4304.

Kalashnikova,A.A., Porter-Goff,M.E., Muthurajan,U.M., Luger,K. and Hansen,J.C. (2013) The role of the nucleosome acidic patch in modulating higher order chromatin structure. *J. R. Soc. Interface*, **10**, 20121022.

Kan,P.-Y., Lu,X., Hansen,J.C. and Hayes,J.J. (2007) The H3 tail domain participates in multiple interactions during folding and self-association of nucleosome arrays. *Mol. Cell. Biol.*, **27**, 2084–2091.

Karmodiya,K., Krebs,A.R., Oulad-Abdelghani,M., Kimura,H. and Tora,L. (2012) H3K9 and H3K14 acetylation co-occur at many gene regulatory elements, while H3K14ac marks a subset of inactive inducible promoters in mouse embryonic stem cells. *BMC Genomics*, **13**, 424.

Karytinos,A., Forneris,F., Profumo,A., Ciossani,G., Battaglioli,E., Binda,C. and Mattevi,A. (2009) A novel mammalian flavin-dependent histone demethylase. *J. Biol. Chem.*, **284**, 17775–17782.

Kato,Y., Kato,M., Tachibana,M., Shinkai,Y. and Yamaguchi,M. (2008) Characterization of *Drosophila* G9a in vivo and identification of genetic interactants. *Genes to Cells*, **13**, 703–722.

Kehle,J., Beuchle,D., Treuheit,S., Christen,B., Kennison,J.A., Bienz,M. and Müller,J. (1998) dMi-2, a hunchback-interacting protein that functions in Polycomb repression. *Science (80-.).*, **282**, 1897–1900.

Kim,J., Daniel,J., Espejo,A., Lake,A., Krishna,M., Xia,L., Zhang,Y. and Bedford,M.T. (2006) Tudor, MBT and chromo domains gauge the degree of lysine methylation. *EMBO Rep.*, **7**, 397–403.

Kim,J., Lu,C., Srinivasan,S., Awe,S., Brehm,A. and Fuller,M.T. (2017) Cell fate: Blocking promiscuous activation at cryptic promoters directs cell type-specific gene expression. *Science (80-.).*, **356**, 717–721.

Kornberg,R.D. (1977) Structure of chromatin. *Annu. Rev. Biochem.*, **46**, 931–954.

Kouzarides,T. (2007) Chromatin modifications and their function. *Cell*, **128**, 693–705.

Kovač,K., Sauer,A., Mačinković,I., Awe,S., Finkernagel,F., Hoffmeister,H., Fuchs,A., Müller,R., Rathke,C., Längst,G., *et al.* (2018) Tumour-associated missense mutations in the dMi-2 ATPase alters nucleosome remodelling properties in a mutation-specific manner. *Nat. Commun.*, **9**.

Kramer,J.M., Kochinke,K., Oortveld,M.A.W., Marks,H., Kramer,D., de Jong,E.K., Asztalos,Z., Westwood,J.T., Stunnenberg,H.G., Sokolowski,M.B., *et al.* (2011) Epigenetic regulation of learning and memory by *Drosophila* EHMT/G9a. *PLoS Biol.*, **9**.

Kunert,N. and Brehm,A. (2008) Mass production of Drosophila embryos and chromatographic purification of native protein complexes. *Methods Mol. Biol.*, **420**, 359–371.

Lakowski,B., Roelens,I. and Jacob,S. (2006) CoREST-like complexes regulate chromatin modification and neuronal gene expression. *J. Mol. Neurosci.*, **29**, 227–239.

Lambrot,R., Lafleur,C. and Kimmins,S. (2015) The histone demethylase KDM1A is essential for the maintenance and differentiation of spermatogonial stem cells and progenitors. *FASEB J.*, **29**, 4402–4416.

Lee,M. and Spradling,A.C. (2014) The progenitor state is maintained by lysine-specific demethylase 1 -mediated epigenetic plasticity during Drosophila follicle cell development. *Genes Dev.*, **28**, 2739–2749.

Lee,M.G., Wynder,C., Cooch,N. and Shiekhattar,R. (2005) An essential role for CoREST in nucleosomal histone 3 lysine 4 demethylation. *Nature*, **437**, 432–435.

Lee,K.S., Yoon,J., Park,J.S. and Kang,Y.K. (2010) Drosophila G9a is implicated in germ cell development. *Insect Mol. Biol.*, **19**, 131–139.

Lee,C.-H., Holder,M., Grau,D., Saldaña-Meyer,R., Yu,J.-R., Ganai,R.A., Zhang,J., Wang,M., LeRoy,G., Dobenecker,M.-W., *et al.* (2018) Distinct Stimulatory Mechanisms Regulate the Catalytic Activity of Polycomb Repressive Complex 2. *Mol. Cell*, **70**, 435-448.e5.

Li,G. and Reinberg,D. (2011) Chromatin higher-order structures and gene regulation. *Curr. Opin. Genet. Dev.*, **21**, 175–186.

Li,B., Carey,M. and Workman,J.L. (2007a) The role of chromatin during transcription. *Cell*, **128**, 707–719.

Li,H., Fischle,W., Wang,W., Duncan,E.M., Liang,L., Murakami-Ishibe,S., Allis,C.D. and Patel,D.J. (2007b) Structural basis for lower lysine methylation state-specific readout by MBT repeats of L3MBTL1 and an engineered PHD finger. *Mol. Cell*, **28**, 677–691.

Livak,K.J. and Schmittgen,T.D. (2001) Analysis of relative gene expression data using real-time quantitative PCR and the $2\text{-}^{\Delta\Delta C}{}^{T}$ method. *Methods*, **25**, 402–408.

Love,M.I., Huber,W. and Anders,S. (2014) Moderated estimation of fold change and dispersion for RNA-seq data with DESeq2. *Genome Biol.*, **15**, 1–21.

Luco,R.F., Pan,Q., Tominaga,K., Blencowe,B.J., Pereira-Smith,O.M. and Misteli,T. (2010) Regulation of alternative splicing by histone modifications. *Science*, **327**, 996–1000.

Luger,K., Mäder,A.W., Richmond,R.K., Sargent,D.F. and Richmond,T.J. (1997) Crystal structure of the nucleosome core particle at 2.8 A resolution. *Nature*, **389**, 251–260.

Lyko,F., Ramsahoye,B.H. and Jaenisch,R. (2000) DNA methylation in Drosophila melanogaster. *Nature*, **408**, 538–540.

Malik,H.S. and Henikoff,S. (2003) Phylogenomics of the nucleosome. *Nat. Struct. Biol.*, **10**, 882–891.

Mantri,M., Krojer,T., Bagg,E.A., Webby,C.A., Butler,D.S., Kochan,G., Kavanagh,K.L., Oppermann,U., McDonough,M.A. and Schofield,C.J. (2010) Crystal Structure of the 2-Oxoglutarate- and Fe(II)-Dependent Lysyl Hydroxylase JMJD6. *J. Mol. Biol.*, 10.1016/j.jmb.2010.05.054.

Maurer-Stroh,S., Dickens,N.J., Hughes-Davies,L., Kouzarides,T., Eisenhaber,F. and Ponting,C.P. (2003) The Tudor domain 'Royal Family': Tudor, plant Agenet, Chromo, PWWP and MBT domains. *Trends Biochem. Sci.*, **28**, 69–74.

McGinty,R.K. and Tan,S. (2015) Nucleosome structure and function. *Chem. Rev.*, **115**, 2255–2273.

Meier,K. and Brehm,A. (2014) Chromatin regulation: How complex does it get? *Epigenetics*, **9**, 1485–1495.

Meier,K., Mathieu,E.L., Finkernagel,F., Reuter,L.M., Scharfe,M., Doehlemann,G., Jarek,M. and Brehm,A. (2012) LINT, a novel dL(3)mbt-containing complex, represses malignant brain tumour signature genes. *PLoS Genet.*, **8**.

Merkling,S.H., Bronkhorst,A.W., Kramer,J.M., Overheul,G.J., Schenck,A. and Van Rij,R.P. (2015) The Epigenetic Regulator G9a Mediates Tolerance to RNA Virus Infection in *Drosophila. PLoS Pathog.*, **11**, 1–25.

Min,J., Allali-Hassani,A., Nady,N., Qi,C., Ouyang,H., Liu,Y., MacKenzie,F., Vedadi,M. and Arrowsmith,C.H. (2007) L3MBTL1 recognition of mono- and dimethylated histones. *Nat. Struct. Mol. Biol.*, **14**, 1229–1230.

Mis,J., Ner,S.S. and Grigliatti,T.A. (2006) Identification of three histone methyltransferases in Drosophila: dG9a is a suppressor of PEV and is required for gene silencing. *Mol. Genet. Genomics*, **275**, 513–526.

Mito,Y., Henikoff,J.G. and Henikoff,S. (2005) Genome-scale profiling of histone H3.3 replacement patterns. *Nat. Genet.*, **37**, 1090–1097.

Molden,R.C., Bhanu,N. V, LeRoy,G., Arnaudo,A.M. and Garcia,B.A. (2015) Multi-faceted quantitative proteomics analysis of histone H2B isoforms and their modifications. *Epigenetics Chromatin*, **8**, 15.

Mulligan,P., Yang,F., Di Stefano,L., Ji,J.-Y., Ouyang,J., Nishikawa,J.L., Toiber,D., Kulkarni,M., Wang,Q., Najafi-Shoushtari,S.H., *et al*. (2011) A SIRT1-LSD1 corepressor complex regulates Notch target gene expression and development. *Mol. Cell*, **42**, 689–699.

Murray,K. (1964) The Occurrence of ε-*N*-methyl Lysine in Histones. *Biochemistry*, **3**, 10–15.

Myrick,D.A., Christopher,M.A., Scott,A.M., Simon,A.K., Donlin-Asp,P.G., Kelly,W.G. and Katz,D.J. (2017) KDM1A/LSD1 regulates the differentiation and maintenance of spermatogonia in mice. *PLoS One*, **12**, 1–17.

Nair,V.D., Ge,Y., Balasubramaniyan,N., Kim,J., Okawa,Y., Chikina,M., Troyanskaya,O. and Sealfon,S.C. (2012) Involvement of Histone Demethylase LSD1 in Short-Time-Scale Gene Expression Changes during Cell Cycle Progression in Embryonic Stem Cells. *Mol. Cell. Biol.*, **32**, 4861–4876.

Nowak,S.J. and Corces,V.G. (2004) Phosphorylation of histone H3: a balancing act between chromosome condensation and transcriptional activation. *Trends Genet.*, **20**, 214–220.

Pickersgill,H., Kalverda,B., de Wit,E., Talhout,W., Fornerod,M. and van Steensel,B. (2006) Characterization of the Drosophila melanogaster genome at the nuclear lamina. *Nat. Genet.*, **38**, 1005–1014.

Pokholok,D.K., Harbison,C.T., Levine,S., Cole,M., Hannett,N.M., Lee,T.I., Bell,G.W., Walker,K., Rolfe,P.A., Herbolsheimer,E., *et al.* (2005) Genome-wide map of nucleosome acetylation and methylation in yeast. *Cell*, **122**, 517–527.

Quénet,D., McNally,J.G. and Dalal,Y. (2012) Through thick and thin: the conundrum of chromatin fibre folding in vivo. *EMBO Rep.*, **13**, 943–944.

Qureshi,I.A., Gokhan,S. and Mehler,M.F. (2010) REST and CoREST are transcriptional and epigenetic regulators of seminal neural fate decisions. *Cell Cycle*, **9**, 4477–4486.

Rathke,C., Baarends,W.M., Jayaramaiah-Raja,S., Bartkuhn,M., Renkawitz,R. and Renkawitz-Pohl,R. (2007) Transition from a nucleosome-based to a protamine-based chromatin configuration during spermiogenesis in Drosophila. *J. Cell Sci.*, **120**, 1689–1700.

Rathke,C., Barckmann,B., Burkhard,S., Jayaramaiah-Raja,S., Roote,J. and Renkawitz-Pohl,R. (2010) Distinct functions of Mst77F and protamines in nuclear shaping and chromatin condensation during *Drosophila* spermiogenesis. *Eur. J. Cell Biol.*, **89**, 326–338.

Rathke,C., Baarends,W.M., Awe,S. and Renkawitz-Pohl,R. (2014) Chromatin dynamics during spermiogenesis. *Biochim. Biophys. Acta - Gene Regul. Mech.*, **1839**, 155–168.

Reid,J.L., Iyer,V.R., Brown,P.O. and Struhl,K. (2000) Coordinate regulation of yeast ribosomal protein genes is associated with targeted recruitment of Esa1 histone acetylase. *Mol. Cell*, **6**, 1297–1307.

Riahi,H., Brekelmans,C., Foriel,S., Merkling,S.H., Lyons,T.A., Itskov,P.M., Kleefstra,T., Ribeiro,C., Van Rij,R.P., Kramer,J.M., *et al.* (2019) The histone methyltransferase G9A regulates tolerance to oxidative stress–induced energy consumption. *PLoS Biol.*, **17**, 1–26.

Ricci,M.A., Manzo,C., García-Parajo,M.F., Lakadamyali,M. and Cosma,M.P. (2015) Chromatin fibers are formed by heterogeneous groups of nucleosomes in vivo. *Cell*, **160**, 1145–1158.

Richter,C., Oktaba,K., Steinmann,J., Müller,J. and Knoblich,J. a (2011) The tumour suppressor L(3)mbt inhibits neuroepithelial proliferation and acts on insulator elements. *Nat. Cell Biol.*, **13**, 1029–1039.

Robinson,P.J.J. and Rhodes,D. (2006) Structure of the '30 nm' chromatin fibre: a key role for the linker histone. *Curr. Opin. Struct. Biol.*, **16**, 336–343.

Rogakou,E.P., Pilch,D.R., Orr,A.H., Ivanova,V.S. and Bonner,W.M. (1998) DNA double-stranded breaks induce histone H2AX phosphorylation on serine 139. *J. Biol. Chem.*, **273**, 5858–5868.

Rossetto,D., Avvakumov,N. and Côté,J. (2012) Histone phosphorylation: a chromatin modification involved in diverse nuclear events. *Epigenetics*, **7**, 1098–1108.

Rudolph,T., Yonezawa,M., Lein,S., Heidrich,K., Kubicek,S., Schäfer,C., Phalke,S., Walther,M., Schmidt,A., Jenuwein,T., *et al.* (2007) Heterochromatin Formation in Drosophila Is Initiated through Active Removal of H3K4 Methylation by the LSD1 Homolog SU(VAR)3-3. *Mol. Cell*, **26**, 103–115.

Rudolph,T., Beuch,S. and Reuter,G. (2013) Lysine-specific histone demethylase LSD1 and the dynamic control of chromatin. *Biol. Chem.*, **394**, 1019–1028.

Saiki,R.K., Gelfand,D.H., Stoffel,S., Scharf,S.J., Higuchi,R., Horn,G.T., Mullis,K.B. and Erlich,H.A. (1988) Primer-directed enzymatic amplification of DNA with a thermostable DNA polymerase. *Science*, **239**, 487–491.

Sakabe,K., Wang,Z. and Hart,G.W. (2010) Beta-N-acetylglucosamine (O-GlcNAc) is part of the histone code. *Proc. Natl. Acad. Sci. U. S. A.*, **107**, 19915–19920.

Sambrrook,J. and Russell,D.W. (2001) Molecular Cloning - A Laboratory Manual. Cold Spring Harbor, New York, CSHL Press.

Santoro,S.W. and Dulac,C. (2012) The activity-dependent histone variant H2BE modulates the life span of olfactory neurons. *Elife*, **1**, e00070.

Saramäki,A., Diermeier,S., Kellner,R., Laitinen,H., Vaïsänen,S. and Carlberg,C. (2009) Cyclical chromatin looping and transcription factor association on the regulatory regions of the p21 (CDKN1A) gene in response to 1alpha,25-dihydroxyvitamin D3. *J. Biol. Chem.*, **284**, 8073–8082.

Schmidt,A., Forne,I. and Imhof,A. (2014) Bioinformatic analysis of proteomics data. *BMC Syst. Biol.*, **8**, S3.

Schneider,I. (1972) Cell lines derived from late embryonic stages of *Drosophila* melanogaster. *J. Embryol. Exp. Morphol.*, **27**, 353–365.

Schotta,G., Ebert,A., Dorn,R. and Reuter,G. (2003) Position-effect variegation and the genetic dissection of chromatin regulation in Drosophila. *Semin. Cell Dev. Biol.*, **14**, 67–75.

Schwarz,P.M., Felthauser,A., Fletcher,T.M. and Hansen,J.C. (1996) Reversible oligonucleosome self-association: dependence on divalent cations and core histone tail domains. *Biochemistry*, **35**, 4009–4015.

Seum,C., Bontron,S., Reo,E., Delattre,M. and Spierer,P. (2007) *Drosophila* G9a is a nonessential gene. *Genetics*, **177**, 1955–1957.

Shahbazian,M.D. and Grunstein,M. (2007) Functions of site-specific histone acetylation and deacetylation. *Annu. Rev. Biochem.*, **76**, 75–100.

Shi,Y., Lan,F., Matson,C., Mulligan,P., Whetstine,J.R., Cole,P.A., Casero,R.A. and Shi,Y. (2004) Histone demethylation mediated by the nuclear amine oxidase homolog LSD1. *Cell*, **119**, 941–953.

Shi,Y.J., Matson,C., Lan,F., Iwase,S., Baba,T. and Shi,Y. (2005) Regulation of LSD1 histone demethylase activity by its associated factors. *Mol. Cell*, **19**, 857–864.

Shimaji,K., Konishi,T., Tanaka,S., Yoshida,H., Kato,Y., Ohkawa,Y., Sato,T., Suyama,M., Kimura,H. and Yamaguchi,M. (2015) Genomewide identification of target genes of histone methyltransferase dG9a during *Drosophila* embryogenesis. *Genes to Cells*, **20**, 902–914.

Shogren-Knaak,M. and Peterson,C.L. (2006) Switching on chromatin: mechanistic role of histone H4-K16 acetylation. *Cell Cycle*, **5**, 1361–1365.

Shogren-Knaak,M., Ishii,H., Sun,J.-M., Pazin,M.J., Davie,J.R. and Peterson,C.L. (2006) Histone H4-K16 acetylation controls chromatin structure and protein interactions. *Science*, **311**, 844–847.

Sims,R.J. 3rd and Reinberg,D. (2008) Is there a code embedded in proteins that is based on post-translational modifications? *Nat. Rev. Mol. Cell Biol.*, **9**, 815–820.

Sobel,R.E., Cook,R.G., Perry,C.A., Annunziato,A.T. and Allis,C.D. (1995) Conservation of deposition-related acetylation sites in newly synthesized histones H3 and H4. *Proc. Natl. Acad. Sci. U. S. A.*, **92**, 1237–1241.

Stabell,M., Eskeland,R., Bjørkmo,M., Larsson,J., Aalen,R.B., Imhof,A. and Lambertsson,A. (2006) The *Drosophila* G9a gene encodes a multi-catalytic histone methyltransferase required for normal development. *Nucleic Acids Res.*, **34**, 4609–4621.

Stielow,B., Sapetschnig,A., Krüger,I., Kunert,N., Brehm,A., Boutros,M. and Suske,G. (2008) Identification of SUMO-Dependent Chromatin-Associated Transcriptional Repression Components by a Genome-wide RNAi Screen. *Mol. Cell*, **29**, 742–754.

Strahl,B.D. and Allis,C.D. (2000) The language of covalent histone modifications. *Nature*, **403**, 41–45.

Suto,R.K., Clarkson,M.J., Tremethick,D.J. and Luger,K. (2000) Crystal structure of a nucleosome core particle containing the variant histone H2A.Z. *Nat. Struct. Biol.*, **7**, 1121–1124.

Szabad,J., Reuter,G. and Schröder,M.B. (1988) The effects of two mutations connected with chromatin functions on female germ-line cells of Drosophila. *MGG Mol. Gen. Genet.*, **211**, 56–62.

Talbert,P.B. and Henikoff,S. (2010) Histone variants--ancient wrap artists of the epigenome. *Nat. Rev. Mol. Cell Biol.*, **11**, 264–275.

Talbert,P.B. and Henikoff,S. (2017) Histone variants on the move: substrates for chromatin dynamics. *Nat. Rev. Mol. Cell Biol.*, **18**, 115–126.

Taverna,S.D., Li,H., Ruthenburg,A.J., Allis,C.D. and Patel,D.J. (2007) How chromatin-binding modules interpret histone modifications: lessons from professional pocket pickers. *Nat. Struct. Mol. Biol.*, **14**, 1025–1040.

Thatcher,T.H. and Gorovsky,M.A. (1994) Phylogenetic analysis of the core histones H2A, H2B, H3, and H4. *Nucleic Acids Res.*, **22**, 174–179.

Thoma,F., Koller,T. and Klug,A. (1979) Involvement of histone H1 in the organization of the nucleosome and of the salt-dependent superstructures of chromatin. *J. Cell Biol.*, **83**, 403–427.

Tontsch,S., Zach,O. and Bauer,H.C. (2001) Identification and localization of M-CoREST (1A13), a mouse homologue of the human transcriptional co-repressor CoREST, in the developing mouse CNS. *Mech. Dev.*, **108**, 165–169.

Trojer,P., Li,G., Sims,R.J. 3rd, Vaquero,A., Kalakonda,N., Boccuni,P., Lee,D., Erdjument-Bromage,H., Tempst,P., Nimer,S.D., *et al*. (2007) L3MBTL1, a histone-methylation-dependent chromatin lock. *Cell*, **129**, 915–928.

Tse,C., Sera,T., Wolffe,A.P. and Hansen,J.C. (1998) Disruption of higher-order folding by core histone acetylation dramatically enhances transcription of nucleosomal arrays by RNA polymerase III. *Mol. Cell. Biol.*, **18**, 4629–4638.

Tsukada,Y., Fang,J., Erdjument-Bromage,H., Warren,M.E., Borchers,C.H., Tempst,P. and Zhang,Y. (2006) Histone demethylation by a family of JmjC domain-containing proteins. *Nature*, **439**, 811–816.

Uckelmann,M. and Sixma,T.K. (2017) Histone ubiquitination in the DNA damage response. *DNA Repair (Amst).*, **56**, 92–101.

Upadhyay,A.K. and Cheng,X. (2011) Dynamics of histone lysine methylation: structures of methyl writers and erasers. *Prog. drug Res. Fortschritte der Arzneimittelforschung. Prog. des Rech. Pharm.*, **67**, 107–124.

Ushijima,Y., Inoue,Y.H., Konishi,T., Kitazawa,D., Yoshida,H., Shimaji,K., Kimura,H. and Yamaguchi,M. (2012) Roles of histone H3K9 methyltransferases during *Drosophila* spermatogenesis. *Chromosom. Res.*, **20**, 319–331.

van den Berg,D.L.C., Snoek,T., Mullin,N.P., Yates,A., Bezstarosti,K., Demmers,J., Chambers,I. and Poot,R.A. (2010) An Oct4-Centered Protein Interaction Network in Embryonic Stem Cells. *Cell Stem Cell*, **6**, 369–381.

van Holde,K. and Zlatanova,J. (2007) Chromatin fiber structure: Where is the problem now? *Semin. Cell Dev. Biol.*, **18**, 651–658.

Vaughn,J.L., Goodwin,R.H., Tompkins,G.J. and McCawley,P. (1977) The establishment of two cell lines from the insect *Spodoptera frugiperda* (Lepidoptera; Noctuidae). *In Vitro*, **13**, 213–217.

Venkatesh,S. and Workman,J.L. (2015) Histone exchange, chromatin structure and the regulation of transcription. *Nat. Rev. Mol. Cell Biol.*, **16**, 178–189.

Wang,W.K., Tereshko,V., Boccuni,P., MacGrogan,D., Nimer,S.D. and Patel,D.J. (2003) Malignant brain tumor repeats: a three-leaved propeller architecture with ligand/peptide binding pockets. *Structure*, **11**, 775–789.

Wei,Y., Mizzen,C.A., Cook,R.G., Gorovsky,M.A. and Allis,C.D. (1998) Phosphorylation of histone H3 at serine 10 is correlated with chromosome condensation during mitosis and meiosis in Tetrahymena. *Proc. Natl. Acad. Sci. U. S. A.*, **95**, 7480–7484.

West,M.H. and Bonner,W.M. (1980) Histone 2B can be modified by the attachment of ubiquitin. *Nucleic Acids Res.*, **8**, 4671–4680.

Widom,J. and Klug,A. (1985) Structure of the 300A chromatin filament: X-ray diffraction from oriented samples. *Cell*, **43**, 207–213.

Williams,S.P., Athey,B.D., Muglia,L.J., Schappe,R.S., Gough,A.H. and Langmore,J.P. (1986) Chromatin fibers are left-handed double helices with diameter and mass per unit length that depend on linker length. *Biophys. J.*, **49**, 233–248.

Wismar,J., Löffler,T., Habtemichael,N., Vef,O., Geissen,M., Zirwes,R., Altmeyer,W., Sass,H. and Gateff,E. (1995) The Drosophila melanogaster tumor suppressor gene lethal(3)malignant brain tumor encodes a proline-rich protein with a novel zinc finger. *Mech. Dev.*, **53**, 141–154.

Wittschieben,B.O., Otero,G., de Bizemont,T., Fellows,J., Erdjument-Bromage,H., Ohba,R., Li,Y., Allis,C.D., Tempst,P. and Svejstrup,J.Q. (1999) A novel histone acetyltransferase is an integral subunit of elongating RNA polymerase II holoenzyme. *Mol. Cell*, **4**, 123–128.

Wong,L.H., McGhie,J.D., Sim,M., Anderson,M.A., Ahn,S., Hannan,R.D., George,A.J., Morgan,K.A., Mann,J.R. and Choo,K.H.A. (2010) ATRX interacts with H3.3 in maintaining telomere structural integrity in pluripotent embryonic stem cells. *Genome Res.*, **20**, 351–360.

Woodcock,C.L. and Ghosh,R.P. (2010) Chromatin higher-order structure and dynamics. *Cold Spring Harb. Perspect. Biol.*, **2**, a000596.

Yang,X.-J. and Seto,E. (2008) The Rpd3/Hda1 family of lysine deacetylases: from bacteria and yeast to mice and men. *Nat. Rev. Mol. Cell Biol.*, **9**, 206–218.

Yang,M., Gocke,C.B., Luo,X., Borek,D., Tomchick,D.R., Machius,M., Otwinowski,Z. and Yu,H. (2006) Structural Basis for CoREST-Dependent Demethylation of Nucleosomes by the Human LSD1 Histone Demethylase. *Mol. Cell*, **23**, 377–387.

You,A., Tong,J.K., Grozinger,C.M. and Schreiber,S.L. (2001) CoREST is an integral component of the CoREST- human histone deacetylase complex. *Proc. Natl. Acad. Sci. U. S. A.*, **98**, 1454–1458.

Yun,M., Wu,J., Workman,J.L. and Li,B. (2011) Readers of histone modifications. *Cell Res.*, **21**, 564–578.

Zhang,K., Chen,Y., Zhang,Z. and Zhao,Y. (2009) Identification and verification of lysine propionylation and butyrylation in yeast core histones using PTMap software. *J. Proteome Res*., **8**, 900–906.

Zhang,Y., Malone,J.H., Powell,S.K., Periwal,V., Spana,E., MacAlpine,D.M. and Oliver,B. (2010) Expression in aneuploid *Drosophila* S2 cells. *PLoS Biol.*, **8**.

Zhang,J., Bonasio,R., Strino,F., Kluger,Y., Holloway,J.K., Modzelewski,A.J., Cohen,P.E. and Reinberg,D. (2013) SFMBT1 functions with LSD1 to regulate expression of canonical histone genes and chromatin-related factors. *Genes Dev.*, **27**, 749–766.

Zhang,X., Huang,Y. and Shi,X. (2015) Emerging roles of lysine methylation on non-histone proteins. *Cell. Mol. Life Sci*., **72**, 4257–4272.

Zhang,P., Torres,K., Liu,X., Liu,C.-G. and Pollock,R.E. (2016) An Overview of Chromatin-Regulating Proteins in Cells. *Curr. Protein Pept. Sci*., **17**, 401–410.

Zhang,J., Jing,L., Li,M., He,L. and Guo,Z. (2019) Regulation of histone arginine methylation/demethylation by methylase and demethylase (Review). *Mol. Med. Rep*., **19**, 3963–3971.

Zheng,C., Lu,X., Hansen,J.C. and Hayes,J.J. (2005) Salt-dependent intra- and internucleosomal interactions of the H3 tail domain in a model oligonucleosomal array. *J. Biol. Chem*., **280**, 33552–33557.

Zheng,Y., Thomas,P.M. and Kelleher,N.L. (2013) Measurement of acetylation turnover at distinct lysines in human histones identifies long-lived acetylation sites. *Nat. Commun*., **4**, 2203.

7. Appendix

Mass-spectrometry results

IP/MS data generated in this study are available at ProteomeXchange, identifier PXD014857 (MS identification of dCoREST interactors)

LC-MS/MS analysis of anti-CoREST co-immunoprecipitation

Appendix Table A1. List of proteins identified by LC-MS/MS analysis in the anti-CoREST co-immunoprecipitation experiment sorted according to the difference between anti-CoREST CoIP and IgG control, showing the unique peptides number and sequence coverage of identified proteins (n=4, FDR=0.01, s0=2). The full dataset is available at ProteomeXchange, identifier PXD014857.

Difference	-log (P-value)	Uniprot ID	Gene name	Unique peptides	Seq. coverage [%]	M. w. [kDa]
12.214	3.227	A0A126GUZ1	pre-mod(md	20	63.4	18.8
12.206	3.185	Q8SY33	gw	55	46.9	143.0
11.983	3.293	Q9VW97	Su(var)3-3	71	65.3	98.4
11.557	6.272	A0A0B4LGA2	CG44249	14	36.9	45.4
11.215	5.592	D5SHR0	twz	16	36.2	40.1
10.875	5.795	Q9VBU6	Dmel\CG118	4	19.7	23.7
10.729	3.129	C7LAG1	CoRest	22	60.4	87.3
10.618	6.086	P34021	EcR	1	2.6	91.2
10.382	4.093	Q9VB52	l(3)mbt	139	65.0	163.0
10.320	4.219	Q32KD4	AGO1	20	24.2	109.8
10.264	3.794	Q9W4W7	EG:100G10.	52	69.7	49.2
9.912	5.530	Q9VQK1	Dmel\CG172	17	31.6	67.4
9.723	2.998	Q9VZ22	Lint-1	71	83.9	67.9
9.719	3.429	Q59E36	CoRest	3	67.5	62.7
9.641	4.193	Q9VZ30	Dmel\CG111	104	36.8	385.0
9.637	3.127	P26017	Pc	6	23.3	44.0
9.532	3.233	Q9VL20	Dmel\CG569	48	52.5	71.9
9.520	4.863	Q0E8X8	CG13551	2	32.7	11.9
9.380	2.658	Q9VJ79	Pde11	24	25.4	155.6
8.950	6.080	Q9V9U6	Dmel\CG189	3	23.6	28.3
8.948	4.526	Q9VWH9	Dmel\CG122	8	27.9	39.1
8.919	5.259	Q9VF92	ear	25	31.9	100.2
8.919	5.346	Q9VIY9	Dmel\CG175	1	2.9	58.7
8.764	3.550	Q9VEB1	Mdh2	6	19.3	35.3
8.683	4.328	M9NHB6	CoRest	2	44.6	34.4
8.620	4.838	Q9W0N9	ebd1	9	17.7	65.4
8.615	4.050	Q0E9E2	PCB	109	70.8	132.7
8.507	4.799	Q24523	bun	6	6.8	118.5
8.326	5.877	Q9VNI3	CG1218	6	9.6	51.1
8.143	3.791	Q9VCH5	Nup98-96	21	12.4	210.1
8.129	3.883	Q94517	Rpd3	57	77.7	58.3

Appendix Table A1. List of proteins identified by LC-MS/MS analysis in the anti-CoREST co-immunoprecipitation experiment sorted according to the difference between anti-CoREST CoIP and IgG control, showing the unique peptides number and sequence coverage of identified proteins (*n*=4, FDR=0.01, s0=2). The full dataset is available at ProteomeXchange, identifier PXD014857. (continuation)

Difference	-log (P-value)	Uniprot ID	Gene name	Unique peptides	Seq. coverage [%]	M. w. [kDa]
8.117	6.834	Q8IQ82	pst	6	12.0	74.6
8.104	1.614	Q9W0U4	Dmel\CG138	1	2.5	55.6
8.019	3.714	P35820	Psc	27	22.5	169.8
8.001	1.595	Q7JVI3	eIF3m	2	9.8	44.1
7.985	6.764	Q86B87	mod(mdg4)	11	25.9	52.4
7.958	3.330	Q9VB08	Sce	12	38.4	47.3
7.895	5.086	Q9W482	lin-52	3	19.7	17.8
7.885	6.144	Q9W0T7	Dis3l2	21	27.0	116.8
7.879	3.347	Q01617	cpo	3	5.8	63.3
7.850	4.500	Q9W543	Rbcn-3B	15	13.4	168.5
7.820	2.731	Q9VNP3	Mes2	53	76.9	48.0
7.794	3.840	Q9VXQ3	Mvd	5	19.3	42.8
7.718	9.002	Q9W0P0	Dmel\CG338	3	11.1	33.7
7.718	5.354	O76878	CG11448	3	13.3	50.1
7.702	5.905	A8DZ10	Dmel\CG343	4	21.0	32.8
7.607	5.076	A0A0B4KFZ8	nvy	13	24.4	76.4
7.561	4.625	Q9VVE2	rogdi	2	6.7	30.5
7.548	2.988	Q9VMC7	Dmel\CG316	14	26.7	79.8
7.520	4.925	O46048	east	121	43.8	250.2
7.453	3.961	Q7K1U0	Arc1	15	49.2	28.9
7.403	6.105	Q9W425	Rbcn-3A	47	16.7	377.3
7.397	3.091	Q7KMP8	Rpn9	4	21.2	43.8
7.365	4.870	M9PBZ3	spen	1	24.4	588.5
7.321	5.848	A0A0B4KHE1	Dmel\CG155	11	25.8	34.7
7.320	4.551	M9MRG5	tai	11	8.8	201.6
7.283	5.946	O44434	qkr58E-3	2	15.1	36.7
7.275	3.488	Q9W2E7	Rae1	4	13.3	38.6
7.221	5.293	Q8IPT9	Dmel\CG105	6	24.1	38.0
7.191	3.447	Q8SX68	CG10915	9	22.2	65.4
7.156	6.064	Q9VNP4	Dmel\CG127	30	47.8	47.7
7.135	4.274	Q9VI58	Tailor	11	32.1	63.9
7.109	5.288	Q7JW66	CG12129	2	9.1	40.3
7.091	4.748	Q03017	cact	6	10.8	53.8
7.031	3.783	P39769	ph-p	9	17.5	167.3
7.030	6.554	Q7K0X9	Syx7	3	12.8	31.8
6.861	4.793	Q9VPL5	Tbc1d15-17	20	34.5	81.8
6.861	6.001	Q9VK42	Dmel\CG993	84	47.5	237.1
6.832	4.985	A0A0B4KGB8	px	13	11.8	206.0
6.828	4.553	A0A023GPV6	Dmel\CG363	3	2.9	124.4
6.742	6.637	A0A0B4KH12	bon	20	18.2	120.4
6.673	4.158	Q9VWC7	lincRNA.10	4	6.2	97.2
6.668	3.670	Q9VYJ7	Dmel\CG400	10	27.3	37.8
6.582	5.671	M9PH72	Dmel\CG423	5	5.7	100.2
6.288	4.762	A0A0B4KGQ7	Dmel\CG331	2	6.8	38.7
6.260	4.135	Q9W0R7	Atac3	16	27.4	63.2
6.244	6.325	Q9Y128	cert	3	7.5	68.5
6.196	5.262	Q95RU8	G9a	99	58.9	181.2
6.115	4.782	A0A0B4K6G6	Dmel\CG751	9	5.8	268.0

Appendix Table A1. List of proteins identified by LC-MS/MS analysis in the anti-CoREST co-immunoprecipitation experiment sorted according to the difference between anti-CoREST CoIP and IgG control, showing the unique peptides number and sequence coverage of identified proteins (*n*=4, FDR=0.01, s0=2). The full dataset is available at ProteomeXchange, identifier PXD014857. (continuation)

Difference	-log (P-value)	Uniprot ID	Gene name	Unique peptides	Seq. coverage [%]	M. w. [kDa]
6.080	4.516	Q9VRP5	scny	1	1.7	114.1
6.078	4.973	P25172	Su(z)2	37	31.5	146.4
6.076	4.141	A0A0B4KEI3	CG1513	1	2.1	53.6
6.065	4.862	Q9VBA0	Dmel\CG633	6	20.9	41.3
6.010	5.529	Q7KV27	Dmel\CG164	3	7.0	63.1
6.003	3.874	Q9VNA8	hd	4	10.0	63.4
5.989	4.331	Q7K3B7	CG11208	4	11.1	62.3
5.950	2.176	Q9W569	EG:171E4.4	2	15.0	14.7
5.874	5.986	Q9W1K4	egl	13	13.7	112.1
5.802	3.977	Q9VDQ3	Dmel\CG493	8	18.4	58.8
5.801	5.858	Q9VLN1	Wdr82	4	10.7	35.4
5.789	5.161	Q9VKQ9	Dpy-30L1	5	50.0	13.8
5.765	4.253	Q9VJ08	B1	1	2.5	89.1
5.708	4.343	Q9I7D3	Capr	3	5.3	103.6
5.706	3.297	Q9VMH1	WDR79	2	6.0	55.9
5.628	2.598	P23696	mts	1	10.7	35.5
5.518	4.531	Q9W0K9	Dmel\CG920	2	10.3	24.3
5.515	4.761	Q7KQZ4	lola	4	21.2	82.2
5.512	3.621	Q24141	mei-S332	1	4.2	44.4
5.394	4.460	Q7K3J0	CCT8	35	74.7	59.4
5.363	3.391	Q7K0E3	Mob4	1	8.5	25.7
5.359	3.844	Q9I7F7	Ack-like	3	3.9	147.5
5.248	3.438	Q9VHL2	CCT7	32	63.8	59.4
5.242	4.874	Q8SWW4	anon-WO014	7	7.1	191.1
5.229	1.972	M9NGE4	mud	1	0.9	242.8
5.151	3.977	P04197	Myb	3	8.1	74.0
5.099	4.376	P17917	PCNA	8	47.3	28.8
5.025	4.083	Q9W5A0	anon-WO015	2	4.7	59.2
4.971	3.909	A1Z9E2	mip120	11	17.3	100.0
4.966	4.287	Q7YU80	par-1	1	13.0	113.7
4.938	4.456	Q8T079	BEST:GH194	19	36.4	65.3
4.912	3.494	Q9VQ58	Dmel\CG153	2	2.6	108.1
4.878	5.144	Q9VKF4	Dmel\CG149	5	25.2	22.5
4.833	4.582	P12613	CCT1	18	45.8	59.6
4.831	4.479	Q9W392	CCT2	39	75.7	58.1
4.816	3.397	Q9VC08	Mink	13	23.1	84.5
4.814	3.719	Q8IR25	sd	1	3.8	42.5
4.782	4.684	Q9VS37	Cdc27	2	4.1	101.3
4.776	5.006	Q9VAG4	Vps16B	1	2.9	50.4
4.761	4.473	M9PF42	Cka	8	16.1	77.1
4.751	5.506	M9PG56	Dmel\CG426	2	4.5	93.3
4.750	4.797	Q867Z4	lola	2	10.3	105.8
4.731	3.671	Q9VXW2	DmRH29	4	4.4	136.3
4.715	3.856	Q04688	Ets97D	7	19.2	52.6
4.703	4.671	P48605	CCT3	38	64.3	59.4
4.700	3.429	Q5BIC3	az2	2	3.7	68.8
4.697	4.070	Q9V474	dbr	3	4.9	110.6
4.696	3.218	Q9W1H5	DCP1	4	15.9	41.4

Appendix Table A1. List of proteins identified by LC-MS/MS analysis in the anti-CoREST co-immunoprecipitation experiment sorted according to the difference between anti-CoREST CoIP and IgG control, showing the unique peptides number and sequence coverage of identified proteins (*n*=4, FDR=0.01, s0=2). The full dataset is available at ProteomeXchange, identifier PXD014857. (continuation)

Difference	-log (P-value)	Uniprot ID	Gene name	Unique peptides	Seq. coverage [%]	M. w. [kDa]
4.662	3.499	P48601	Rpt2	4	10.7	49.3
4.628	1.974	Q960V1	simj	5	13.2	95.4
4.614	5.101	Q9VK69	CCT4	30	62.7	57.1
4.608	1.429	Q9VX77	Chchd2	1	7.1	17.3
4.598	2.457	A0A0B4KFX5	CtBP	1	30.9	41.3
4.589	5.173	P29845	Hsc70-5	27	35.9	74.1
4.586	3.370	M9PH19	msn	4	3.9	152.6
4.577	3.914	Q9V9T9	betaGlu	3	4.5	79.3
4.553	4.253	Q7K159	mip40	3	13.1	30.1
4.552	2.939	Q0E931	Dgp-1	1	2.8	72.5
4.549	3.859	Q9VPC0	Pitslre	4	5.3	108.8
4.536	2.338	Q9W542	mip130	3	2.8	110.4
4.533	4.510	Q7KKI0	CCT5	43	81.9	59.3
4.532	2.538	Q24318	Dp	2	6.7	46.7
4.514	2.624	Q59E01	Dmel\CG979	4	6.9	76.4
4.495	1.347	Q9VR89	l(1)G0004	1	6.7	26.7
4.493	3.090	Q9VLJ8	Uba4	2	4.9	50.2
4.430	4.149	Q7K2Q8	Trs31	4	28.4	22.3
4.429	2.149	Q7KRY7	scrib	2	2.5	191.3
4.369	2.174	Q9VSD6	msk	1	1.0	119.3
4.345	2.684	A0A0B4KFX4	Rcd1	3	4.9	112.9
4.340	2.731	Q9VND7	Dmel\CG293	2	10.6	33.6
4.252	2.677	Q9VT60	iPLA2-VIA	10	14.9	96.9
4.242	0.997	Q94524	Dlc90F	1	15.3	12.5
4.242	3.418	P10180	ct	3	1.9	233.4
4.221	3.487	B7Z0I8	anon-EST:L	6	2.8	378.6
4.200	4.085	Q9W3Z4	Dmel\CG334	10	24.1	50.4
4.176	1.878	Q9VWY6	Taf8	1	6.7	36.6
4.147	2.082	Q9VRV5	D19A	3	3.8	96.2
4.131	2.190	P48609	Cdk5	1	4.1	33.2
4.120	3.435	E1JGM9	par-1	1	16.9	88.5
4.120	4.533	Q9VC61	REPTOR	4	9.4	82.3
4.096	3.918	O77459	ken	4	13.0	67.0
4.087	4.302	P05205	Su(var)205	7	36.4	23.2
4.045	4.562	Q9VXQ5	CCT6	32	55.0	58.2
4.023	3.748	Q2MGP0	CG32737 OR	1	2.0	71.6
4.009	3.710	P16568	BicD	25	47.2	89.0
3.992	1.886	M9NDL7	Reps	3	4.8	93.4
3.987	2.893	Q59E33	scaf6	1	2.0	107.6
3.965	1.324	Q9V436	Rpn12	3	14.4	30.2
3.879	3.810	Q9V3Z4	Rpn5	7	15.5	57.7
3.856	2.492	P40798	stc	1	1.3	121.9
3.846	3.656	Q7KLV9	Rpn6	15	40.8	47.3
3.845	1.856	O61444	Mkk4	2	5.2	47.5
3.845	4.669	A0A0B4LFE2	CG8079	2	2.2	55.6
3.839	6.265	A0A0B4K7P1	p53	6	21.9	38.2
3.838	1.928	Q9VY91	Pdcd4	2	3.5	56.4
3.833	3.842	Q9VGQ8	Arfip	5	20.3	38.8

Appendix Table A1. List of proteins identified by LC-MS/MS analysis in the anti-CoREST co-immunoprecipitation experiment sorted according to the difference between anti-CoREST CoIP and IgG control, showing the unique peptides number and sequence coverage of identified proteins (n=4, FDR=0.01, s0=2). The full dataset is available at ProteomeXchange, identifier PXD014857. (continuation)

Difference	-log (P-value)	Uniprot ID	Gene name	Unique peptides	Seq. coverage [%]	M. w. [kDa]
3.807	2.609	M9PGG0	ArfGAP3	2	7.4	54.5
3.801	4.973	Q8T498	Dmel\CG426	2	2.6	171.6
3.798	3.939	Q9V4D4	bip2	1	0.9	154.5
3.757	2.772	Q9VX15	DmRFC2	1	4.5	39.6
3.752	3.194	Q9V3G7	Rpn7	14	45.0	45.4
3.713	3.925	Q9VXG1	hang	9	6.9	213.8
3.706	2.031	Q7JVL3	Prp38	1	4.5	40.1
3.701	2.549	Q9VBR1	Vps33B	3	5.8	71.2
3.701	1.655	O46036	CtBP	1	24.5	50.4
3.660	2.583	Q9XYZ4	mre11	2	2.6	69.3
3.652	2.942	Q9V3H2	Rpn11	6	22.1	34.4
3.648	3.000	Q8MMD2	Eps-15	11	10.3	132.1
3.642	2.109	P53034	RfC4	2	7.6	37.2
3.614	3.193	P20028	RpI135	1	0.8	128.4
3.558	3.737	A1Z7A8	coil	5	11.4	70.5
3.556	1.553	Q8T6I0	Past1	1	1.3	61.0
3.542	4.018	Q03427	LamC	2	5.6	69.9
3.526	4.561	Q9VAA9	Dmel\CG794	3	6.5	52.8
3.506	1.029	P02517	Hsp26	2	14.9	23.0
3.501	1.436	Q9VPF1	Dmel\CG519	1	3.7	42.3
3.494	2.037	Q9VEN9	Patr-1	3	6.9	108.2
3.469	2.595	Q7JX95	CG11123	1	1.7	75.7
3.463	1.357	Q9NF31	ph-d	1	12.6	143.2
3.438	2.621	Q24472	Rbf	1	2.1	96.8
3.400	4.901	P17789	ttk	4	10.7	68.8
3.396	5.118	Q9W2D0	CG4021	1	7.5	37.0
3.349	2.383	Q9VK33	Sfmbt	2	3.0	133.7
3.342	1.660	Q9VX34	DmRH14	3	5.8	92.8
3.337	1.328	Q9W3J4	Dmel\CG212	1	3.7	53.3
3.324	1.974	Q9VB49	mrt	1	2.3	85.8
3.311	1.332	Q9U9Q4	eIF3h	1	5.0	38.4
3.310	3.138	Q6NP69	gfzf	7	10.1	119.3
3.306	4.550	Q9VZ27	CDK2AP1	2	14.6	29.3
3.299	2.811	P23128	me31B	2	8.1	51.9
3.286	2.463	Q7KU01	PNUTS	1	1.1	120.6
3.281	4.573	Q7JWH6	CG1888	2	9.9	42.3
3.275	1.998	A1Z9I5	tum	2	1.8	69.8
3.264	3.953	M9PEL3	qm	3	13.2	37.4
3.263	2.913	A8DYB0	CG13185	1	0.2	631.3
3.259	4.219	P98149	Dif	1	1.6	73.9
3.238	4.479	Q94527	Rel	1	1.0	109.8
3.148	2.994	E1JJ72	Taf1	6	5.1	235.6
3.126	2.504	X2JJ32	Dmel\CG7766	1	1.7	136.7
3.117	3.498	Q0E8J0	MEP-1	4	6.8	124.1
3.111	3.224	X2JGE9	l(1)G0196	2	1.9	130.7
3.100	2.160	B7Z0X1	Shmt	5	16.9	51.0
3.095	3.526	P25161	Rpn3	9	28.5	56.0
3.094	5.202	Q9VZF5	pav	12	16.2	100.7

Appendix Table A1. List of proteins identified by LC-MS/MS analysis in the anti-CoREST co-immunoprecipitation experiment sorted according to the difference between anti-CoREST CoIP and IgG control, showing the unique peptides number and sequence coverage of identified proteins (*n*=4, FDR=0.01, s0=2). The full dataset is available at ProteomeXchange, identifier PXD014857. (continuation)

Difference	-log (P-value)	Uniprot ID	Gene name	Unique peptides	Seq. coverage [%]	M. w. [kDa]
3.092	3.097	Q8IPN8	mtd	1	0.9	94.4
3.088	4.243	Q08605	Trl	6	11.8	54.8
3.072	3.477	Q9V3V6	Rpt5	4	15.7	47.8
3.053	3.775	Q9V406	crp	20	40.1	67.2
3.035	1.223	Q9VN50	eIF3f1	1	3.9	31.1
3.008	3.378	P28166	zfh1	2	2.1	116.6
2.970	5.331	Q9VUB5	upSET	2	0.8	336.4
2.963	0.842	Q9VD81	RpI12	1	11.7	13.6
2.963	2.065	Q7KRY6	ball	1	3.3	66.0
2.961	3.927	Q960S0	BtbVII	7	8.7	78.4
2.959	4.087	Q7PLI2	Nipped-B	1	0.6	223.3
2.949	3.065	Q9W0K4	bab2	6	9.1	114.6
2.939	3.835	Q9VIP9	barr	1	1.6	82.8
2.928	1.308	Q8IQV5	Dmel\CG172	2	3.6	83.5
2.911	1.565	M9NEL3	kis	12	5.2	560.9
2.903	1.712	P49906	Taf11	2	15.3	22.1
2.889	2.344	A0A0B4LFQ2	Incenp	2	5.0	83.4
2.864	2.203	Q9XZ06	Nup93-1	2	3.3	93.9
2.851	1.944	Q7KMQ0	Rpt1	3	7.9	48.5
2.843	5.806	Q9VSY2	Dmel\CG368	1	7.4	23.0
2.836	2.882	Q9V405	Rpt3	4	11.1	47.0
2.826	3.508	Q9VKJ1	CG4751	6	5.9	150.0
2.811	1.390	Q8INN5	Unc-115b	1	3.9	82.1
2.810	3.537	P02518	Hsp27	5	25.4	23.6
2.792	2.926	Q7KQM6	CG11148	3	4.4	173.7
2.789	2.172	E1JIM1	nsl1	1	1.9	99.1
2.788	2.160	Q9VAW3	Gfat2	1	2.0	76.5
2.784	1.104	A0A0B4KG68	Tm1	1	6.0	29.1
2.779	2.745	Q9XZT7	Taf10b	5	30.8	15.8
2.774	2.804	M9PG55	Dmel\CG106	1	1.7	150.4
2.764	1.632	A8DYJ0	EndoB	1	3.3	41.3
2.761	4.947	M9PID3	HIPP1	1	1.4	99.7
2.758	2.816	P91638	smid	6	8.5	104.3
2.753	2.045	Q9VBZ5	Ythdf	2	3.4	78.9
2.735	1.896	Q9W590	Ns3	1	2.0	70.2
2.725	3.744	Q7KRI2	lolal	8	49.6	14.5
2.714	3.878	O18413	Rpt6	1	6.2	45.9
2.702	3.354	Q86PF3	cindr	11	21.7	67.1
2.699	1.618	Q9VL18	eEF1delta	1	9.0	28.9
2.690	2.668	Q24325	Taf2	1	1.4	139.5
2.683	3.912	P46863	Klp61F	4	4.7	121.2
2.675	4.661	P47825	Taf4	6	11.8	92.1
2.672	3.264	O02649	Hsp60A	43	63.2	60.8
2.664	2.451	Q8IRH5	FBpp007260	1	2.1	80.9
2.661	3.237	Q9VUR2	Dmel\CG123	10	18.9	88.7
2.633	2.283	X2JE07	Dmel\CG167	1	1.7	109.0
2.625	2.267	Q8T390	EndoA	2	13.8	41.4
2.623	2.773	A0A0B4KGP6	Fmr1	3	5.4	64.9

Appendix Table A1. List of proteins identified by LC-MS/MS analysis in the anti-CoREST co-immunoprecipitation experiment sorted according to the difference between anti-CoREST CoIP and IgG control, showing the unique peptides number and sequence coverage of identified proteins (*n*=4, FDR=0.01, s0=2). The full dataset is available at ProteomeXchange, identifier PXD014857. (continuation)

Difference	-log (P-value)	Uniprot ID	Gene name	Unique peptides	Seq. coverage [%]	M. w. [kDa]
2.610	2.758	Q9VE85	Nup43	3	11.5	40.1
2.603	1.686	P12982	Pp1-87B	1	4.0	34.5
2.546	3.785	Q9VSH4	CFlm-68k	4	7.8	66.1
2.533	3.808	Q9VXR5	BEST:LD382	1	1.8	69.5
2.533	1.950	Q9VTH2	Dmel\CG426	2	3.2	133.1
2.530	2.017	Q9VJD1	GCS2beta	5	6.8	61.5
2.501	3.578	Q9NJH0	eEF1gamma	25	44.3	49.0
2.494	2.005	Q7KNA0	CG8230	1	1.7	79.1
2.481	3.204	Q9VHY5	Taf7	3	7.6	51.4
2.479	2.556	Q9VXE6	Nup153	5	3.7	196.6
2.479	3.174	A1Z8M2	tou	4	1.9	322.2
2.472	3.823	P26270	Rpn8	12	46.2	38.1
2.455	1.568	P13709	fs(1)h	1	1.6	205.3
2.402	2.970	Q9VJZ5	Tap42	2	2.6	43.3
2.395	2.999	L0MLQ9	4E-T	12	20.2	110.6
2.383	3.466	P52172	srp	8	9.5	134.2
2.378	5.027	Q9XYP8	Grip91	1	1.5	103.7
2.360	3.473	Q8SX89	kuk	16	29.3	60.2
2.356	3.240	Q9V455	Kap-alpha3	5	12.1	57.0
2.354	4.525	O97159	Mi-2	7	4.9	223.1
2.353	3.120	M9PFM9	crol	1	2.8	75.1
2.350	1.783	Q9V3Y5	BcDNA:LD23	1	2.0	112.7
2.337	4.358	Q9VLT5	poe	1	0.3	590.7
2.328	1.267	Q9VWG1	Dmel\CG142	7	48.1	20.8
2.306	1.088	Q9VGA4	MBD-R2	1	0.9	130.2
2.300	2.197	P49847	Taf6	10	24.4	65.7
2.296	2.859	Q7K0D8	Nup50	2	5.5	59.4
2.289	1.695	Q9VZE6	CG11583	1	4.7	41.6
2.281	2.291	O44081	Nop60B	2	11.0	25.8
2.269	1.430	P14199	ref(2)P	4	12.5	65.3
2.263	4.018	Q961C3	Dmel\CG847	10	20.5	62.4
2.262	2.243	Q9NCC3	SH3PX1	2	4.2	63.2
2.252	2.827	Q9V9A7	l(2)04524	7	20.8	62.6
2.250	2.473	Q9VWQ3	Dmel\CG696	13	31.9	53.0
2.234	2.676	A0A0B4KGG9	CtBP	1	26.6	41.9
2.232	2.255	Q9V3P6	Rpn2	3	5.1	113.2
2.229	2.412	Q7YZA2	CG7065	3	3.8	136.8
2.188	4.303	Q8MZI3	BcDNA:HL01	3	6.1	88.2
2.179	4.165	P36179	Pp2A-29B	5	9.0	65.4
2.176	3.303	X2JEU3	Dmel\CG173	18	25.8	100.1
2.171	3.382	M9PE74	nocte	17	11.5	235.0
2.164	2.950	Q7K3L1	mars	12	17.9	101.9
2.158	2.931	Q9VHI7	Dmel\CG119	3	12.9	40.3
2.132	1.431	P48592	RnrS	1	2.5	45.1
2.119	2.884	Q9VCA8	mask	11	4.5	423.1
2.118	2.848	Q9VW54	Rpn1	2	3.6	102.3
2.109	1.496	P08928	Lam	1	2.1	71.3
2.097	3.093	Q9V4C8	Hcf	7	6.7	160.2

Appendix Table A1. List of proteins identified by LC-MS/MS analysis in the anti-CoREST co-immunoprecipitation experiment sorted according to the difference between anti-CoREST CoIP and IgG control, showing the unique peptides number and sequence coverage of identified proteins (n=4, FDR=0.01, s0=2). The full dataset is available at ProteomeXchange, identifier PXD014857. (continuation)

Difference	-log (P-value)	Uniprot ID	Gene name	Unique peptides	Seq. coverage [%]	M. w. [kDa]
2.090	3.703	Q27268	Hel25E	6	25.7	48.7
2.082	2.658	M9PH75	BcDNA:GH23	4	1.8	357.4
2.082	2.400	O62621	betaCOP	1	1.1	102.7
2.081	1.936	M9NDM3	rhea	1	0.8	235.3
2.071	2.895	Q9W1V3	Fib	7	31.1	34.6
2.051	2.646	Q9VUE5	stwl	14	24.7	112.9
2.046	1.572	Q7KND8	Mad1	1	1.2	85.0
2.016	1.889	Q9VNF7	MTA1-like	6	9.4	92.8
2.010	1.353	Q9W061	mu2	2	3.0	138.3
2.009	2.195	Q7JQN4	Rs1	2	2.9	87.8
2.005	2.648	P49905	Taf12	3	29.4	17.6
1.998	3.679	Q9W526	EG:67A9.2	1	3.0	62.3
1.994	1.502	P07487	Gapdh2	2	5.7	35.4
1.985	2.107	P55035	Rpn10	9	28.5	42.6
1.984	1.473	Q8SXM8	LysRS	4	6.6	64.7
1.974	2.243	Q9V8R9	cora	2	2.0	173.9
1.973	2.897	Q24478	Cp190	10	14.9	121.7
1.969	2.563	P48598	eIF4E1	7	30.9	29.2
1.966	2.861	Q9NBD7	chb	5	5.5	165.6
1.948	2.053	Q9U9Q1	RfC38	2	5.9	40.8
1.939	3.890	Q7K2G1	Rpn13	5	19.5	42.0
1.937	4.634	Q9VUM1	Prp31	2	4.0	55.5
1.928	3.304	P35600	Gnf1	3	4.0	108.6
1.920	3.503	Q02748	eIF4A	4	15.9	45.9
1.920	2.927	Q8IRX4	br	1	3.1	55.5
1.916	3.083	Q9VU35	anon-WO011	1	13.6	11.0
1.916	2.405	Q9VQ76	tho2	4	4.4	188.5
1.912	3.860	P52486	Ubc4	1	6.0	22.5
1.890	2.085	P23257	gammaTub23	8	22.5	53.3
1.890	3.204	P02516	Hsp23	8	75.8	20.6
1.878	3.979	P08841	betaTub60D	8	44.5	50.8
1.878	2.152	Q9VPR5	Sf3b1	1	1.6	149.6
1.876	2.445	Q86BS3	Chro	9	16.1	101.1
1.857	3.260	P46461	comt	3	5.8	82.6
1.846	2.495	Q8SX83	spen	1	24.2	593.5
1.842	2.696	P15348	Top2	7	6.6	164.4
1.825	2.149	Q9VAW5	larp	5	4.2	178.1
1.820	4.010	P06605	alphaTub84	27	53.1	49.9
1.818	2.221	A0A0B4LH25	CG4266	1	1.1	130.1
1.816	2.210	Q9W517	wapl	1	0.9	185.2
1.814	2.839	Q7KKH3	Mys45A	1	2.1	82.0
1.771	3.058	Q9W1N1	pita	2	3.7	71.6
1.770	3.731	R9PY26	htk	2	1.7	192.6
1.759	2.488	O61380	eIF4G1	24	19.6	183.9
1.711	2.820	Q9W0S7	Tudor-SN	3	6.0	103.1
1.700	2.630	A0A0B4LF82	Sin3A	6	3.5	220.4
1.694	2.727	Q8IPX7	Rrp40	4	18.1	25.0
1.649	3.831	Q24560	betaTub56D	27	74.7	50.1

Appendix Table A1. List of proteins identified by LC-MS/MS analysis in the anti-CoREST co-immunoprecipitation experiment sorted according to the difference between anti-CoREST CoIP and IgG control, showing the unique peptides number and sequence coverage of identified proteins (n=4, FDR=0.01, s0=2). The full dataset is available at ProteomeXchange, identifier PXD014857. (continuation)

Difference	-log (P-value)	Uniprot ID	Gene name	Unique peptides	Seq. coverage [%]	M. w. [kDa]
1.635	2.808	Q8I0S9	Mccc1	11	25.2	69.4
1.635	3.959	Q9VN25	eIF3a	3	4.0	133.9
1.625	3.276	Q9VN21	lost	3	5.1	59.7
1.600	3.110	P41073	Pep	7	15.4	75.6
1.594	3.213	Q0E940	eIF3b	2	3.0	80.4
1.574	4.071	Q9VBU9	RpS27	4	31.0	9.4

LC-MS/MS analysis of anti-FLAG co-immunoprecipitation

Appendix Table A2. List of proteins identified by LC-MS/MS analysis in the anti-FLAG co-immunoprecipitation experiment of FLAG-dCoREST-L sorted according to the difference between FLAG-dCoREST-L CoIP and control, showing the unique peptides number and sequence coverage of identified proteins (n=4, FDR=0.2, s0=1). The full dataset is available at ProteomeXchange, identifier PXD014857.

Difference	-log (P-value)	Uniprot ID	Gene name	Unique peptides	Seq. coverage [%]	M. w. [kDa]
7.438	3.562	C7LAG1	CoRest	48	55.3	87.3
6.339	1.540	Q9W5N2	RpL38	3	32.9	8.2
5.765	1.997	Q9VB14	RpS10a	2	10.4	18.2
5.357	2.003	Q9W4W7	EG:100G10.6	5	18.8	49.2
5.277	1.586	P31009	RpS2	4	22.5	28.9
5.141	2.013	Q9VWG3	RpS10b	9	63.8	17.9
5.060	2.295	Q9VW	Su(var)3-3	6	8.5	95.9
4.737	1.915	Q9VR42	Dmel\CG3008	1	2.3	69.3
4.638	2.126	P04359	RpL32	8	44.0	16.0
4.618	1.326	P48149	RpS15Aa	5	57.7	14.8
4.383	2.338	O76927	RpS21	12	86.7	9.2
4.343	1.339	Q9VB52	l(3)mbt	16	13.7	163.0
4.332	1.842	O17445	RpL15	6	19.6	24.3
4.263	2.215	Q9VMU4	RpL37A	6	46.7	10.3
4.140	2.069	Q9VZS5	RpL28	12	61.1	16.0
4.129	2.006	Q9V9W2	RpL6	12	53.5	27.7
4.104	2.175	Q9VJ19	RpL30	8	66.7	12.2
4.018	3.189	P38979	sta	15	64.8	30.2
4.014	1.375	Q9VBN5	RpL27	9	55.6	15.9
3.947	2.598	P48588	RpS25	8	51.3	13.2
3.924	1.629	P80455	RpS12	8	51.1	15.2
3.803	2.495	P50882	RpL9	15	65.3	21.4
3.691	2.075	P32100	RpL7	21	50.4	29.6
3.593	1.910	Q24154	RpL29	4	26.3	8.9
3.491	1.821	Q9VHE5	RpL34b	9	33.9	18.4
3.446	2.363	Q9VNE9	RpL13A	9	36.6	23.6
3.422	2.460	P55841	RpL14	15	59.0	19.2
3.378	2.278	O18640	Rack1	15	51.9	35.6
3.371	1.965	Q94517	Rpd3	20	35.7	58.3
3.358	2.816	Q9VNB9	RpL35A	11	51.6	17.7
3.346	1.724	P46223	RpL7A	15	45.8	30.7
3.326	2.405	P39018	RpS19a	19	75.6	17.3
3.241	2.691	Q9VDH8	RpS30	3	9.1	14.6
3.144	2.063	Q9VS34	RpL18	13	46.8	21.7
3.136	2.174	P41093	RpL18A	13	61.0	21.0
3.104	2.518	Q9V9M7	RpL21	13	67.9	18.5
3.057	2.240	Q9V3G1	RpL8	16	52.0	27.9
3.046	1.655	Q9VLT7	RpL36A	4	23.1	12.5
3.012	1.646	P49630	RpL36	6	45.2	13.5
2.983	1.842	P41094	RpS18	10	52.6	17.6
2.983	1.890	Q9W1B9	RpL12	5	30.3	17.7
2.940	2.525	P02518	Hsp27	5	28.6	23.6
2.938	2.422	Q9VTP4	RpL10Ab	10	41.5	24.3
2.879	4.257	Q9W334	RpS28b	6	84.6	7.5
2.712	1.842	P02516	Hsp23	8	63.4	20.6

Appendix Table A2. List of proteins identified by LC-MS/MS analysis in the anti-FLAG co-immunoprecipitation experiment of FLAG-dCoREST-L sorted according to the difference between FLAG-dCoREST-L CoIP and control, showing the unique peptides number and sequence coverage of identified proteins (n=4, FDR=0.2, s0=1). The full dataset is available at ProteomeXchange, identifier PXD014857. (continuation)

Difference	-log (P-value)	Uniprot ID	Gene name	Unique peptides	Seq. coverage [%]	M. w. [kDa]
2.675	2.239	P09180	RpL4	33	65.8	45.0
2.601	1.888	O16797	RpL3	20	42.8	46.9

Appendix Table A2. List of proteins identified by LC-MS/MS analysis in the anti-FLAG co-immunoprecipitation experiment of FLAG-dCoREST-L sorted according to the difference between FLAG-dCoREST-L CoIP and control, showing the unique peptides number and sequence coverage of identified proteins (n=4, FDR=0.2, s0=1). The full dataset is available at ProteomeXchange, identifier PXD014857. (continuation)

Appendix Table A3. List of proteins identified by LC-MS/MS analysis in the anti-FLAG co-immunoprecipitation experiment of FLAG-dCoREST-M sorted according to the difference between FLAG-dCoREST-M CoIP and control, showing the unique peptides number and sequence coverage of identified proteins (n=4, FDR=0.2, s0=1). The full dataset is available at ProteomeXchange, identifier PXD014857.

Difference	-log (P-value)	Uniprot ID	Gene name	Unique peptides	Seq. coverage [%]	M. w. [kDa]
7.969	3.148	Q59E36	CoRest	47	65.4	62.7
6.589	1.991	Q9W4W7	EG:100G10.6	7	20.9	49.2
6.121	1.940	Q9VB14	RpS10a	2	10.4	18.2
5.846	2.126	P02515	Hsp22	5	36.2	19.8
5.816	1.835	Q9VR42	Dmel\CG3008	1	2.3	69.3
5.540	2.316	Q9VWG3	RpS10b	8	56.9	17.9
5.459	1.517	Q9XZT7	Taf10b	4	30.8	15.8
5.446	2.383	P04359	RpL32	11	70.9	16.0
5.312	4.414	P38979	sta	17	60.4	30.2
5.189	1.670	Q9VB52	l(3)mbt	21	17.5	163.0
5.105	2.118	P31009	RpS2	9	31.8	28.9
5.073	2.133	O17445	RpL15	17	39.7	24.3
4.921	3.210	P02518	Hsp27	11	62.4	23.6
4.884	2.984	P29845	Hsc70-5	4	8.6	74.1
4.715	3.692	Q9VDH8	RpS30	4	12.9	14.6
4.641	2.867	P02516	Hsp23	12	63.4	20.6
4.634	3.589	Q9VNB9	RpL35A	18	67.5	17.7
4.570	3.114	P55841	RpL14	16	68.1	19.2
4.529	2.517	P32100	RpL7	25	67.9	29.6
4.471	3.768	O76927	RpS21	15	100.0	9.2
4.450	2.572	Q9VJ19	RpL30	8	55.0	12.2
4.383	5.610	Q9W334	RpS28b	10	96.9	7.5
4.354	2.439	Q9V9W3	RpL6	20	53.4	29.7
4.353	1.370	B7YZQ7	Nurf-38	3	21.4	32.6
4.282	2.766	Q9VMU4	RpL37A	7	65.2	10.3
4.250	3.655	O16130	RpL39	5	39.2	6.3
4.181	1.380	Q9VWG1	Dmel\CG14207	7	36.1	20.8
4.160	1.993	P48149	RpS15Aa	3	27.7	14.8
4.157	2.159	Q9VZS5	RpL28	20	66.7	16.0
4.127	2.989	P50882	RpL9	11	48.9	21.4
4.123	2.283	Q9VHE5	RpL34b	13	51.8	18.4
4.102	2.210	P49630	RpL36	6	53.9	13.5
4.083	3.015	P48588	RpS25	10	53.0	13.2
4.037	2.427	Q9W1B9	RpL12	6	27.3	17.7
4.035	2.963	P39018	RpS19a	24	91.7	17.3
4.018	2.588	Q24154	RpL29	6	36.8	8.9
4.010	2.829	Q9V3G1	RpL8	20	60.2	27.9
3.986	1.276	Q7KBL8	ix	1	9.0	21.1
3.977	2.678	Q9VNE9	RpL13A	10	37.1	23.6
3.941	2.673	Q9V535	tsu	1	10.3	19.0
3.922	1.959	P46223	RpL7A	19	60.5	30.7
3.884	3.170	Q9V9M7	RpL21	11	61.6	18.5
3.839	1.978	P80455	RpS12	6	49.6	15.2
3.813	2.826	Q9VTP4	RpL10Ab	10	43.8	24.3
3.787	2.408	Q9VLT7	RpL36A	5	32.7	12.5
3.786	1.863	Q24186	RpS5a	8	26.3	25.4
3.767	2.783	Q9VVU2	RpL26	13	62.4	17.3

Appendix Table A3. List of proteins identified by LC-MS/MS analysis in the anti-FLAG co-immunoprecipitation experiment of FLAG-dCoREST-M sorted according to the difference between FLAG-dCoREST-M CoIP and control, showing the unique peptides number and sequence coverage of identified proteins (n=4, FDR=0.2, s0=1). The full dataset is available at ProteomeXchange, identifier PXD014857. (continuation)

Difference	-log (P-value)	Uniprot ID	Gene name	Unique peptides	Seq. coverage [%]	M. w. [kDa]
3.707	2.433	Q9VS34	RpL18	18	55.3	21.7
3.679	2.482	Q9VZJ3	Rcd5	5	8.3	63.5
3.669	1.696	O97125	Hsp68	2	5.5	69.7
3.669	2.392	Q9VXX8	RpL37a	11	54.8	10.6
3.614	2.334	P46222	RpL11	10	37.5	21.1
3.591	0.682	Q8IG95	Mes2	10	39.0	41.1
3.586	2.482	P41093	RpL18A	12	62.7	21.0
3.561	2.253	P41094	RpS18	12	58.6	17.6
3.560	0.946	Q9W5E1	Roc1a	1	15.7	12.5
3.554	0.848	Q9VZ22	Lint-1	17	29.2	67.9
3.544	1.374	P19889	RpLP0	13	41.3	34.2
3.538	2.730	P09180	RpL4	42	69.8	45.0
3.520	1.381	Q7JZW2	RpS15	7	38.5	17.0
3.520	1.402	Q9VBN5	RpL27	10	60.7	15.9
3.423	2.421	Q9VKQ9	Dpy-30L1	2	26.9	13.8
3.388	2.211	P55828	RpS20	9	58.3	13.5
3.382	1.528	Q9W499	RpL35	8	38.2	14.4
3.313	1.040	Q9V455	Kap-alpha3	2	7.2	57.0
3.262	2.571	O16797	RpL3	28	49.0	46.9
3.223	0.818	Q7KRI2	lolal	1	10.2	14.5
3.171	3.320	O18640	Rack1	14	44.7	35.6
3.160	1.870	Q94517	Rpd3	16	26.7	58.3
3.057	1.082	Q7K180	Map60	8	24.8	47.6
3.010	1.711	P11147	Hsc70-4	30	43.3	71.1
2.974	1.731	Q9W0A8	RpL23A	20	50.9	29.5
2.937	1.657	P55935	RpS9	18	70.8	22.6
2.871	2.154	Q7K1Q7	RpLP0-like	6	28.1	29.4
2.797	1.468	P15357	RpS27A	2	27.6	17.9
2.779	1.307	Q95RU8	G9a	5	6.2	181.2
2.764	1.408	Q03334	RpS13	13	62.3	17.2
2.755	3.671	Q9VH69	RpS29	6	73.2	6.6
2.743	1.103	Q9W229	RpS24	7	51.1	15.0
2.733	1.720	P08570	RpLP1	4	58.9	11.5
2.662	1.463	Q06559	RpS3	12	43.1	27.5
2.588	1.613	Q9V597	RpL31	12	69.4	14.5
2.581	0.855	Q9V4C8	Hcf	7	7.1	160.2
2.574	1.523	Q9W5R8	RpL5	17	44.1	34.0
2.539	1.636	Q9VA91	RpS7	12	60.8	22.2
2.456	1.388	P25007	Cyp1	3	15.4	24.7
2.443	1.288	Q9VJY6	RpL24	9	53.5	17.5
2.412	1.316	P36241	RpL19	18	50.7	24.0
2.362	2.587	P41126	RpL13	17	51.4	25.0
2.322	1.283	Q8MLY8	RpS8	19	68.3	23.8
2.284	1.307	P48159	RpL23	12	58.6	14.9
2.279	1.379	P29843	Hsc70-1	2	6.1	70.7
2.247	1.326	Q9W237	RpS16	13	63.5	16.8
2.223	1.122	P50887	RpL22	10	35.8	30.6
2.222	1.918	P13008	RpS26	6	49.1	13.3

Appendix Table A3. List of proteins identified by LC-MS/MS analysis in the anti-FLAG co-immunoprecipitation experiment of FLAG-dCoREST-M sorted according to the difference between FLAG-dCoREST-M CoIP and control, showing the unique peptides number and sequence coverage of identified proteins (*n*=4, FDR=0.2, s0=1). The full dataset is available at ProteomeXchange, identifier PXD014857. (continuation)

Difference	-log (P-value)	Uniprot ID	Gene name	Unique peptides	Seq. coverage [%]	M. w. [kDa]
2.219	1.169	P55830	RpS3A	22	63.1	30.3
2.178	1.257	Q8T3U2	RpS23	12	60.8	16.0
2.150	2.501	P18101	RpL40	1	25.0	14.7
2.109	1.152	P29327	RpS6	14	51.2	28.4
2.100	1.242	P17704	RpS17	12	63.4	15.3
2.049	1.051	Q0E9B6	RpS11	15	64.5	18.1
1.999	1.686	Q8T0Q2	Dmel\CG9775	1	5.4	34.2

ChIP-seq results

Raw ChIP-seq data generated in this study have been deposited in the ArrayExpress database at EMBL-EBI (www.ebi.ac.uk/arrayexpress) under accession number E-MTAB-8341.

RNA-seq results

S2 cells

Raw RNA-seq data generated in this study have been deposited in the ArrayExpress database at EMBL-EBI (www.ebi.ac.uk/arrayexpress) under accession number E-MTAB-7440.

Drosophila testes

Raw RNA-seq data generated in this study have been deposited in the ArrayExpress database at EMBL-EBI (www.ebi.ac.uk/arrayexpress) under accession number E-MTAB-7439.
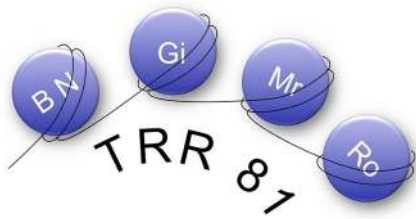
PhD Portfolio — MGK

Summary of PhD training

Name of PhD student:
Igor Mačinković

Affiliation:
Institute of Molecular Biology and Tumour Research (IMT)
School of Medicine
Philipps University Marburg
Hans-Meerwein-Straße 2
D-35043 Marburg
tel: +49-6421-28-66854
fax: +49-6421-28-66842
e-mail: igor.macinkovic@imt.uni-marburg.de

Start of PhD work:
February 14, 2015

Topic of PhD thesis work:
Distinct CoREST complexes act in a cell-type-specific manner

Thesis committee:
1. Prof. Dr Alexander Brehm
2. Prof. Dr Guntram Suske
3. Prof. Dr Raymond Poot

Meetings of the thesis committee:
Two Skype conferences with all three thesis committee members
- 30. July 2015
- 04. April 2017
Other presentations where only first two members were present
- Kleinwalsertal, February 23, 2015
- Gießen, April 02, 2015
- Kleinwalsertal, February 26, 2016
- Kleinwalsertal, February 28, 2018

PhD training

General courses

-

Specific courses
- GE Healthcare Seminar - Chromatography (Marburg, October 13, 2015)
- GE Healthcare Seminar - Chromatography (Marburg, January 25, 2016)
- Galaxy Course (Gießen, October 05, 2016)
- SAP-MM "Besteller für Neueinsteiger" (Marburg, July 09, 2018)

Seminars and workshops
- Transregio 81 Seminar: CoREST complexes in Drosophila (Gießen, April 02, 2015)
- Transregio 81 Seminar: Distinct CoREST complexes act in a cell-type-specific manner (Gießen, April 02, 2015)

Presentations:
Journal Club:
- A Specific LSD1/KDM1A Isoform Regulates Neuronal Differentiation through H3K9 Demethylation (Marburg, April 14, 2015)
- INO80 Chromatin Remodeler Facilitates Release of RNA Polymerase II from Chromatin for Ubiquitin-Mediated Proteasomal Degradation (Marburg, January 12, 2016)
- CHD4 is a Peripheral Component of the Nucleosome Remodeling and Deacetylase Complex (Marburg, June 14, 2016)
- Distortion of histone octamer core promotes nucleosome mobilization by a chromatin remodeler (Marburg, February 02, 2017)
- *Drosophila* CP190- and dCTCF-mediated enhancer blocking is augmented by SUMOylation (Marburg, August 17, 2017)
- L(3)mbt and the LINT complex safeguard cellular identity in the *Drosophila* ovary (Marburg, May 03, 2018)
- Phosphorylation of Histone H4T80 Triggers DNA Damage Checkpoint Recovery (Marburg, December 06, 2018)
- The histone methyltransferase G9a regulates tolerance to oxidative stress-induced energy consumption (Marburg, June 06, 2019)

Chromatin Methods Club:
- Protein-Protein Interaction (Co-IP, GST-pulldown, chromatography, etc.) (Marburg, November 03, 2015)

Retreats:
- 8th Winter School of the Collaborative Research Centre TRR81 "Chromatin Changes in Differentiation and Malignancies" Marburg-Giessen-Bad Nauheim-Rotterdam CoREST complexes in *Drosophila* (Kleinwalsertal, February 26 - March 02, 2018)
- 6th Winter School of the Collaborative Research Centre TRR81 "Chromatin Changes in Differentiation and Malignancies" Marburg-Giessen-Bad Nauheim-Rotterdam CoREST complexes in *Drosophila* (Kleinwalsertal, February 21-26, 2016)
- 5th Winter School of the Collaborative Research Centre TRR81 "Chromatin Changes in Differentiation and Malignancies" Marburg-Giessen-Bad Nauheim-Rotterdam Characterization of CoREST complexes in *Drosophila* (Kleinwalsertal, February 22-27, 2015)

(Inter)national conferences
- 3rd TRR81 Symposium on "Chromatin Changes in Differentiation and Malignancy", (Philipps-University Marburg, Germany, September 14-16, 2015) — poster presentation
- 4th TRR81 Symposium on "Chromatin Changes in Differentiation and Malignancy", (Egmond aam Zee, Netherlands, September 18-20, 2017) — poster presentation
- CSHL Epigenetics & Chromatin meeting (Cold Spring Harbor, USA, September 11-15, 2018) — poster presentation
- 5th TRR81 Symposium on "Chromatin Changes in Differentiation and Malignancy", (Bad Nauheim, Germany, September 09-11, 2019) — poster presentation

Organisation of student workshops/minisymposia on specific topics
- 12th TRR81 PhD Mini-Symposium "Advanced Methods in Chromatin and Gene Expression Research" (Marburg, Germany, April 08, 2019)

Internships in laboratories of the TRR81 in Rotterdam
-

Others
- Supervising a practical course for students of human biology (Marburg, February 11-13, 2015)
- Supervising a lab internship course for two students of human biology (Marburg, March 02-31, 2015)
- Supervising a lab internship course for a student of human biology (Marburg, August 07 – September 01, 2017)
- Supervising a BSc lab work for a student of human biology (Marburg, February 26 – June 23, 2020)

- Supervising a practical course for students of medicine (Marburg, June 15-18, and 24, 2015)
- Supervising a practical course for students of medicine (Marburg, June 17-22, 2016)
- Supervising a practical course for students of medicine (Marburg, June 21, 26-27, 2017)
- Supervising a practical course for students of medicine (Marburg, June 11-13, 2018)
- Supervising a practical course for students of medicine (Marburg, June 13-14, and 19, 2019)

- Seminar — Fachmodule Proteinbiochemie WS 2015/2016 — "CoREST complexes in *Drosophila*" (Marburg, November 19, 2015)
- Seminar — Fachmodule Proteinbiochemie WS 2016/2017 — "CoREST complexes in *Drosophila*" (Marburg, November 24, 2016)
- Seminar — Fachmodule Proteinbiochemie WS 2016/2017 — "CoREST complexes in *Drosophila*" (Marburg, November 16, 2017)
- Seminar — Fachmodule Proteinbiochemie WS 2018/2019 — "CoREST complexes in *Drosophila*" (Marburg, November 22, 2018)
- Seminar — Fachmodule Proteinbiochemie WS 2019/2020 — "CoREST complexes in *Drosophila*" (Marburg, November 21, 2019)

Curriculum vitae

Personal Information

Surname:	Mačinković
First name:	Igor
Date of birth:	September 10th, 1983
Place of birth:	Belgrade, Republic of Serbia
Nationality:	Serbian

Education

2.2015 — present	**PhD student in the lab of Prof. Dr Alexander Brehm** Institute of Molecular Biology and Tumour Research School of Medicine, Philipps-University Marburg, Marburg *Ph.D. dissertation:* *"Distinct CoREST complexes act in a cell-type-specific manner"*	
10.2009 — 07.2010	**MSc in Biochemistry** University of Belgrade, Faculty of Chemistry, Belgrade *Master's thesis:* *"Optimisation of conditions for detection of GST activity under denaturing conditions"*	
10.2002 — 07.2009	**Graduated Biochemist** University of Belgrade, Faculty of Chemistry, Belgrade *Diploma thesis:* *"Expression optimization of recombinant thaumatin-like protein from kiwi fruit — rAct d 2 tagged with GST"*	
09.1998 — 05.2002	Gymnasium "Branko Radičević," Stara Pazova *Matriculation work:* *"Microbes and their application in genetic engineering"*	

Fellowships

10.2014 — 02.2015	**TRR81 Fellowship** Institute of Molecular Biology and Tumour Research School of Medicine , Philipps-University Marburg, Marburg
01.2013 — 12.2013	**EFI-MRIC Fellowship** Chair of Bioinorganic Chemistry Department of Chemistry and Pharmacy Friedrich-Alexander-University Erlangen-Nuremberg

Working experience

11.2010 — 12.2012	**Staff scientist** Institute for Biochemistry of Medical Faculty Friedrich-Alexander-University Erlangen-Nuremberg

Publications

1. Mačinković I, Theofel I, Hundertmark T, Kovač K, Awe S, Lenz J, Forné I, Lamp B, Nist A, Imhof A, Stiewe T, Renkawitz-Pohl R, Rathke C, Brehm A, **Distinct CoREST complexes act in a cell-type-specific manner**, *Nucleic Acids Research* (**2019**) Dec 16;47(22):11649-11666

2. Kovač K, Sauer A, Mačinković I, Awe S, Finkernagel F, Hoffmeister H, Fuchs A, Müller R, Rathke C, Längst G, Brehm A, **Tumour-associated missense mutations in the dMi-2 ATPase alters nucleosome remodelling properties in a mutation-specific manner**, *Nature Communications* (**2018**) May 29;9(1):2112

3. Dorninger F, Herbst R, Kravic B, Camurdanoglu BZ, Macinkovic I, Zeitler G, Forss-Petter S, Strack S, Khan MM, Waterham HR, Rudolf R, Hashemolhosseini S, Berger J, **Reduced muscle strength in ether lipid-deficient mice is accompanied by altered development and function of the neuromuscular junction**, *Journal of Neurochemistry* (**2017**), Dec; 143(5):569-583

4. Jox T, Buxa MK, Bohla D, Ullah I, Mačinković I, Brehm A, Bartkuhn M, Renkawitz R, ***Drosophila* CP190- and dCTCF-mediated enhancer blocking is augmented by SUMOylation**, *Epigenetics and Chromatin* (**2017**), Jul 4; 10:32

5. Kreher J, Kovač K, Bouazoune K, Mačinković I, Ernst AL, Engelen E, Pahl R, Finkernagel F, Murawska M, Ullah I, Brehm A, **EcR recruits dMi-2 and increases efficiency of dMi-2-mediated remodelling to constrain transcription of hormone-regulated genes**, *Nature Communication* (**2017**), Apr 5; 8:14806

6. Park CM*, Macinkovic I*, Filipovic MR, Xian M, **Use of the "Tag-switch" Method for Detection of Protein *S*-Sulfhydration**, *Methods in Enzymology* (**2015**); 555:39-56 (* equal contribution)

7. Weddmann R, Berlein S, Macinkovic I, Bölz S, Miljkovic J, Munoz L, Herrmann M, Filipovic MR, **Working with "H2S": Facts and apparent artifacts**, *Nitric Oxide* (**2014**), Sep 15; 41:85-96

8. Zhang D*, Macinkovic I*, Davarie-Baez NO, Pan J, Park CM, Carroll KS, Filipovic MR, Xian M, **Detection of protein *S*-sulfhydration by a tag-switch technique**, *Angewandte Chemie International Edition* (**2014**), Jan 7; 53(2):575-81 (* equal contribution)

9. Mačinković IS, Abughren M, Mrkic I, Grozdanović MM, Prodanović R, Gavrović-Jankulović M, **Employment of colorimetric enzyme assay for monitoring expression and solubility of GST fusion proteins targeted to inclusion bodies**, *Journal of Biotechnology* (**2013**), Dec; 168(4):506-10

List of academic teachers

My academic teachers at the University of Belgrade were the following professors:

Šerban, Nedeljkoivć, Vučković, Tešić, Pavlović, Dojčilović, Marić, Vrećica, Stanisavljev, Miodragović, Došen Mićović, Jankov, Manojlović, Niketić, Vrvić, Veličković, Korać, Spasić, Vajs, Tomić, Giba, Gavrović Jankulović, Vujčić, Savić Pavićević, Brajušković, Milojković Opsenica, Dimitrijević, Kataranovska

Acknowledgements

Dear reader, before you start reading the last page of this PhD thesis, I would like to write a few lines dedicated to the people who supported me during my work on this dissertation.

First, I would like to thank Prof. Dr Alexander Brehm, who allowed me to perform my experiments in his laboratory, who guided me and taught me real science. It was a pleasure having you as a supervisor for the last six years. Additionally, I would like to thank my PhD thesis committee members, Prof. Dr Guntram Suske and Prof. Dr Raymond Poot, for their scientific impacts on this thesis.

Second, I would like to thank Dr Ina Theofel, Dr Tim Hundertmark and Dr Christina Rathke from the Department of Biology, Philipps-University; Dr Ignasi Forné from Protein Analysis Unit, BioMedical Centre, Faculty of Medicine, LMU Munich and Dr Andrea Nist and Dr Boris Lamp from Genomics Core Facility, Institute of Molecular Oncology, Philipps-University for their experimental and scientific support. Furthermore, I would like to thank Dr Peeyush Sahu, Dr Robert Liefke, Prof. Dr Marek Bartkuhn and Tobias Zimmermann for assistance in the bioinformatics field; and Jonathan Lenz and Prof. Dr Colin Dingwall for their critical reading of this work and English language corrections.

I want to thank my lab colleagues: Kristina, Jonathan, Stephan, and Ulla, as well as the other member of Brehm's lab for their experimental support. Thank you all for the precious moments, for suggestions and advice, for translating my summary in the German language. Besides, one special thank you to Dr Kovač, my flatmate, my travel mate, but, first of all, my friend, for being there for me.

Bastian, Joanna, Lisa, Sabrina, Sara, Satis, Peeyush— it was my pleasure doing this PhD in your surrounding.

Thanks to Dr Mandy Paul-Karasungur and Yunus Karasungur — I hope I finally made it, thanks for believing in me!

Special thanks to all my friends. They encompassed me in the crucial moments on this journey and created an enormous impact on my "think outside the box" decisions.

In the end, thanks to my family. Јеби га, а шта сад?!

Ehrenwörtliche Erklärung

„Ich Igor Mačinković, geboren am 10.09.1983 in Belgrad, Serbien, erkläre ehrenwörtlich, dass ich die dem Fachbereich Medizin Marburg zur Promotionsprüfung eingereichte Arbeit mit dem Titel „**Distinct CoREST complexes act in a cell-type-specific manner**", im Institut für Molekularbiologie und Tumorforschung (Geschäftsführender Direktor: Prof. Dr. Alexander Brehm) unter Leitung von Prof. Dr. Alexander Brehm ohne sonstige Hilfe selbst durchgeführt und bei der Abfassung der Arbeit keine anderen als die in der Dissertation aufgeführten Hilfsmittel benutzt habe. Ich habe bisher an keinem in- oder ausländischen Medizinischen Fachbereich ein Gesuch um Zulassung zur Promotion eingereicht, noch die vorliegende oder eine andere Arbeit als Dissertation vorgelegt. Ich versichere, dass ich sämtliche wörtlichen oder sinngemäßen Übernahmen und Zitate kenntlich gemacht habe. Mit dem Einsatz von Software zur Erkennung von Plagiaten bin ich einverstanden.

Vorliegende Arbeit wurde (oder wird) in folgenden Publikationsorganen veröffentlicht:

1) Kreher J, Kovač K, Bouazoune K, <u>Mačinković I</u>, Ernst AL, Engelen E, Pahl R, Finkernagel F, Murawska M, Ullah I, Brehm A, **EcR recruits dMi-2 and increases efficiency of dMi-2-mediated remodelling to constrain transcription of hormone-regulated genes**, *Nature Communications* (2017), Apr 5; 8:14806

2) Jox T, Buxa MK, Bohla D, Ullah I, <u>Mačinković I</u>, Brehm A, Bartkuhn M, Renkawitz R, ***Drosophila* CP190- and dCTCF-mediated enhancer blocking is augmented by SUMOylation**, *Epigenetics and Chromatin* (2017), Jul 4; 10:32

3) Kovač K, Sauer A, <u>Mačinković I</u>, Awe S, Finkernagel F, Hoffmeister H, Fuchs A, Müller R, Rathke C, Längst G, Brehm A, **Tumour-associated missense mutations in the dMi-2 ATPase alters nucleosome remodelling properties in a mutation-specific manner**, *Nature Communications* (2018) May 29;9(1):2112

4) <u>Mačinković I</u>, Theofel I, Hundertmark T, Kovač K, Awe S, Lenz J, Forné I, Lamp B, Nist A, Imhof A, Stiewe T, Renkawitz-Pohl R, Rathke C, Brehm A, **Distinct CoREST complexes act in a cell-type-specific manner**, *Nucleic Acids Research* (2019) Dec 16;47(22):11649-11666. doi: 10.1093/nar/gkz1050

Marburg, den 12.08.2020   Igor Mačinković

Die Hinweise zur Erkennung von Plagiaten habe ich zur Kenntnis genommen.

Marburg, den 12.08.2020   Prof. Dr. A. Brehm